

EDITORIAL BOARD

Editor-in-Chief

Igor Krivtsun

E.O. Paton Electric Welding Institute of the NASU, Kyiv, Ukraine

Deputy Editor-in-Chief

Michael Gasik

Aalto University, Espoo, Finland

Deputy Editor-in-Chief

Jacob Kleiman

Integrity Testing Laboratory, Markham, Canada

Editorial Board Members

Serhii Akhonin

E.O. Paton Electric Welding Institute of the NASU, Kyiv, Ukraine

Olena Berdnikova

E.O. Paton Electric Welding Institute of the NASU, Kyiv, Ukraine

Chunlin Dong

Guangzhou Jiao Tong University, China

Shiyi Gao

China-Ukraine Institute of Welding,
Guangdong Academy of Sciences, Guangzhou, China

Len Gelman

The University of Huddersfield, UK

Andrey Gumenyuk

Bundesanstalt für Materialforschung und –prüfung (BAM),
Berlin, Germany

Vitalii Knysh

E.O. Paton Electric Welding Institute of the NASU, Kyiv, Ukraine

Volodymyr Korzhyk

E.O. Paton Electric Welding Institute of the NASU, Kyiv, Ukraine

Victor Kvasnytskyi

NTUU «Igor Sikorsky Kyiv Polytechnic Institute», Ukraine

Leonid Lobanov

E.O. Paton Electric Welding Institute of the NASU, Kyiv, Ukraine

Eric Macdonald

The University of Texas at El Paso, USA

Serhiy Maksymov

E.O. Paton Electric Welding Institute of the NASU, Kyiv, Ukraine

Dhanesh G. Mohan

School of Engineering University of Sunderland England,
United Kingdom

João Pedro Oliveira

Universidade NOVA de Lisboa, Portugal

Mykola Pashchin

E.O. Paton Electric Welding Institute of the NASU, Kyiv, Ukraine

Valeriy Pozniakov

E.O. Paton Electric Welding Institute of the NASU, Kyiv, Ukraine

Uwe Reisgen

Welding and Joining Institute, Aachen, Germany

Massimo Rogante

Rogante Engineering, Civitanova Marche, Italy

Cezary Senderowski

Mechanics and Printing Institute, Warsaw University
of Technology, Poland

Magdalena Speicher

Kempen University of Applied Sciences, Germany

Mattias Thuvander

Chalmers University of Technology, Goteborg, Sweden

Valentyn Uchanin

Karpenko Physico-Mechanical Institute of the NASU, Lviv, Ukraine

Gerald Wilhelm

University of Applied Sciences of Munich, Germany

Yongqiang Yang

South China University of Technology, Guangzhou, China

Executive Editor

Oleksandr Zelnichenko

International Association "Welding", Kyiv, Ukraine

Address of Editorial Office

E.O. Paton Electric Welding Institute, 11 Kazymyr Malevych Str., 03150, Kyiv, Ukraine

Tel.: (38044) 205 23 90, E-mail: patonpublishinghouse@gmail.com; journal@paton.kiev.ua

<https://patonpublishinghouse.com/eng/journals/tpwj>

The Journal was registered by the National Council of Ukraine on Television and Radio Broadcasting on 09.05.2024,
carrier identifier R30-04569; ISSN 0957-798X; DOI: <http://dx.doi.org/10.37434/tpwj>

Subscriptions, 12 issues per year:

348 Euro — annual subscription for the printed (hard copy) version, air postage and packaging included;

288 Euro — annual subscription for the electronic version (sending issues in pdf format or providing access to IP addresses).

Representative Offices of "The Paton Welding Journal":

BRAZIL, Arc Dynamics

Address: Nova Iguacu, Rio de Janeiro, Brazil

Daniel Adolpho, Tel.: +55 21 9 6419 5703, E-mail: dadolpho@arcdynamics.com.br

BULGARIA, Bulgarian Welding Society

Address: Blvd. Asen Yordanov No.10, Sofia 1592, Bulgaria

Pavel Popgeorgiev, Tel.: +359 899 96 22 20, E-mail: office@bws-bg.org

CHINA, China-Ukraine Institute of Welding, Guangdong Academy of Sciences

Address: Room 210, No. 363 Changxing Road, Tianhe, Guangzhou, 510650, China

Zhang Yupeng, Tel.: +86-20-61086791, E-mail: patonjournal@gwi.gd.cn

POLAND, PATON EUROPE Sp. z o. o.

Address: ul. Kapitałowa 4, 35-213, Rzeszów, Poland

Anton Stepakhno, Tel.: +38067 509 95 67, E-mail: Anton.Stepakhno@paton.ua

The content of the Journal includes articles received from authors from around the world in the field of welding, cutting, cladding, soldering, brazing, coating, 3D additive technologies, electrometallurgy, material science, NDT and selectively includes translations into English of articles from the following journals, published in Ukrainian:

- «Автоматичне Зварювання» (Automatic Welding), [https://patonpublishinghouse.com/eng/journals/as](https://patonpublishinghouse.com/eng/journals/as;);
- «Suchasna Elektrometalurhiya» (Electrometallurgy Today), [https://patonpublishinghouse.com/eng/journals/sem](https://patonpublishinghouse.com/eng/journals/sem;);
- «Tekhnichna Diahnostyka ta Neruinivnyi Kontrol» (Technical Diagnostics & Nondestructive Testing), <https://patonpublishinghouse.com/eng/journals/tdnk>.

CONTENTS

ORIGINAL ARTICLES

V.S. Kachynskyi, D. Allford, M.P. Drachenko, I.V. Ziakhor, V.I. Klymenko, S.M. Samotryasov
DEVELOPMENT OF THE TECHNOLOGY OF PRESSURE WELDING WITH A MAGNETICALLY IMPELLED ARC OF SMALL-DIAMETER PIPES USING SUPERCAPACITORS* 3

Ke Liming, P.D. Stukhliak, V.M. Mudrichenko
FEATURES OF THE STRUCTURE OF COATINGS OF TUNGSTEN AND CHROMIUM CARBIDES DURING DETONATION-GAS SPRAYING WITH ENERGY ACCUMULATION IN A MULTICHAMBER DEVICE* 11

N.V. Vihilianska, O.M. Burlachenko, O.P. Gryshchenko, I.O. Koziakov, V.F. Gorban
FORMATION OF COATINGS OF THE FeTi–SiC SYSTEM DURING THERMAL SPRAYING OF POWDER PRODUCED BY THE METHOD OF MECHANOCHEMICAL SYNTHESIS* 19

Z. Mirijanashvili, G. Dadianidze, O. Tsagareishvili, B. Salaridze, L. Chkhartishvili
OBTAINING WEAR-RESISTANT COATINGS BY SURFACING WITH POWDER CORE WELDING WIRE 26

A.A. Babinets
USING THE HEREDITY EFFECT FOR CONTROL OF THE STRUCTURE OF THE DEPOSITED METAL DURING ELECTRIC ARC SURFACING WITH FLUX-CORED WIRES (REVIEW)* 30

S.V. Petrov, S.G. Bondarenko, Sh. Roshanpour, A.M. Shakhnovsky
CONTINUOUS PRODUCTION OF LARGE VOLUMES OF PLASMA ACTIVATED WATER FOR AGRICULTURE 42

INFORMATION

77th ANNUAL ASSEMBLY OF THE INTERNATIONAL INSTITUTE OF WELDING AND INTERNATIONAL WELDING AND JOINING CONFERENCE 54

VII INTERNATIONAL CONFERENCE “WRT-2024” 56

*Translated Article(s) from “Avtomatychne Zvaryuvannya” (Automatic Welding), No. 5, 2024.



DEVELOPMENT OF THE TECHNOLOGY OF PRESSURE WELDING WITH A MAGNETICALLY IMPELLED ARC OF SMALL-DIAMETER PIPES USING SUPERCAPACITORS

V.S. Kachynskiy¹, D. Allford², M.P. Drachenko¹, I.V. Ziakhor¹,
V.I. Klymenko¹, S.M. Samotryasov¹

¹E.O. Paton Electric Welding Institute of the NASU
11 Kazymyr Malevych Str., 03150, Kyiv, Ukraine, Kyiv

²Arc Specialties. 1730 Stebbins Drive, Houston, TX 77043-2807, USA

ABSTRACT

Pipes of small diameters of up to 100 mm are used at various industrial and agricultural facilities. The methods of manual arc welding or automatic welding are traditionally used for joining the pipes. The issue of using supercapacitors in equipment for magnetically impelled arc butt welding (MIAB) process, to reduce peak loads on the electrical network, is considered. The need for such equipment is primarily determined by the tasks of “green” technologies. Application of supercapacitors in power sources allows ensuring further on the optimal parameters of pulse welding processes, in order to improve their quality and work productivity. A prototype of a new generation of power source for MIAB welding of pipes of a small diameter in the field and stationary conditions using an autonomous power supply source has been developed and manufactured.

KEYWORDS: welding current formers, magnetically impelled arc butt welding, autonomous sources of powerful current pulses and power supply, supercapacitors

INTRODUCTION

The world is becoming ever more dependent on electricity as the main source of energy. In view of this trend and increasing global competition, the manufacturers focused on increase of the efficiency and reduction of power consumption.

Energy efficiency of welding equipment is one of the main tasks of its further improvement. This also concerns the pulse processes of welding various parts. Application of supercapacitors as power sources for resistance spot welding ensures a significant weight reduction, compared to the usual approaches (transformer and power source) with further ergonomic advantages [1]. One of the developed at PWI processes of joining pipes is magnetically impelled arc butt (MIAB) welding [2]. In order to reduce peak loads from equipment power on the mains during welding of pipes under field and stationary production conditions [3], studies were performed on development of an equipment complex for MIAB process with power supply from an autonomous power plant (APP) based on supercapacitors. For optimal selection of its power, preliminary analysis of power consumption was performed, proceeding from the value of power consumed under load. The capacitors are charged at a low rate for a long period of time and discharge quickly, ensuring high currents with minimal influence on peak consumption from the mains. Capacitor charging at low current levels also allows the manufacturers to connect the welding systems without upgrading the

distribution power of their plants. The supercapacitors accumulate energy similar to a flywheel, storing the energy for a long period of time, and then quickly releasing this energy, when required. This approach is more effective at power application and reduces the expenses for the infrastructure and capital equipment.

At application of classical supply circuits, achieving high efficiencies (EF) of the welding equipment involves considerable difficulties. It is anticipated that application of capacitive energy storages based on supercapacitors will allow solving the energy storage issue. Application of supercapacitors in pipe welding equipment will allow reducing energy consumption and the demand for power supply, will significantly reduce the weight and overall dimensions of welding equipment, and will allow development of autonomous welding complexes with power supply from mobile power plants for working under the field and stationary conditions.

The question of development of pulse current generators (PCG) for MIAB welding is urgent. The experimental mock-up of MIAB welding equipment was based on the method of forming a powerful pulse of welding current, which involves application of supercapacitors (SC) as energy storage [4–6]. It allows significantly lowering the level of peak loads on the mains and, consequently, the value of the source installed power. One of the important tasks at development of MIAB welding equipment is formation of a powerful current pulse at the final stage of welding before upsetting the heated pipe edges.

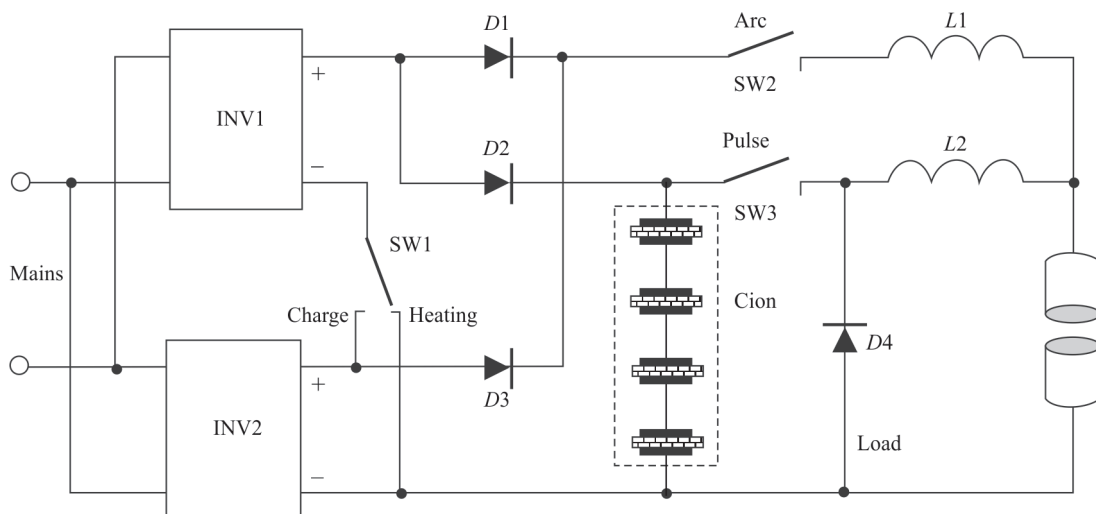


Figure 1. Scheme of pulse forcing of the welding arc: INV1, INV2 — the inverter voltage converters; SW1–SW3 — mechanical current switches; D1–D4 — diodes; Cion — supercapacitor battery; L1, L2 — forming inductors; the Load is the MIAB welding unit

Until lately, direct welding current sources of Lincoln Electric — DC1000 or Miller-DC1000 with up to 1000 A peak current pulse were used for this purpose. A circuit (Figure 1) of a pulse welding current source, in which SC battery was used to form pulse current, was developed and tested by the results of the conducted studies.

The circuit includes two inverter converters DC INV1 and INV2 with rated welding current of 150 A, separating diodes $D1$, $D2$, $D3$; reverse protection diode $D4$; forming inductances $L1$, $L2$; circuit mode switches SW1, SW2, SW3 and energy storage, based on a battery of Cion SC connected in series. The device work cycle consists of three phases: 1 — phase of charging the pulse energy storage; 2 — phase of heating the edges to be welded by a pilot arc; 3 — phase of pulsed increase of the arc current for pipe edge melting.

Cion pulse energy storage is charged through separating diode $D2$ from inverters INV1 and INV2 connected in series via SW1 switch. Capacitor charge voltage is controlled by the monitoring and control circuit (not shown in Figure 1). Preheating of the pipes being welded is performed from inverters INV1 and INV2, connected in parallel by switch SW1, and connected to the item via diodes $D1$, $D3$, choke $L1$ and switch SW2. Arc current forcing pulse is executed at closing of contactor SW3 by the following circuit: +Cion, SW3, $L2$, load, –Cion. Diode $D3$ protects contactor SW3 from failure when extinguishing the arc forcing current pulse. Switches SW1, SW2, SW3 are controlled by the monitoring and control circuit (not shown in Figure 1).

PCG laboratory mockup with a controlled current pulse shape was made for performance of further studies of the welding processes. In it power current switches based on fully controlled semi-conductor structures are used [7, 8].

In keeping with modern tendencies in power electronics [8], power transistors with MOSFET structure were used for welding processes at conditionally low voltage of the current pulse. Their selection is substantiated by the peculiarities of their properties that allows performing parallel connection of the transistors of a conditionally unlimited number, and enables building powerful current switches. Supercapacitor batteries (SCB) were applied as the power source to form powerful current pulses. SCB application as powerful current sources allows essentially reducing PCG weight and size characteristics, compared to the traditional solutions, in which the industrial mains are used as the pulse current source. Moreover, mains power can be much lower, as the SCB forms the current pulse. Here, just the power required for SCB charging, distributed over SCB charging time, is consumed from the mains.

The generalized structural-functional scheme of the pulse current generator with charging circuit optimization for application in MIAB welding equipment is given in Figure 2.

In PCG circuit stepdown type voltage converter (SVC) with pulse-width modulation (PWM) are used as current pulse formers, where M1 module forms the current of pipe edge heating, and M2 module generates the pulse of edge melting current. Application of PCG modular structure allows improvement of the conditions of power loss dissipation, as well as more flexible adaptation of the power part of the circuit for different welding applications.

Overall monitoring and control of the circuit operation is performed by the control unit (CU). SC battery charging is conducted by charging device (CD), which in its turn is powered from the initial voltage inverter with power corrector INV1. SVC is controlled from local PWM controllers.

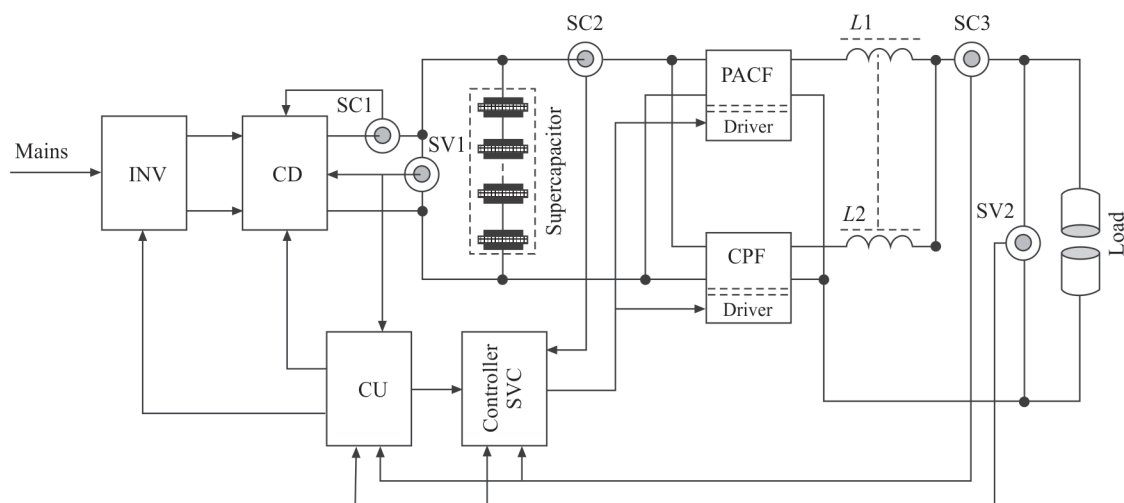


Figure 2. Generalized structural-functional scheme of pulse current generator for MIAB welding: INV — power inverter; CD — charging device; CU — control unit; SVC — controller of stepdown voltage converters; PACF — preheating arc current former; CPF — current pulse former; SC, SV — current and voltage sensors

Table 1. Chemical composition of pipe metal, wt. %

Steel grade	C	Si	Mn	Ni	S	Cu	P	Cr	V
09G2S	0.11	0.61	1.48	0.21	0.021	0.21	0.02	0.23	0.11

DEVELOPMENT OF EXPERIMENTAL TECHNOLOGY OF MIAB WELDING, USING AN AUTONOMOUS POWER SUPPLY SOURCE

Pipes from structural low-alloyed steel 09G2S which can withstand a wide working temperature range from –70 to +450 °C, were used for investigations. High mechanical strength allows using steels of this grade in the oil industry, pipeline construction and agriculture. Table 1 gives the chemical composition of the pipe metal.

In order to conduct studies on welding steel pipes of Ø38×3 mm, welding current and arc voltage and relative movement of pipes being welded were programmed, in keeping with the cyclogram (Figure 3). At the start of the process, during time t_1 , the pipes are pressed together to provide reliable contact of their edges and the arc power source is switched on, and then the pipes are moved apart for the arc gap width, thus exciting the arc. The arc is first burning at higher current I_1 during time t_2 . Then the welding current decreases to current I_2 and the pipes are heated during time t_3 . After the necessary heating of the pipe edges has been achieved, the welding current from SC is increased up to value I_3 , and then pipe upsetting and welded joint formation are performed. After time t_5 the arc power source is switched off, and after time t_6 the upsetting force is removed. The welding cycle is over.

The welded pipe sample is shown in Figure 4. Welding was performed with application of the developed autonomous PCG power source for MIAB welding equipment.

A study with current increase after heating, but without upsetting, was performed additionally (Figure 5). Results showed that the pipe edges before upsetting are uniformly melted over the entire heated metal surface that promotes optimal formation of the welded joint.

MECHANICAL TEST RESULTS

Mechanical testing was conducted in keeping with API 1104 standard [9]. Test results are given in Table 2.

DEVELOPMENT OF SPECIFICATION PROCEDURE FOR MIAB WELDING WITH AN AUTONOMOUS POWER SOURCE

Proceeding from the developed parameters of MIAB welding process, recording of the procedure of welding with application of supercapacitors from an autonomous power source was conducted. Based on the results of the conducted mechanical tests, the weld-

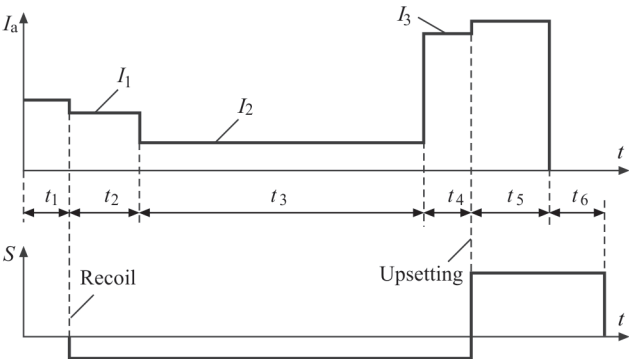


Figure 3. Cyclogram of MIAB welding process: I_a — welding current; S — pipe movement during welding; t — welding time



Figure 4. Welded joint of a pipe of Ø38×3 mm
ing procedure recording was further developed into the welding procedure specification (WPS). Figure 6 gives the specification of the welding procedure, developed for Ø38×3 mm pipes from 09G2S steel.

RESULTS OF METALLOGRAPHIC INVESTIGATIONS

Investigations were conducted on microsections of welded joints of Ø38×3 mm pipes, which were polished on high-speed wheels, using diamond pastes of different dispersity. Metal structure was revealed by chemical etching in 4 % alcohol solution of HNO₃. Investigations were performed in Neophot-32 and Versomet micro-

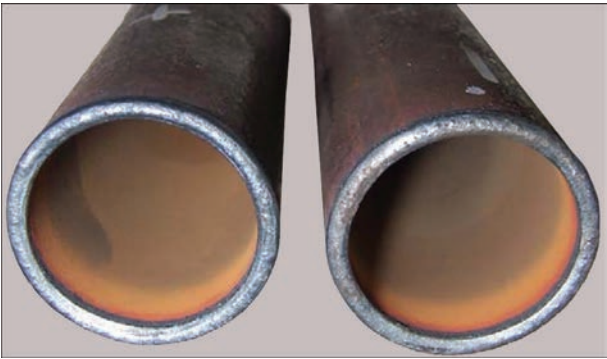


Figure 5. Appearance of pipe edges before upsetting
scopes at different magnifications. Microhardness was determined at 1 N load in M-400 microhardness meter of Leco Company. Grain size was determined by GOST 5639–82 scales. Digital image of the microstructures was obtained using Olympus camera.

The joint line is quite pronounced along the entire weld height. The width of the joint line band is 30–50 µm, near the flash it is up to 180 µm (Figure 7).

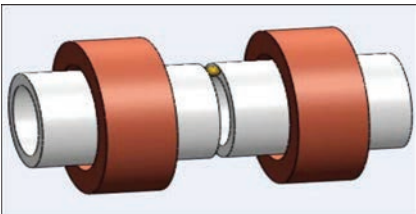

E.O. Paton Electric Welding Institute of the NAS of Ukraine					
Procedure specification of MIAB welding with an autonomous welding source					
API 1104 Specification Welding process: MIAB welding Steel grade: 09G2S MIAB welding machine model: MD-101			PWI WPS/MIAB – 001 Process mode: automatic WPS: Procedure for carbon steels Pipe diameter: 38 mm Wall thickness: 3 mm		
Joint configuration			Joined parts		
					
Joint characterization			Shielding gases and materials		
Joint type – butt joint			Shielding gases: not used Internal blowing: not used Welding wire: not used Water cooling: not used		
Welding parameters for pipes of 38 mm dia					
Stage number	Welding current, A	Welding time, <i>t</i>	Arc voltage, V	Arc gap, mm	Upsetting force, kN
1	220–240	2.5–2.7	24–27	1.7	41–44
2	180–190	10–12			
3	570–610	0.2–0.4			
Prepared:			Certified:		
Date:			Date:		

Figure 6. WPS for MIAB welding using an autonomous power source

Table 2. Mechanical properties of pipe welded joints

Steel grade	Pipe wall diameter/ wall thickness, mm	σ_t , MPa		$KCV_{+20\text{ }^\circ\text{C}}$, J/cm ²	
		Base metal	Welded joint	Base metal	Welded joint
09G2S	38×3	488±11	492±12	56±12	52±13

The microstructure is a ferrite-pearlite mixture, where pearlite is found in the form of thin plates within the ferrite precipitates.

Hardness measurement was performed in the weld, HAZ and base metal. The measured hardness values on test samples are as follows:

- welded joint: $HV1-2070-2200$ MPa
- HAZ: overheated subzone $HV1-1910-2210$ MPa, overheated zone width $1200-1300$ μm ;
- complete recrystallization subzone $HV1-1610-1790$ MPa, subzone width 1400 μm ;
- base metal: $HV1-1510-1710$ MPa.

Proceeding from the results of mechanical tests and metallographic investigations it was established that the pipe welded joints are within the admissible limits, in keeping with standards, applied in industry of Ukraine and other countries.

TECHNICAL MEANS FOR AUTONOMOUS MIAB WELDING COMPLEX

In case it is necessary to conduct MIAB welding of pipes under field and stationary production conditions [2, 10–12], at low input power levels, there is the need use supercapacitors and power supply from APP. Analysis and optimization of charge-discharge processes in capacitive energy storages (CES) is one of the main tasks in design of pulse technological installations, to which MIAB equipment belongs. At selection of the method of CES charging, we usually proceed from technical-economic indices, where the price-quality criterion is used. As is known [13, 14], at technical realization of charging devices, three charging methods are mainly used:

- Charging from constant voltage source ($U_{\text{ch}} = \text{const}$);

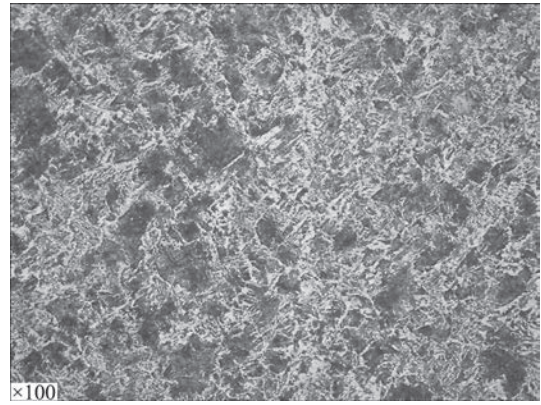


Figure 7. Joint line and HAZ of the welded joint ($\times 200$)

- Charging from direct current source ($I_{\text{ch}} = \text{const}$);
- Charging in the constant power mode ($P_{\text{ch}} = \text{const}$).

In work [15] it is shown that application of inductive-capacitive converters (ICC) as current sources in charging devices can provide the efficiency close to 100 %.

As regards technical realization of MIAB welding units, Figure 8 shows a variant of structural-functional scheme of the unit with application of SCB for energy accumulation. Such a schematic is the most advanced technologically in terms of optimal use of APP resources, in view of absence of peak loads during operation of the welding complex. SC charging is performed directly from a special charging device (CD) with application of ICC technology that allows maximum use of SC, and PFC application at the device input increases the efficiency of electric plant power utilization. This is due to the fact that at the device operation during the welding cycle, the plant load power is practically constant, that is related to application of energy storage based on SC.

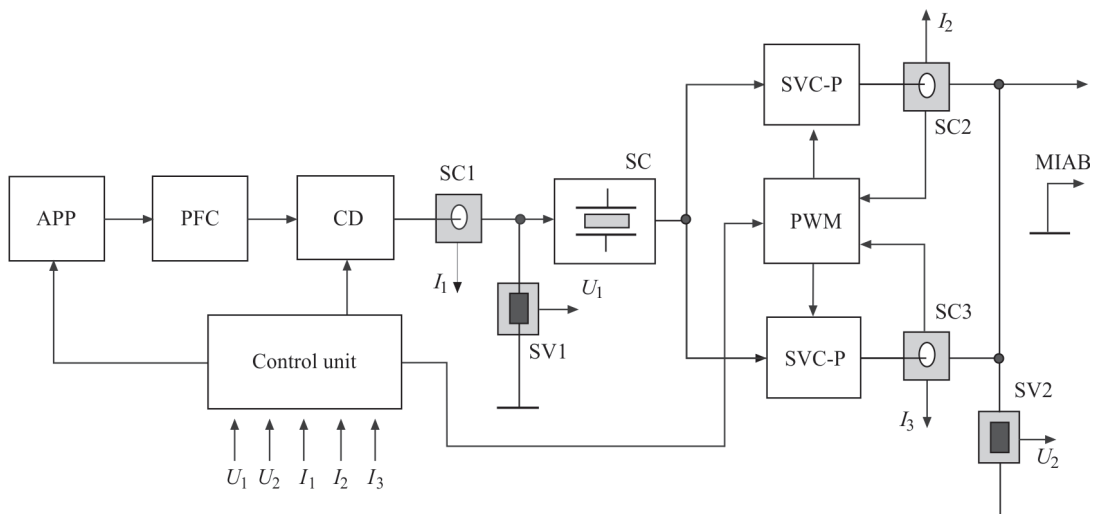


Figure 8. Structural-functional scheme of power supply system for welding by MIAB method with energy storage based on supercapacitors: APP; PFC — power factor corrector; CD — charging device for supercapacitor battery; SC — supercapacitor battery; SVC-P — stepdown converter of preheating arc supply voltage; PWM — pulse-width modulation controller; SVC-P — stepdown converter of pulse arc supply voltage; SV1, SV2 and SC1–SC3 — voltage and current sensors

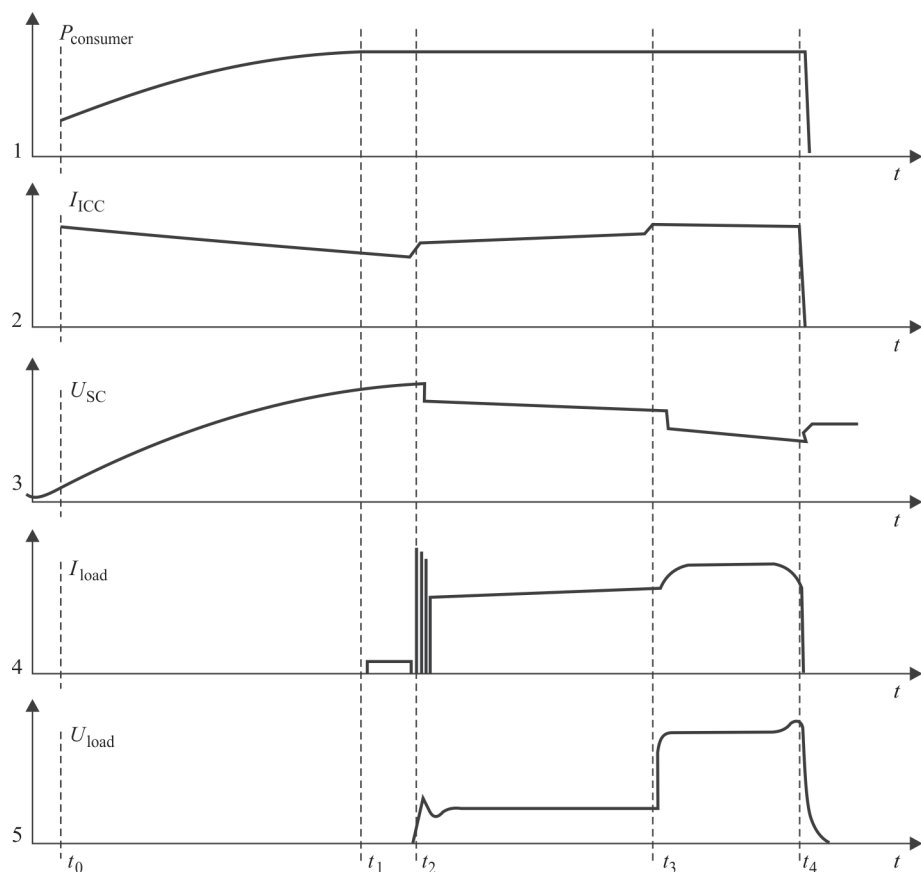


Figure 9. Current and voltage diagrams in the time interval of the complex work cycle: 1 — power consumed from APP; 2 — SCB charging current; 3 — SCB voltage; 4 — load current; 5 — load voltage

The operation of MIAB welding power source can be broken into the following main phases, Figure 9: SC energy storage charging ($t_0 - t_1$); heating of the edges to be welded by a low-ampere arc ($t_2 - t_3$); edge melting by a forced arc ($t_3 - t_4$); upsetting (t_4). Current pulse extinguishing takes place in the upsetting mode.

Each mode of power source operation is characterized by its own circuit operation algorithm, and consequently, different losses in the power unit proper, which should also be taken into account at selection of APP power level.

For stable operation of stepdown converters of welding arc voltage, the voltage at SVC input should not drop below $1.5U_a$. For maximum use of the properties of SC-based energy storage, the SC battery discharge by more than $0.5U_{SCmax}$ is not rational.

Figure 10, *a* shows one of the variants of experimental sample of the power supply system for MIAB welding machine (Figure 10, *b*), based on 6 kW mini-power plant, and Figure 11 is its structural-functional block-diagram.

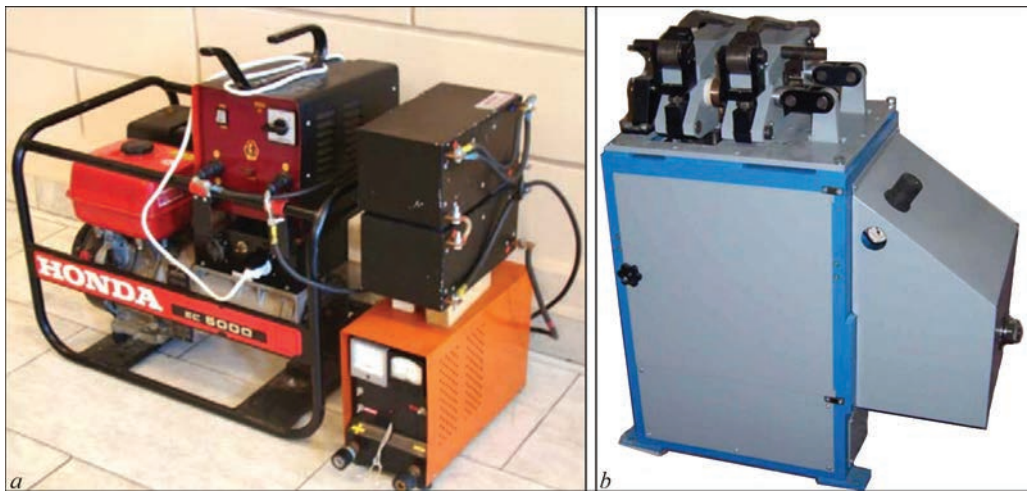


Figure 10. Autonomous power complex based on 6 kVA mini-power plant (*a*) and MIAB welding unit for MD101 pipes (*b*)

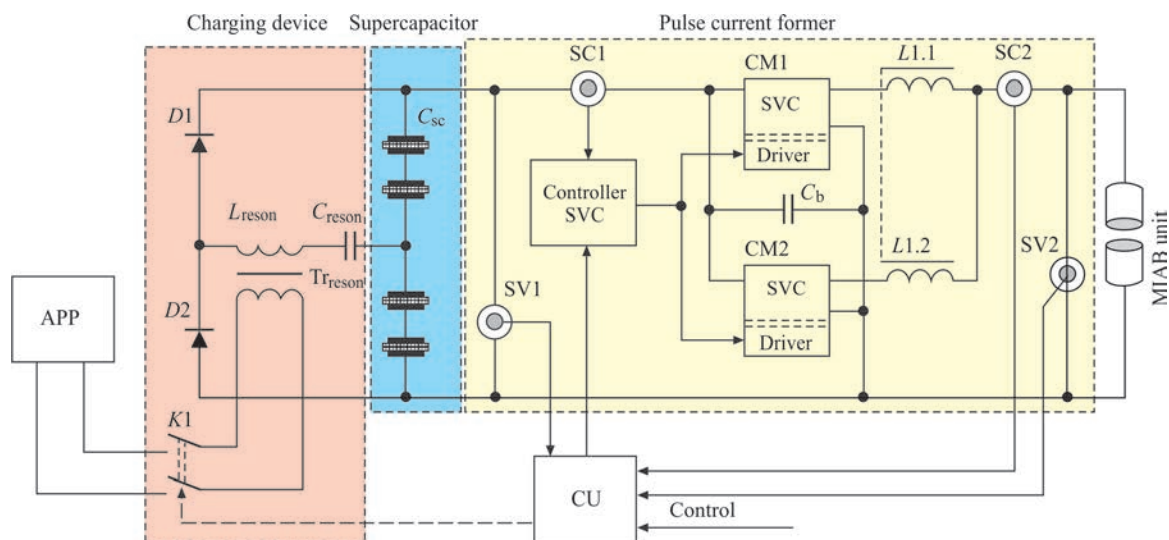


Figure 11. Structural-functional block-diagram of an autonomous power complex for MIAB welding: C_{sc} — supercapacitor battery; CM1 — stepdown converter of preheating arc supply voltage; SVC controller — pulse-width modulation controller; CM2 — stepdown converter of pulse arc supply voltage; CU — complex control unit; SV and SC — voltage and current sensors; $L1.1$, $L1.2$ — inductive storage chokes

Technical characteristics of the experimental autonomous power complex for welding small-diameter pipes by MIAB welding method are as follows:

- power of autonomous gasoline unit: $P = 6$ kVA, $\cos \varphi > 0.8$;
- supercapacitor battery: $C = 60$ F, $U = 68$ V;
- range of current pulse amplitude values: $I_p = 0.4\text{--}2.0$ kA;
- range of preheating arc current values: $I_{pr} = 75\text{--}200$ A;
- range of current pulse time values: $T_1 = 0.05\text{--}1.0$ s.

CONCLUSIONS

1. With application of MIAB welding process with an autonomous power source based on supercapacitors the energy consumption costs can be lowered by 50–70 %, compared to the conventional welding process.

2. A pilot-production technology was developed for MIAB welding with supercapacitors.

3. Supercapacitors have the engineering potential for generation of the required welding current with the specified arc voltage and pulse duration at MIAB welding of small-diameter pipes.

4. Modern tendencies of development in the field of electric energy storages indicate that capacitive type devices are the most promising for pulse technological installations. This is particularly true for capacitors with a double electric layer — supercapacitors, where the specific capacitance already now is higher than 20 F/h. As their inner resistance is equal to units of mOhms, they can be effectively used in pulse technological units.

5. At development of units for pulse welding processes, it is necessary to take into account such an im-

portant capacitor parameter as energy efficiency. This is related to the fact that the discharge degree is determined by the minimal level of voltage, at which a specific technological process can occur, and with optimization in the processes of the charging-discharging of capacitive energy storages.

6. Application of supercapacitors in MIAB welding units significantly improves the energy efficiency of welding, and technological quality of welded joints, lowers the welding equipment cost, and reduces the peak loads on the mains.

7. Further work on determination of the effectiveness of supercapacitor application in the welding processes will be aimed at investigation of the process of MIAB welding and formation of welded joints of larger diameter pipes from steel of different classes.

REFERENCES

1. Jerry E. Gould, Hee Chang, (2013) Estimations of compatibility of supercapacitors for use as power sources for resistance welding guns. Doc. IIW III-1208-02, *Welding in the World*, 57(6), 887–894.
2. Kachinsky, V.S., Kuchuk-Yatsenko, S.I., Koval, M.P., Goncharenko, E.I. (2016) Technology and equipment for press magnetically-impelled arc welding of position joints of small-diameter pipes in site and stationary conditions. *The Paton Welding J.*, 5–6, 29–34. DOI: <https://doi.org/10.15407/tpwj2016.06.05>
3. Kachinskiy V.S., Krivenko V.G., Ignatenko V.Yu. (2002) Magnetically impelled arc butt welding of hollow and solid parts. Doc. IIW III-1208-02, *Welding in the World*, 46(7–8).
4. Gautham Prasad G, NidheeshShetty, Simran Thakur, Rakshitha and Bommegowda K.B. (2019) Supercapacitor technology and its applications: A review. *IOP Conf. Series: Mater. Sci. and Engin.*, 561 012105. DOI: <https://doi.org/10.1088/1757-899X/561/1/012105>.
5. Korotynsky, A.E., Drachenko, N.P., Shapka, V.A. (2014) Peculiarities of application of supercapacitors in devices for

- pulse welding technologies, *The Paton Welding J.*, **9**, 34–38. DOI: <https://doi.org/10.15407/tpwj.2014.09.05>
6. Korotynskiy, O.E., Skopyuk, M.I., Vertetska, I.V. (2021) High-efficient sources for arc welding on the base of capacitive energy storage systems. *The Paton Welding J.*, **3**, 43–48. DOI: <https://doi.org/10.37434/tpwj.2021.03.08>
 7. Korotynskiy, O.Ye., Drachenko, M.P., Zhernosekov, A.M., Vertetska, I.V. (2024) Welding current formers using artificial long lines. *The Paton Welding J.*, **1**, 27–31. DOI: <https://doi.org/10.37434/tpwj.2024.01.04>
 8. Shidlovsky, A.K., Shcherba, A.A., Suprunovskaya, N.I. (2009) *Energy processes in electropulse installations with capacitive energy storage*. Kyiv, NANU–IED.
 9. (2013) API standard 1104: Welding of pipelines and related facilities, API.
 10. Leigh, F., Cec, S., Gabriel S. (2003) *MIAB welding: Break-through technology for high productivity field welding of pipelines*. APIA National Convention Pipelines — Yesterday, Today and Tomorrow Convened by the Australian Pipeline Industry Association.
 11. Edson, D.A. (1982) *Magnetically impelled arc faying surfaces welding of thick wall tubes*. Doc. IIW, IM-726–82.
 12. Hiller, F., Schmidt, M., Breiksch, J. (2003) *Use of the magnetarc welding process in the production of truck cab suspension systems*. Thyssen Krupp Techforum.
 13. Opre, V.M. (2008) Generators of rectangular current pulses. *Power Electronics*, **1**, 56–61.
 14. Gromovenko, V.M., Opre, V.M., Shchegoleva, N.A. (1997) Charging devices of split capacitive storage devices. *Electrical Engineering*, **3**, 46–48.
 15. Pentegov, I.V. (1982) *Fundamentals of the theory of charging circuits of capacitive energy storage*. Kyiv, Naukova Dumka [in Russian].

ORCID

V.S. Kachynskiy: 0000-0001-9695-6434,
M.P. Drachenko: 0000-0002-4485-2403,
I.V. Ziakhor: 0000-0001-7780-0688,
V.I. Klymenko: 0000-0002-8709-5924,
S.M. Samotryasov: 0000-0003-4891-9625

CONFLICT OF INTEREST

The Authors declare no conflict of interest

CORRESPONDING AUTHOR

V.S. Kachynskiy
E.O. Paton Electric Welding Institute of the NASU
11 Kazymyr Malevych Str., 03150, Kyiv, Ukraine.
E-mail: vskweld@gmail.com

SUGGESTED CITATION

V.S. Kachynskiy, D. Allford, M.P. Drachenko, I.V. Ziakhor, V.I. Klymenko, S.M. Samotryasov (2024) Development of the technology of pressure welding with a magnetically impelled arc of small-diameter pipes using supercapacitors. *The Paton Welding J.*, **10**, 3–10. DOI: <https://doi.org/10.37434/tpwj.2024.10.01>

JOURNAL HOME PAGE

<https://patonpublishinghouse.com/eng/journals/tpwj>

Received: 24.04.2024

Received in revised form: 09.09.2024

Accepted: 29.10.2024

SUBSCRIPTION-2025



“The Paton Welding Journal” is Published Monthly Since 2000 in English, ISSN 0957-798X (Print), ISSN 3041-2293 (Online); doi.org/10.37434/tpwj.

“The Paton Welding Journal” can be also subscribed worldwide from catalogues subscription agency EBSCO.

If You are interested in making subscription directly via Editorial Board, fill, please, the coupon and send application by E-mail.

12 issues per year, back issues available.

348 Euro, subscriptions for the printed (hard copy) version, air postage and packaging included.

288 Euro, subscriptions for the electronic version (sending issues of Journal in pdf format or providing access to IP addresses).

The archives for 2009–2023 are free of charge on
[www://patonpublishinghouse.com/eng/journals/tpwj](http://www.patonpublishinghouse.com/eng/journals/tpwj)

Address

International Association “Welding”
11 Kazymyr Malevych Str., 03150, Kyiv, Ukraine
Tel.: (38044) 205 23 90

E-mail: patonpublishinghouse@gmail.com, E-mail: journal@paton.kiev.ua
[www://patonpublishinghouse.com/eng/journals/tpwj](http://www.patonpublishinghouse.com/eng/journals/tpwj)

FEATURES OF THE STRUCTURE OF COATINGS OF TUNGSTEN AND CHROMIUM CARBIDES DURING DETONATION-GAS SPRAYING WITH ENERGY ACCUMULATION IN A MULTICHAMBER DEVICE

Ke Liming, P.D. Stukhliak, V.M. Mudrichenko

Scientific-Research Institute of Welding Technologies named after E.O. Paton in Zhenjiang Province
233 Yonghui Road, Xiaoshan District, Hangzhou City, Zhejiang Province, China

ABSTRACT

This paper presents the results of studies of the structure of coatings obtained from powders based on chromium ($75\text{Cr}_3\text{C}_2 + 25\text{NiCr}$) (wt.%) and tungsten carbides ($\text{WC} + 12\text{Co}$) (wt.%) by detonation-gas spraying with energy accumulation in multi-chamber devices. It has been established that this technology provides high-density coatings with a thickness of 200–500 μm with porosity of less than 1 % and microhardness $HV_{0.05} = 1235 \pm 80$ ($\text{WC} + 12\text{Co}$) (wt.%) and 1547 ± 150 ($75\text{Cr}_3\text{C}_2 + 25\text{NiCr}$) (wt.%). A characteristic feature of these coatings is the formation of a substructure with the size of 1–8 μm and of carbide-type strengthening phases with dimensions of 100–800 nm, which are evenly distributed in the volume of the coating material. It was established that a high level of structural strengthening of these coatings is provided by formation of a material with a dispersed subgranular structure with a uniform distribution of particles of strengthening phases in it.

KEYWORDS: protective coatings, multichamber detonation-cumulative spraying, microstructure, microhardness, substructure, structural strengthening

INTRODUCTION

Improvement of operational reliability of the mechanisms of oil-pumping equipment in technological facilities envisages application of wear-resistant coatings, exposed to elevated temperatures in service. In this research area a promising approach is application of materials based on chromium and tungsten carbides. Formation of such composites and coatings on their base is performed by thermal spraying [1–3], including highly productive method of detonation spraying at process speed, exceeding the velocity of sound several times [4–7].

Compared to other methods of producing the coatings [8–12] such as flame, plasma or laser methods and hybrid technologies, the method of multichamber detonation spraying provides better technological effect of coating formation through realization of the cumulative energy effect in specially designed chambers [6, 7]. In this case, the pressure of pulsed gas flow rises that results in an increase of the velocities of detonation combustion products in the nozzle (1800 m/s) and velocity of powder transportation (1200–1500 m/s) to the surface to form the coatings. This method allows forming sound poreless nanostructured coatings, including those based on carbides, with high adhesion and cohesion characteristics and density [13–16].

Interesting from the scientific and practical viewpoint is application of dispersed WC-Co , $\text{Cr}_3\text{C}_2\text{-NiCr}$

powder materials that have proven themselves well at formation of protective coatings on the surfaces of parts, and components of mechanisms and machines of different functional purposes. Selection of the abovementioned materials is due to the temperature conditions of their operation at 500–520 and 820–870 $^{\circ}\text{C}$, respectively, under the conditions of erosion and cavitation wear and at dynamic alternating loads. Formation of WC- and $\text{Cr}_3\text{C}_2\text{-}$ based materials with Co and Ni content leads to appearance of a nanocrystalline structure and zones with a non-crystalline structure in the coating material [3, 17, 18]. It allows improving the wear resistance and crack resistance due to strengthening on the interface and increasing the strength of adhesion bonding of the coatings with the base.

Application of the abovementioned materials is not limited by oil-transportation equipment. Particularly promising is application of such protective coatings in the mining industry, for equipment used in oil well drilling, agricultural machinery and for metal-cutting tools, and equipment repair by restoration of the wearing surfaces. Application for all the types of valves, water turbines, rolls for sheet steel rolling, shafts for protection of their working surfaces is promising.

At present insufficient attention is paid to studying the features of formation of the abovementioned coatings, produced by the method of multichamber detonation spraying and to determination of their struc-

tural-phase characteristics, influencing their service properties.

The objective of the work is investigation of the structure of coatings from powders of different systems: WC–Co; Cr_3C_2 –NiCr, produced by the method of multichamber detonation spraying and of the influence of structural-phase characteristics on hardness values.

MATERIALS AND INVESTIGATION PROCEDURES

Coatings for investigation performance were deposited at the Scientific-Research Institute of Welding Technologies named after E.O. Paton in Zhenjiang Province (PRC) in a robotic detonation-gas spraying system developed at PWI (Figure 1).

Coating deposition was performed by a multichamber detonation device (Figure 1), which includes: specially profiled forechamber which allows significantly shortening the section of transition from the arcing to detonation mode; main cylindrical chamber used for development of the detonation process, creation of the main gas-dynamic pressure of detonation combustion products, which accelerate and heat the powder; circular chamber, designed for forming an additional gas-dynamic flow, which “backs up” in the cylindrical barrel the detonation products from the second (main) chamber, and expands the powder heating and acceleration zone. Application of such a design of multichamber detonation device provides intensification of the detonation arcing mode, accumulation of detona-

tion energy, and creation of the effect of detonation wave compression [6, 7].

The following powders were used for coating deposition: WC + 12Co (wt.%) (AMPERIT® 518.074); $75\text{Cr}_3\text{C}_2 + 25\text{NiCr}$ (wt.%) (AMPERIT®585.003) with particle size of 15–45 μm , Abrasive-jet treatment of the base material surface (St. 3) with white electrocorundum of F16 grade was performed (1–2 mm fraction) before spraying. Spraying mode was as follows: gun movement speed — 1500 mm/min; gun barrel length/diameter ratio (l/d) — 325/16 mm; oxygen flow rate — $\text{O}_2 = 41$ l/min (chamber 1), $\text{O}_2 = 35$ l/min (chamber 2); in each chamber the flow rate of air was 11 l/min and flow rate of C_3H_8 was 11 l/min; powder flow rate — 1600 g/h. Spraying distance (distance from the multichamber device nozzle to steel base surface) was 60–70 mm. Coating No. 1 (WC + 12 Co) was sprayed in three passes, No. 2 (WC + 12 Co) and No. 3 ($75\text{Cr}_3\text{C}_2 + 25\text{NiCr}$) were deposited in seven passes.

Microstructural studies of the coatings were conducted with application of light microscopy (Zeiss Axio Imager M2m microscope). Coating thickness (δ), microhardness (HV), dimensions of the structural components — lamel width (h_l) and their volume fraction (V_p , %), and porosity (P , %) were determined. Coating porosity and volume fraction of the lamels were determined using metallographic software with application of “Pro Imaging” software package (Zeiss Axio Imager M2m). Microhardness was measured in VH1102 instrument (USA) at 0.5 kg load.

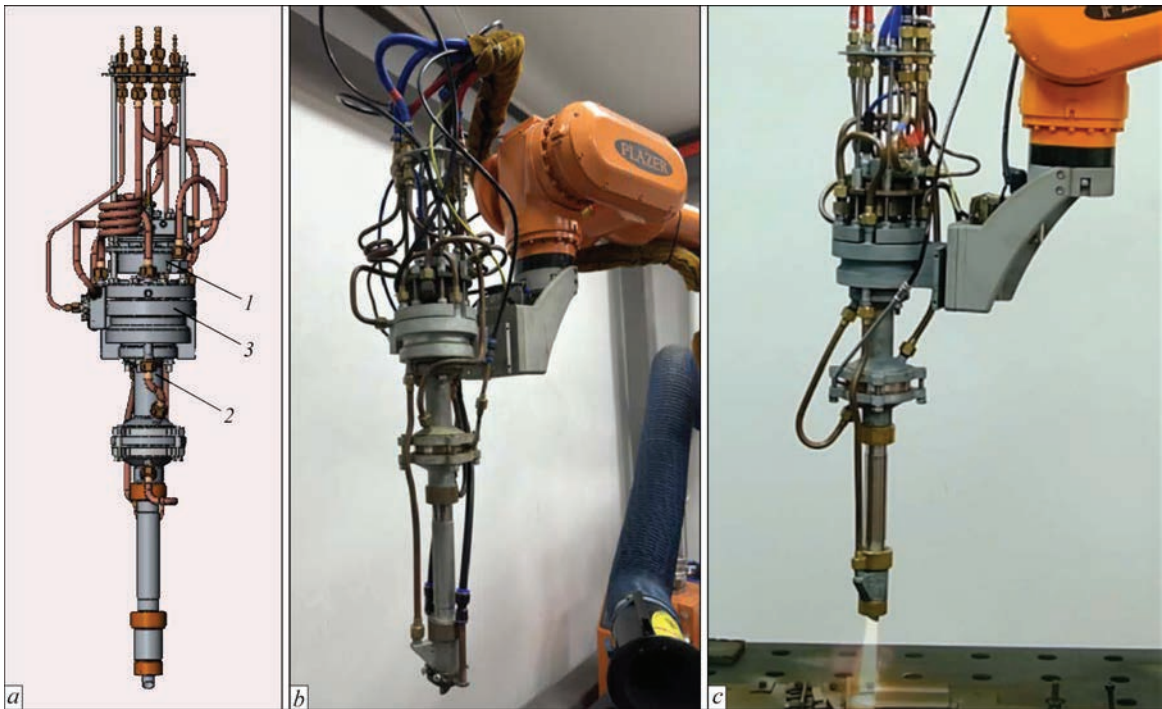


Figure 1. Appearance of multichamber detonation device (*a*, *b*) and process of detonation-gas spraying (*c*) with energy accumulation in the multichamber device: 1 — forechamber; 2 — main chamber; 3 — cylindrical chamber

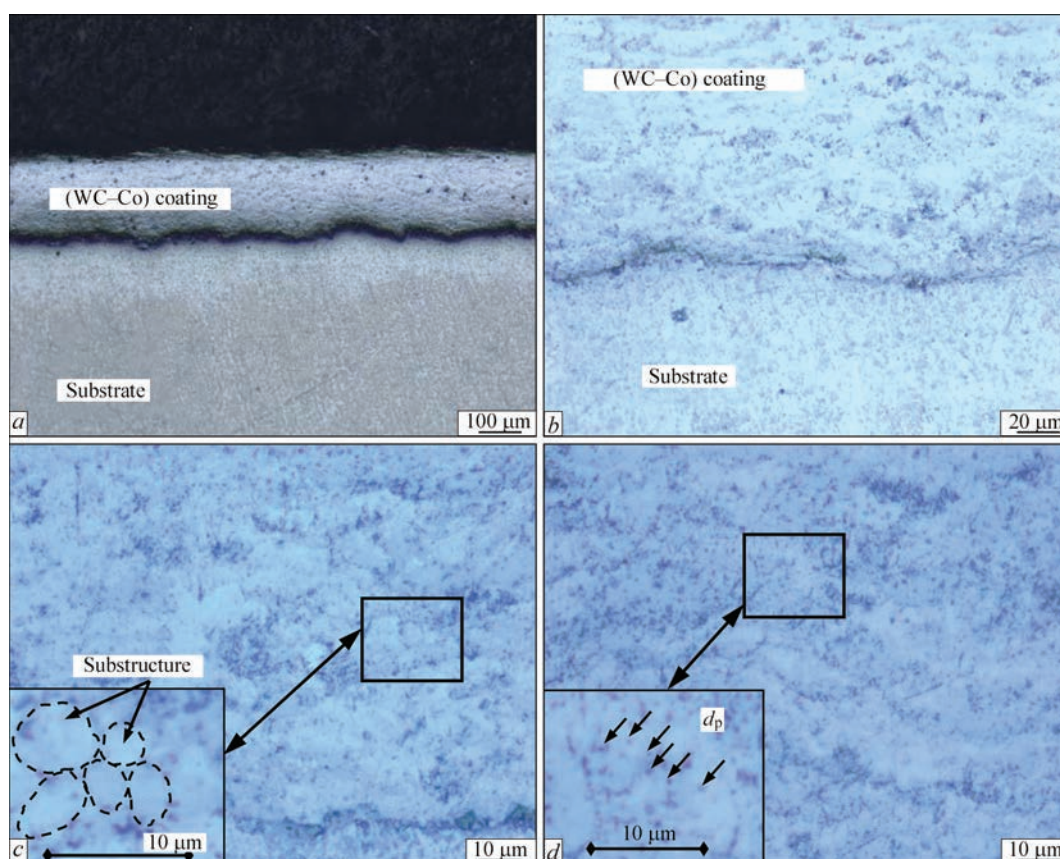


Figure 2. Microstructure of coating No. 1 from (WC + 12Co) powders (*a* — $\times 100$; *b* — $\times 500$; *c*, *d* — $\times 1000$)

INVESTIGATION RESULTS

Three types of coatings were produced from the initial powders: No. 1 — from (WC + 12Co) powder of thickness $\delta = 200 \mu\text{m}$ (Figure 2, *a*); No. 2 — (WC + 12Co) of thickness $\delta = 520 \mu\text{m}$ (Figure 3, *a*); No. 3 — ($75\text{Cr}_3\text{C}_2$ –25NiCr) of thickness $\delta = 500 \mu\text{m}$ (Figure 4, *a*). Coating materials differ by the volume fraction of the lamels (Table 1).

Coating from (WC + 12Co) powder is characterized by volume fraction of the lamels (V_l) of 5–10 % (coating No. 1) and of 10–15 % (coating No. 2) in the matrix, respectively (Figures 2, *b*; Figure 3, *b*). Spraying of Cr_3C_2 –NiCr ensures lamellation with $V_l = 25$ –30 % (Figure 4, *b*).

At application of Cr_3C_2 –NiCr powder in the material of coating No. 3 the lamel width is $h_l = 1$ –20 μm (Table 2). Here, formation of the grain structure at $D_{gr} = 10$ –20 μm (Figure 4, *b*) and of a substructure with size $d_s = 2$ –8 μm (Figure 4, *c*, *d*) with microhardness $HV_{0.5} = 1417 \pm 67 \text{ MPa}$ (across coating thickness) and $HV_{0.5} = 1547 \pm 150 \text{ MPa}$ (along the thickness of the coating middle zone) (Table 2) was observed. Presence of particles of dispersed phases with size $d_p = 0.15$ –0.3 μm is also characteristic with their uniform distribution at distances $\lambda_p = 0.2$ –0.45 μm (Figure 4, *c*).

In case of producing coating No. 2 from (WC + 12Co) powder the lamel width $h_l = 20$ –30 μm , grain

size is $D_{gr} = 10$ –20 μm at microhardness $HV_{0.5} = 1235 \pm 80$ (across coating thickness) and $HV_{0.5} = 1209 \pm 80 \text{ MPa}$ (along the coating middle zone length), Table 2. Also observed was formation of a substructure with size $d_s = 1.2$ –3.0 μm (Figure 3, *c*) in the presence of dispersed phase particles of size $d_p = 0.15$ –0.45 μm at distances $\lambda_p = 0.25$ –0.6 μm (Figure 3, *d*).

Material of coatings No. 1 sprayed using (WC–Co) powder is characterized by formation of grain and subgrain structures with sizes $D_{gr} = 10$ –20 μm (Figure 2, *b*) and $d_s = 2$ –5 μm (Figure 2, *c*, *d*) with microhardness $HV_{0.5} = 1120 \pm 100 \text{ MPa}$ (across the thickness) and $HV_{0.5} = 1184 \pm 66 \text{ MPa}$ (along the length of the coating middle zone), Tables 1, 2. The size of dispersed phase particles is $d_p = 0.1$ –0.8 μm , distance between them is $\lambda_p = 0.16$ –1.0 μm (Figure 2, *d*). The main phases forming in the material of coatings from

Table 1. Structural parameters of the coatings

Coating	$\delta, \mu\text{m}$	$HV_{0.5}$		$V_l, \%$
		Across the thickness	Along the length	
No. 1 (WC–Co)	200	1120 \pm 100	1184 \pm 66	5–10
No. 2 (WC–Co)	520	1235 \pm 80	1209 \pm 80	10–15
No. 3 (Cr_3C_2 –NiCr)	500	1417 \pm 67	1547 \pm 150	25–30

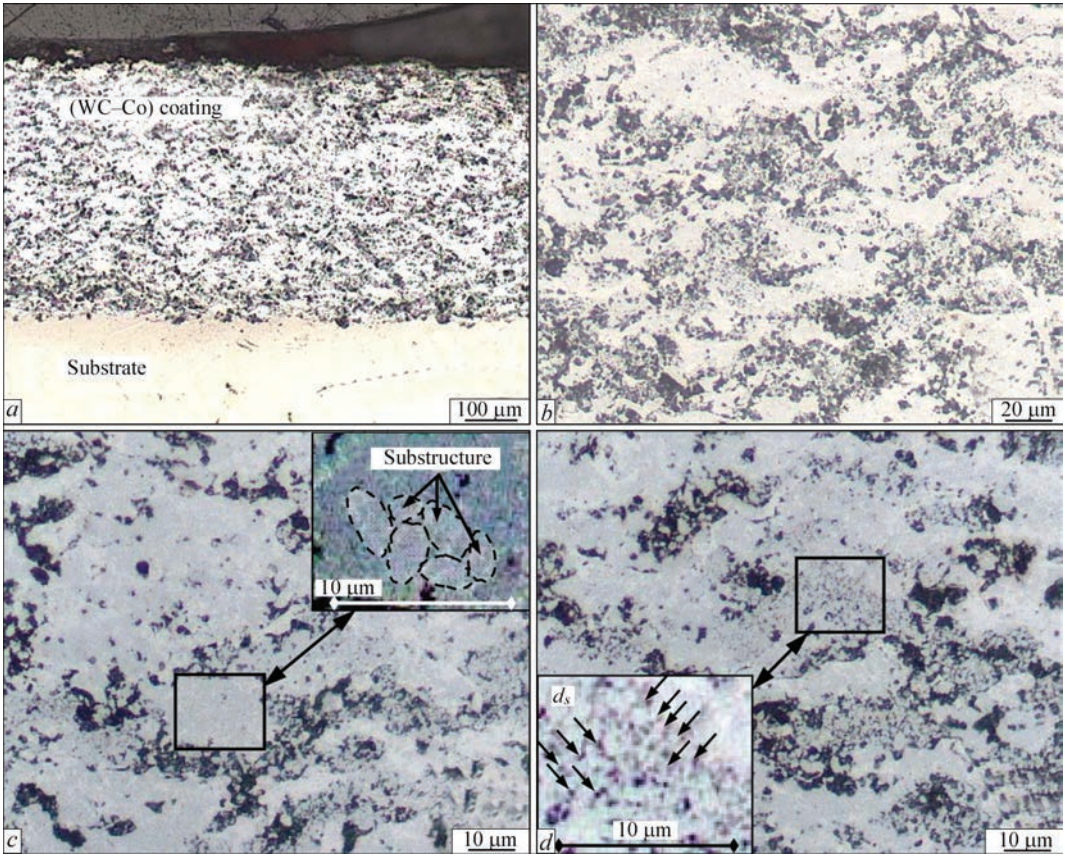


Figure 3. Microstructure of coating No. 2 from WC-Co powder (*a* — $\times 100$; *b* — $\times 500$; *c*, *d* — $\times 1000$)

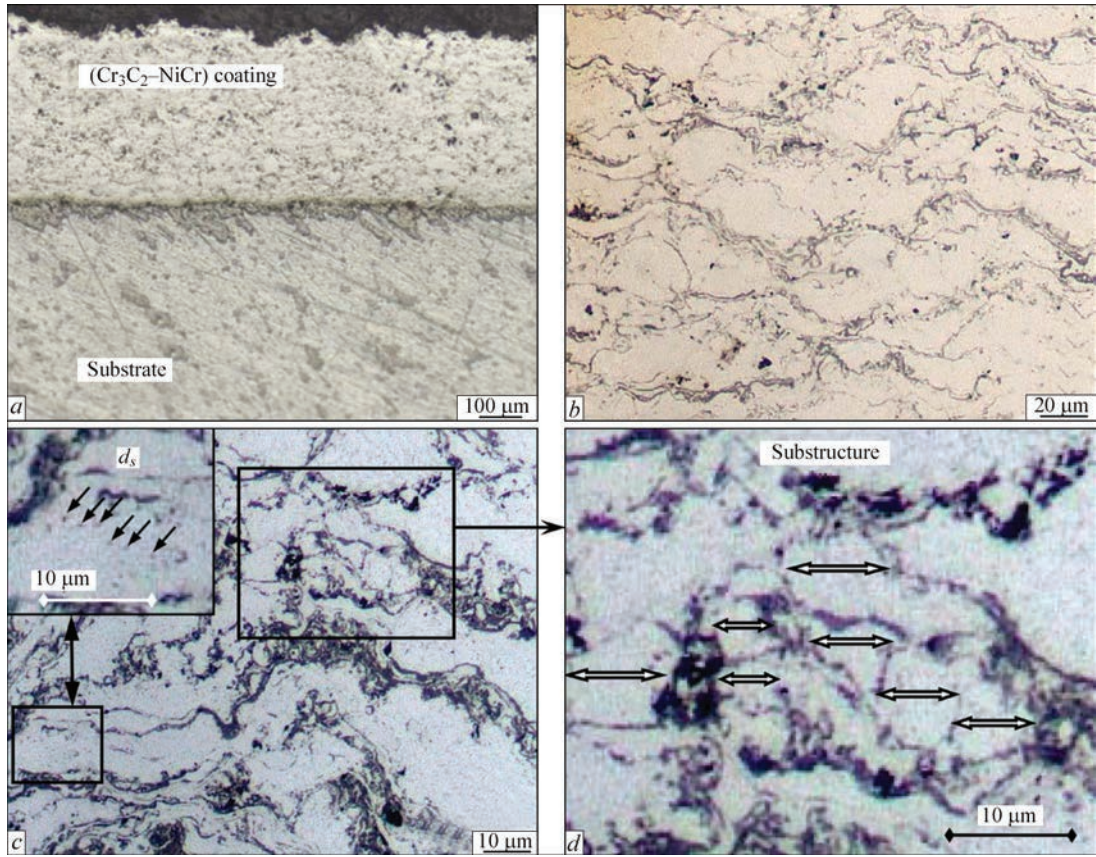


Figure 4. Microstructure of coating No. 3 from $\text{Cr}_3\text{C}_2\text{-NiCr}$ powder: *a* — $\times 100$; *b* — $\times 500$; *c*, *d* — $\times 1000$ (*d* — enlarged fragment from Figure 4, *c*)

Table 2. Microstructural parameters of coating material

Coating	Structural parameters				
	$h_p, \mu\text{m}$	$D_{gr}, \mu\text{m}$	$D_s, \mu\text{m}$	$d_p, \mu\text{m}$	$\lambda_p, \mu\text{m}$
No. 1 (WC-Co)	20–30	10–40	2.0–5.0	0.15–0.45	0.25–0.60
No. 2 (WC-Co)	8–20	10–20	1.2–3.0	0.10–0.80	0.16–1.00
No. 3 (Cr ₃ C ₂ -NiCr)	2–20	10–20	2.0–8.0	0.15–0.30	0.20–0.45

powders based on tungsten carbide are WC and W₂C [19, 20].

Thus, metallographic studies of material structure in coatings produced by the method of multichamber detonation spraying of powders based on tungsten and chromium carbides, showed the following. The coatings are characterized by porosity of less than 1 %, and differ by microhardness and lamellation. The level of material microhardness is without significant gradients. Microhardness is practically the same in coatings of different thickness (Nos 1 and 2), sprayed from WC-based powder (Figure 5).

The highest microhardness was observed in Cr₃C₂-NiCr coating (Figure 5). At detailed measurements of $HV_{0.5}$ of different structural components, such as unmolten particles (Figure 6, *a*), light (Figure 6, *b*) and dark lamels (Figure 6, *c*) it was established that their microhardness was found to differ as follows: $HV_{0.5}$ = 579–1147 (unmolten particles); $HV_{0.5}$ = 826–1776

(light lamels); $HV_{0.5}$ = 1039–1573 (dark lamels). This is indicative of the activity of phase formation process when producing the coatings. Application of Cr₃C₂-NiCr powder for spraying of coatings led to appearance of particles of Cr₃C₂ (30–50 %) and Cr₇C₃ + Cr₂O₃ phases (30–40 %) [13, 21–23].

Compared to Cr₃C₂-NiCr coating in coatings from WC-Co powder the microhardness decreases 1.2 times on average. At spraying of (WC-Co) powder in the material of coating No.1 (of thickness δ = 200 μm) the lamel width and grain size increase 2.2 times at substructure coarsening 2.6 times.

Measurements of phase particle size and distribution in the coating matrix were conducted. Software for metallographic microscope Zeiss Axio Imager M2m was used. Analysis of microstructure fragments obtained at magnifications of $\times 1000$ (Figure 2, *d*; Figure 3, *d*; Figure 4, *c*) further magnification of the images 10–15 times was performed.

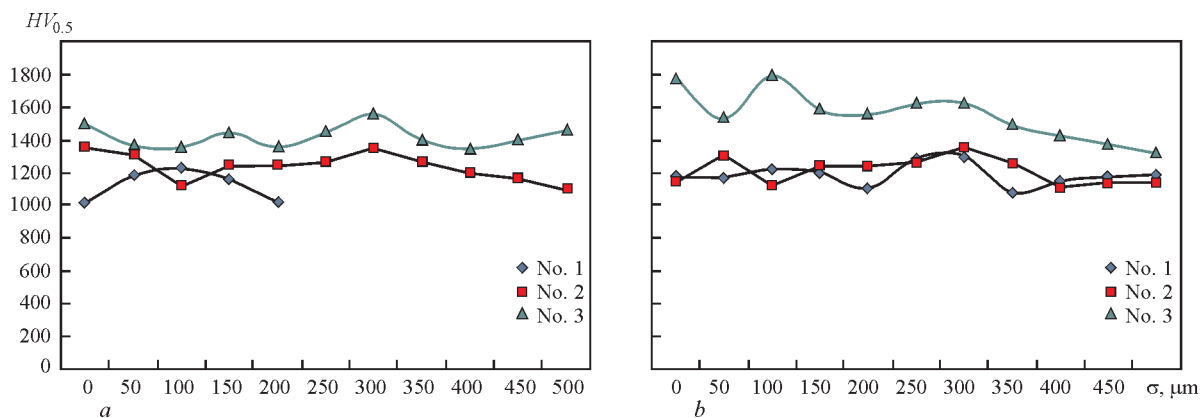


Figure 5. Change of microhardness across the thickness (δ) of coatings and length (L) of middle zone of coatings produced from WC-Co (Nos 1, 2) and Cr₃C₂ + NiCr (No. 3) powders

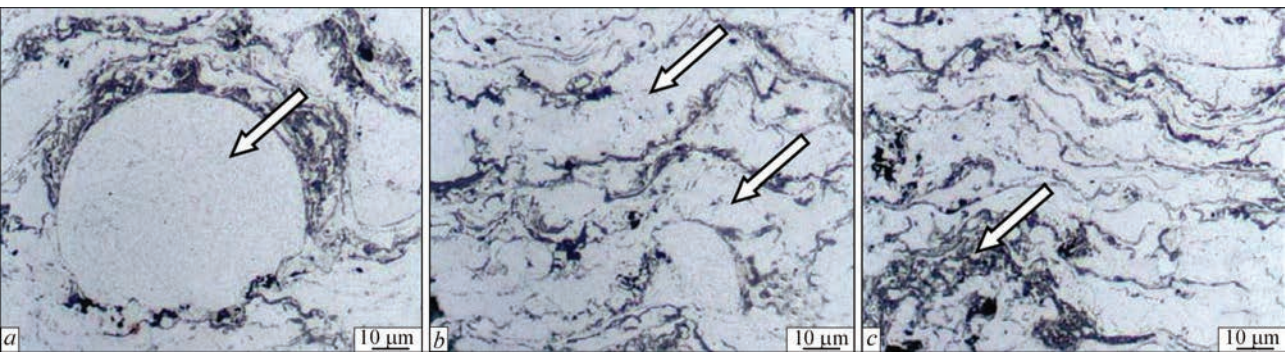


Figure 6. Different structural components in coating No. 3 (Cr₃C₂-NiCr): unmolten particles (*a*), light (*b*) and dark lamels (*c*)

Table 3. Calculated values of coating material structural strengthening

Coating	Structural strengthening				
	$\Delta\sigma_0$	$\Delta\sigma_{gr}$	$\Delta\sigma_s$	$\Delta\sigma_{d.s}$	$\Sigma\Delta\sigma_y$ (average)
No. 1 (WC–Co)	46	17–5* 128–181**	291–460	1341–1849	2208
No. 2 (WC–Co)	60	10–16* 135–192**	375–593	811–2159	2206
No. 3 (Cr ₃ C ₂ –NiCr)	34	32–3* 75–150**	230–460	750–1812	1809

*Lamels. **Grain.

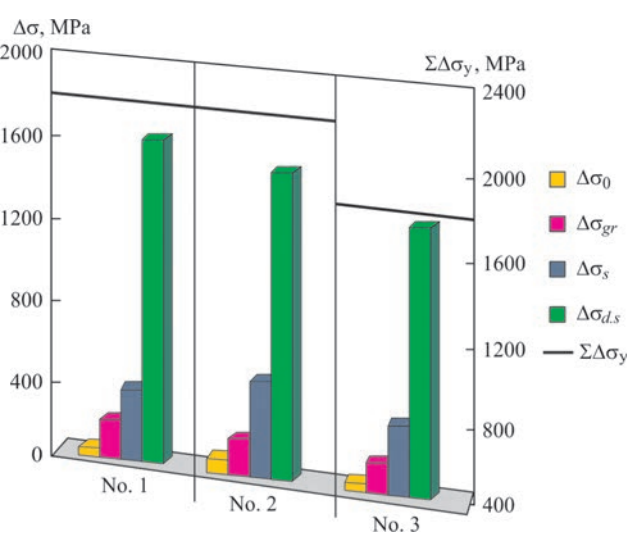


Figure 7. Histograms of the contribution of average values of structural strengthening of coatings from the following powders: Nos 1, 2 — (WC–Co); No. 3 — (Cr₃C₂–NiCr): — lattice friction ($\Delta\sigma_0$), grain ($\Delta\sigma_{gr}$), subgrain ($\Delta\sigma_s$) and dispersion ($\Delta\sigma_{d.s}$) strengthening

In case of application of (Cr₃C₂–NiCr) powder, the size of dispersed phase particles $d_p = 150\text{--}300$ nm in the coating matrix is negligibly small compared to coatings No. 1 (WC–Co), where $d_p = 150\text{--}450$ nm (Table 2). Distance (λ_p) between the particles is also reduced, which is characterized by increase of their volume fraction in the coating matrix up to 30 %. However, in coating No. 2 (WC–Co) at minimal sizes of dispersed phases ($d_p = 100$ nm) and distances between them ($\lambda_p = 160$ nm) their volume fraction in the coating matrix rises up to 43 %. This will ensure a high level of dispersion strengthening of the coating material [13, 15, 21–24].

It should be noted that a characteristic feature of the produced coatings is presence of dispersed phase particles (Figure 2, *d*; Figure 3, *d*; Figure 4, *c*) of the size from 100–150 up to 300–800 nm at substructure formation (Figure 2, *c*; Figure 3, *c*; Figure 4, *d*).

In order to study the influence of the structure on the mechanical characteristics of the coating material the structural strengthening index ($\Sigma\Delta\sigma_y$) was analyti-

cally assessed, allowing for the contribution of each of the structural parameters (size of lamels and grains — D_{gr} , subgrain — d_s , dispersed phase particles — d_p and distances between them λ_p) [21–24]. Calculation of the structural strengthening components σ_0 ; σ_{gr} ; σ_s ; $\sigma_{d.s}$ was performed (Table 3, Figure 7). A similar approach was also tried out on other materials, where significant results were obtained as regards the experimental values of mechanical properties in the structure of different materials — steels of different class, aluminium and titanium alloys, tungsten single-crystals, protective coatings, etc. [25–27].

As a result it was established that the average integral values of strengthening ($\Sigma\Delta\sigma_y$) for (WC–Co) coatings No. 1 (thickness $\delta = 200$ μm) and No. 2 ($\delta = 500$ μm) are equal to $\Sigma\Delta\sigma_y = 2208$ MPa and $\Sigma\Delta\sigma_y = 2206$ MPa, respectively (Figure 7, Table 3). A slight reduction of $\Sigma\Delta\sigma_y$ is observed in the material of (Cr₃C₂–NiCr) coating. In all the cases, the maximal contribution (up to 70 %) into the total strengthening value is made by strengthening of the coating matrix due to dispersed particles of nanosized phases (Orowan dispersion strengthening): $\Delta\sigma_{d.s} = 1595$ MPa (coating No. 1); $\Delta\sigma_{d.s} = 1485$ MPa (coating No. 2); $\Delta\sigma_{d.s} = 1281$ MPa (No. 3). Here, the contribution of grain and subgrain strengthening for the studied coatings is equal to 8–9 % ($\Delta\sigma_{gr}$) and 17–22 % ($\Delta\sigma_s$), respectively.

Thus, the high level of structural strengthening of coatings from powders based on WC and Cr₃C₂ at application of the method of multichamber cumulative-detonation spraying is ensured predominantly due to dispersion strengthening by phase particles at their uniform distribution in the coating material.

CONCLUSIONS

The structural features were revealed in coatings from (WC + 12Co) (wt.%) powders deposited on the steel surface by the method of multichamber cumulative-detonation spraying. A high density coating of 200–500 μm thickness was produced with less than 1 % porosity, with a gradientless microhardness level.

A characteristic features of the coating microstructure formed at multichamber cumulative-detonation spraying, is formation of a dispersed substructure of 1–8 μm size and carbide-type strengthening phases of 100–800 nm size, evenly distributed in the coating material volume. Such submicron and nanosized substructure of the carbide phases provides higher values of coating microhardness $HV_{0.5} = 1014\text{--}1352$ for (WC + 12Co) (wt.%) coating and $HV_{0.5} = 1256\text{--}1785$ for (75Cr₃C₂ + 25NiCr) (wt.%).

It was found that the high level of structural strengthening of the produced coatings is ensured due to dispersion strengthening by submicron and nanosized carbide phases at their uniform distribution in the coating material.

REFERENCES

1. Yushchenko, K.A., Borisov, Yu.S., Kuznetsov, V.D., Korzhyk, V.M. (2007) *Surface engineering*. Kyiv, Naukova Dumka [in Ukrainian].
2. Korzhyk, V.N., Likhoshva, V.P., Tkachenko, E.A. (2014) *Strengthening and renovation by surface engineering*. Kyiv, Nash Format [in Russian].
3. Borisov, Yu.S., Korzhyk, V.N. (1995) Amorphous gas-thermal coatings: Theory and experimental data. *Thermal Plasma and New Materials Technology*, **2**, 255–269. Cambridge Inter-science Publ.
4. Korzhyk, V.N., Astakhov, E.A., Chernyshov, A.V. (1990) *Detonation spraying of amorphous and microcrystalline coatings*. Kyiv, Znanie [in Russian].
5. Borisov, Yu.S., Korzhyk, V.N., Astakhov, E.A., Chernyshov, A.V. (1993) Influence of the composition of the detonating medium on the formation of amorphous-crystalline coatings. *Avtomatich. Svarka*, **6**, 83–93 [in Russian].
6. Barykin G.Yu., Korzhyk, V.N., Chernyshov, O.V. (1995) *Device for detonation spraying of coatings*. Pat. of Ukraine [in Ukrainian].
7. Kolisnichenko, O.V., Tyurin, Yu.N., Tovbin, R. (2017) Efficiency of process of coating spraying using multichamber detonation unit. *The Paton Welding J.*, **10**, 18–23. DOI: <https://doi.org/10.15407/tpwj2017.10.03>
8. Hrygorenko, G.M., Adeeva, L.I., Tunik, A.Y. et al. (2020) Formation of microstructure of plasma-arc coatings obtained using powder wires with steel skin and B4C + (Cr, Fe)₇C₃ + Al filler. *Metallfizika i Noveishie Tekhnol.*, **42**(9), 1265–1282. <https://mfint.imp.kiev.ua/ua/abstract/v42/i09/1265.html>
9. Grigorenko, G.M., Adeeva, L.I., Tunik, A.Y. et al. (2019) Structurization of coatings in the plasma arc spraying process using B4C + (Cr, Fe)₇C₃-cored wires. *Powder Metall. Met. Ceram.*, **58**(5–6), 312–322.
10. Kuzmych-Ianchuk, I.K., Borisov, Yu.S., Bernatskyi, A.V. (2014) Laser-microplasma reactive powder spraying of titanium coatings with nitride phases. *Applied Mechanics and Materials*, **682**, 276–281. Transact. Tech. Publ. Ltd. DOI: <https://doi.org/10.4028/www.scientific.net/AMM.682.276>
11. Shelyagin, V., Krivtsun, I., Borisov, Yu. et al. (2005) Laser-arc and laser-plasma welding and coating technologies. *The Paton Welding J.*, **8**, 44–49.
12. Imbriovych, O., Povstyanoy, O., Zaleta, S. et al. (2021) The influence of synthesis regimes on operational properties of oxide ceramic coatings on an aluminum alloy. In: *Advances in Design, Simulation and Manufacturing. DSMIE-2021*. Eds by V. Ivanov et al. Lecture Notes in Mechanical Engineering, 536–545. Springer, Cham. DOI: https://doi.org/10.1007/978-3-030-77719-7_53
13. Korzhyk, V.M., Berdnikova, O.M., Stukhliak, P.D. et al. (2023) Structural features of the Cr₃C₂–NiCr and Ni–Cr coatings produced by multichamber detonation spraying. *Poroshk. Metalugiya*, **11–12** [in Ukrainian].
14. Korzhyk, V., Berdnikova, O., Stukhliak, P. et al. (2024) Strength and crack resistance structural criteria of composite coatings produced by the method of multichamber detonation spraying. *Solid State Phenomena*, **355**, 123–129. DOI: <https://doi.org/10.4028/p-qjM7yA>
15. Markashova, L., Tyurin, Y., Berdnikova, O. et al. (2019) Effect of nano-structured factors on the properties of the coatings produced by detonation spraying method. *Lecture Notes in Mechanical Engineering*, 109–117. DOI: https://doi.org/10.1007/978-981-13-6133-3_11
16. Oliker, V.E., Syrovatka, V.L., Timofeeva, I.I. (2005) Effect of titanium aluminide powder properties and detonation spraying conditions on phase and structure formation of coatings. *Poroshk. Metallurgiya*, **9–10**, 74–84 [in Russian].
17. Kunitsky, Yu.A., Korzhik, V.N., Borisov, Yu.S. (1988) *Non-crystalline metallic materials and coatings in engineering*. Kyiv, Tekhnika [in Russian].
18. Shpak, A.P., Korzhyk, V.N., Kunitsky, Yu.A., Shmatko, O.A. (2004) *Materials with nano- and quasi-crystalline structure*. Kyiv, Akademperiodika [in Russian].
19. Haoqiang Zhang, Hao Liu, Chengxiang Ren et al. (2023) Microstructure and properties of the Stellite6/WC composite coatings prepared by laser cladding. *Lasers in Manufacturing and Materials Processing*, **10**(4), 1–14. DOI: <https://doi.org/10.1007/s40516-023-00228-3>
20. Baijiang, Chen, Mengkuo, Xu. (2020) Preparation and performance analysis of micro-nano composite coatings reinforced with WC particles. *Materials Research Express*, **11**(2). DOI: <https://doi.org/10.1088/2053-1591/ad2888>
21. Titkov, Y., Berdnikova, O., Tyurin, Y. et al. (2020) Effect of structure on the properties of composite CrC + NiCr coatings. *Springer Proc. in Physics*, **240**, 151–159.
22. Markashova, L., Tyurin, Y., Berdnikova, O. et al. (2019) Effect of nano-structured factors on the properties of the coatings produced by detonation spraying method. *Lecture Notes in Mechanical Engineering*, 109–117. DOI: https://doi.org/10.1007/978-981-13-6133-3_11
23. Sydorets, V., Berdnikova, O., Polovetskyi, Y. et al. (2020) Modern techniques for automated acquiring and processing data of diffraction electron microscopy for nano-materials and single-crystals. *Mat. Sci. Forum*, **992**, 907–915.
24. Berdnikova, O.M., Tyurin, Yu.M., Kolisnichenko, O.V. et al. (2022) Nanoscale structures of detonation-sprayed metal-ceramic coatings of the Ni–Cr–Fe–B–Si system. *Nanosistemy, Nanomaterialy, Nanotekhnologii*, **20**(1), 97–109.
25. Berdnikova, O., Sydorets, V., Alekseienko, T. (2014) Structure and properties of laser-welded joints from high-strength steels. *Applied Mechanics and Materials*, **682**, 240–245. DOI: <https://doi.org/10.4028/www.scientific.net/AMM.682.240>
26. Berdnikova, O., Kushnarova, O., Bernatskyi, A. et al. (2020) Structure peculiarities of the surface layers of structural steel under laser alloying. In: *Proc. of IEEE 10th Inter. Conf. on Nanomaterials: Applications & Properties*, 02IT01-1-02IT01-4. DOI: <http://doi.org/10.1109/nap51477.2020.9309615>
27. Berdnikova, O., Kushnarova, O., Bernatskyi, A. et al. (2021) Structure features of surface layers in structural steel after laser-plasma alloying with 48(WC–W₂C) + 48Cr + 4Al powder. In: *Proc. of IEEE 11th Inter. Conf. on Nanomaterials: Appli-*

cations & Properties, 01–04. DOI: <https://doi.org/10.1109/NAP51885.2021.9568516>

ORCID

P.D. Stukhliak: 0000-0001-9067-5543,
V.M. Mudrichenko: 0009-0005-8311-2685

CONFLICT OF INTEREST

The Authors declare no conflict of interest

CORRESPONDING AUTHOR

P.D. Stukhliak
Scientific-Research Institute of Welding
Technologies named after E.O. Paton
in Zhenjiang Province

233 Yonghui Road, Xiaoshan District,
Hangzhou City, Zhejiang Province, China.
E-mail: stukhlyakpetro@gmail.com

SUGGESTED CITATION

Ke Liming, P.D. Stukhliak, V.M. Mudrichenko
(2024) Features of the structure of coatings
of tungsten and chromium carbides during
detonation-gas spraying with energy
accumulation in a multichamber device.

The Paton Welding J., **10**, 11–18.

DOI: <https://doi.org/10.37434/tpwj2024.10.02>

JOURNAL HOME PAGE

<https://patonpublishinghouse.com/eng/journals/tpwj>

Received: 21.06.2024

Received in revised form: 27.08.2024

Accepted: 22.10.2024

INTERNATIONAL TRADE FAIR

JOINING ▲ CUTTING ▲ SURFACING

JOIN
THE FUTURE

15. – 19.09.2025

SCHWEISSEN
& SCHNEIDEN



No. 1
IN THE WORLD

MESSE ESSEN

[www.schweissen-schneiden.com](#) | [#schweissenundschniden](#) |

FORMATION OF COATINGS OF THE FeTi–SiC SYSTEM DURING THERMAL SPRAYING OF POWDER PRODUCED BY THE METHOD OF MECHANOCHEMICAL SYNTHESIS

N.V. Vihilianska¹, O.M. Burlachenko¹, O.P. Gryshchenko¹, I.O. Koziakov¹, V.F. Gorban²

¹E.O. Paton Electric Welding Institute of the NASU

11 Kazymyr Malevych Str., 03150, Kyiv, Ukraine

²Frantsevich Institute for Problems of Materials Science of the NASU

3 Omeliana Pritsaka Str., 03142, Kyiv, Ukraine

ABSTRACT

The study of the formation of composite coatings of the FeTi–SiC system, produced by spraying using thermal spraying methods: subsonic (plasma) and supersonic (detonation), was carried out. Composite powder, produced by the method of mechanochemical synthesis of ferrotitanium and silicon carbide powder mixture, was used as the feedstock for spraying. Selection of the composition of powder mixture of ferrotitanium and silicon carbide for the process of mechanochemical synthesis was carried out on the basis of thermodynamic calculations of changes in the values of isobaric-isothermal potentials (Gibbs energy) of reactions in the FeTi–SiC system with selection of the reaction whose passage is the most favorable from a thermodynamic point of view. As a result of mechanochemical synthesis, a composite powder of the FeTi–(SiC, TiC, Ti₃Si₃) system with an amorphous-nanocrystalline structure was produced. Heterogeneous composite coatings consisting of a Fe₂Ti metal matrix with uniformly distributed ceramic inclusions of titanium carbide and silicide and oxide components were produced by plasma and detonation spraying methods. By studying the mechanical characteristics, it was established that the produced thermal sprayed coatings of the FeTi–SiC system are classified as materials with a microcrystalline heterophase structure by the type of structural state. The microhardness of the coatings is 8.5 and 8.0 GPa for plasma and detonation coatings, respectively.

KEYWORDS: mechanochemical synthesis, thermal spraying, composite powder, coating, mechanical properties

INTRODUCTION

Degradation of the surface of parts caused by the influence of aggressive media (abrasive wear, corrosion, high temperature) leads to a reduction in the service life of equipment as a result of the failure of its components [1, 2]. Increasing the service life of equipment can be achieved by creating a protective layer on the surface of parts that is resistant to mechanical, chemical and thermal effects. The combination of toughness and plasticity of the metal matrix with hardness, corrosion, wear and heat resistance of ceramic inclusions makes metal-ceramic (cermet) materials promising for use as a protective layer and allows expanding the service characteristics of parts [3]. At present, iron and its alloys, as well as ferroalloys, are widely used as a metal matrix, which ensure lower production costs for metal-ceramic materials [4–9]. High values of hardness and Young's modulus, good resistance to corrosion and oxidation make silicon carbide a promising candidate for use as a ceramic component in metal-ceramic materials [10].

Thermal spraying (TS) technology is an effective and economical method to produce a metal-ceramic protective layer on the surface of a part [11]. The main difficulties in the formation of metal-ceramic coatings are weak interfacial bond between ceramic inclusions

and a metal matrix, uneven distribution of dispersed ceramic inclusions in the matrix, and also the risk of interfacial interaction, which leads to the formation of undesirable compounds and coating embrittlement [12]. The use of mechanochemical synthesis (MChS) technology allows producing composite powders (CP), which can be used in TS of protective coatings with a homogeneous structure [13].

The aim of the work was to study the process of coating formation under thermal spraying methods using a powder of the FeTi–SiC system produced by mechanochemical synthesis and to determine the mechanical properties of the resulting coatings.

MATERIALS AND RESEARCH PROCEDURE

FeTi–SiC composite powder, produced by the MChS method from ferrotitanium powders (Ti content — 47 wt.%; particle size — 63–100 μm) and silicon carbide (particle size ~3 μm) was used as the feedstock for thermal spraying, (Figure 1). The microhardness of FeTi particles is in average 3.8 ± 1 GPa, and that of SiC particles is 30 GPa.

The phase analysis of the initial powders showed (Figure 2) that the silicon carbide powder has a single-phase structure, and ferrotitanium has a two-phase structure consisting of FeTi and Fe_{0.2}Ti_{0.8} phases.

The MChS process was carried out in a planetary mill (Activator-2S1) at a drum rotation speed

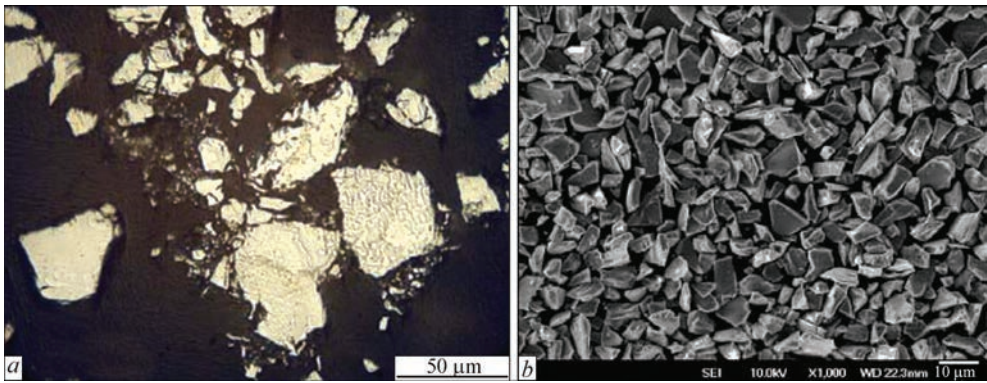


Figure 1. Microstructure of FeTi powder (a) and appearance of SiC powder (b)

of 1500 rpm and a ball mass-to-powder mass ratio of 10:1 in an air environment for 5 h. To eliminate sticking of the processed charge to the grinding bodies and walls of the drum, as well as to intensify the process of synthesis of new phases, a surfactant, oleic acid was added to the mixture ($C_{17}H_{33}COOH$) in the amount of 0.5 wt.%.

Coatings of CP FeTi–SiC were deposited by thermal spraying methods using both subsonic and supersonic high-temperature jets, which differ in the level of kinetic and thermophysical characteristics: subsonic method — plasma spraying (PS) and supersonic method — detonation spraying (DS). Plasma spraying was carried out in the “UPU-8M” installation using a mixture of Ar–N₂ as a plasma-forming gas. The detonation coating was applied in the “Perun-S” installation using a mixture of air–O₂–propane + butane as a combustible gas and with a cycle frequency of 6.6 s^{−1}. The spraying modes are given in Table 1. The technological spraying parameters were selected based on previous studies on spraying coatings using these methods from composite powders produced by the MChS method.

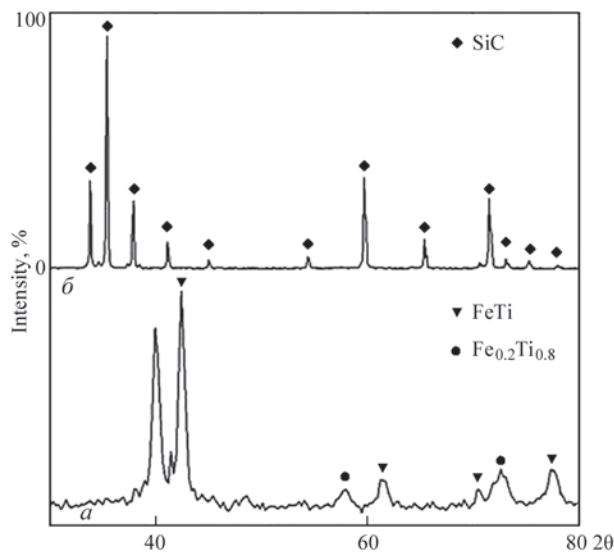


Figure 2. X-ray diffraction patterns of initial powders: a — FeTi; b — SiC

The study of CP and coatings produced from these powders was carried out using a comprehensive methodology that included metallographic, X-ray diffraction (XRD) and microdurotometric analysis (PMT-3 microhardness tester, at an indenter load of 25 g when investigating powder and 50 g for coating study).

X-ray phase analysis (XRD) was performed using a “DRON-3” diffractometer in CuK_α-radiation with a graphite monochromator at a step movement of 0.1° and an exposure time of 4 s at each point with the subsequent computer processing of the obtained digital data. The phase identification was performed using the international ICDD PDF-2 or PDF-4 database. The size of crystallites in the coatings was estimated by the Debye–Scherrer formula:

$$d = \frac{K\lambda}{\beta \cos \theta},$$

where d is the average size of coherent scattering regions (domains, crystallites), which can be lower or equal to the grain size; K is the dimensionless particle shape factor (Scherrer’s constant); λ is the X-ray radiation wavelength; β is the reflex width at half-height (in radians and in units of 2 θ); θ is the diffraction angle (Bragg’s angle).

The porosity of the coatings was determined using the Image-Pro Plus software.

The micromechanical characteristics of the surface of thermal coatings were determined by the microindentation method using a “MICRON-GAMMA” nanoindentometer [19]. The values of the characteris-

Table 1. Spraying modes of FeTi–SiC system coatings

Spraying method	Spraying mode			
	Current, A	Voltage, V	Flow rate of working gases, m ³ /h	Spraying distance, mm
PS	500	50	Ar – 0.7; N ₂ – 0.56	100
DS	–	–	Propane–butane – 0.5; O ₂ – 1.55; Air – 0.65	100

tics were calculated automatically according to ISO 14577-1:2015.

The aim of the studying coatings by the microindentation method was to:

- determine the structural state of plasma and detonation coatings produced from MChS FeTi–SiC powders;
- determine (based on the data on the mechanical properties of coatings) values of criteria that evaluate the behaviour of coatings under wear processes.

RESULTS OF THE STUDY AND THEIR DISCUSSION

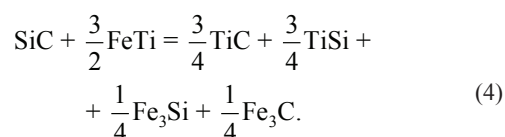
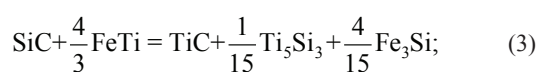
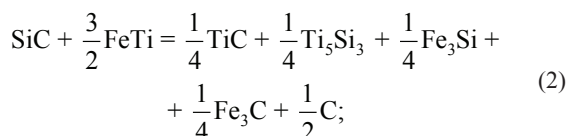
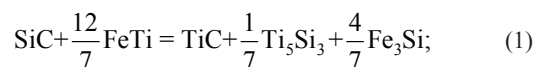
In order to determine the phases that can be obtained in the FeTi–SiC system, the change in the value of the isobaric-isothermal potential (Gibbs energy) ΔG_T^0 was evaluated for the reactions of silicon carbide with simple elements (Ti, Fe). In the TS process, powder particles entering a high-temperature jet are significantly heated and, therefore, thermodynamic calculations were performed in the temperature range of 298–3000 K [14–16]. The following types of interaction were considered in the Ti and Fe–SiC systems (Figures 3, 4):

1. formation of a mixture of carbide and silicide phases of titanium or iron;
2. formation of titanium carbide, iron carbide and precipitation of free silicon;
3. formation of titanium silicides, iron silicides and precipitation of free carbon.

As is seen, for the Ti–SiC system, from a thermodynamic point of view, reaction 1 in the temperature range of 298–2100 K and reaction 2 in the tempera-

ture range of 2100–3000 K are the most favourable (Figure 3). In the Fe–SiC system, reaction 1 in the temperature range of 298–680 K, reaction 2 in the temperature range of 1060–1180 K, and reaction 3 in the temperature ranges of 680–1020 and 1640–3000 K are the most favourable (Figure 4).

Thus, the following reactions are possible in the FeTi–SiC system:



Calculations of the change in the value of the isobaric-isothermal potential showed that reactions 1 and 4 are the most favourable in the FeTi–SiC system from a thermodynamic point of view (Figure 5). At the same time, the content of silicon carbide in the mixture should amount to 21 wt.%. Therefore, a powder mixture of the composition 79FeTi–21SiC (wt.%) was used for the research. The final phase composition of both the MChS product as well as coatings may differ from the calculated one due to the non-equilibrium of

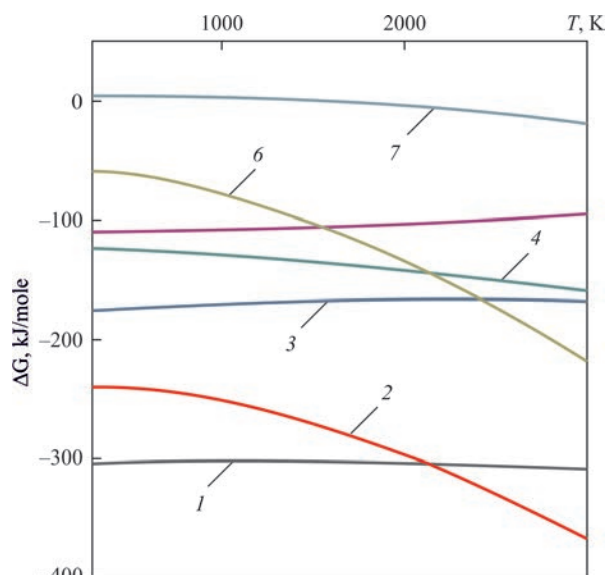


Figure 3. Temperature dependence of the change in the Gibbs energy of the reaction of silicon carbide with Ti: 1 — $\text{SiC} + 8/3\text{Ti} = 1/3\text{Ti}_5\text{Si}_3 + \text{TiC}$; 2 — $\text{SiC} + 2\text{Ti} = \text{TiC} + \text{TiSi}$; 3 — $\text{SiC} + 3/2\text{Ti} = \text{TiC} + 1/2\text{TiSi}_2$; 4 — $\text{SiC} + 5/3\text{Ti} = 1/3\text{Ti}_5\text{Si}_3 + \text{C}$; 5 — $\text{SiC} + \text{Ti} = \text{TiC} + \text{Si}$; 6 — $\text{SiC} + \text{Ti} = \text{TiSi} + \text{C}$; 7 — $\text{SiC} + 1/2\text{Ti} = \text{TiSi}_2 + \text{C}$

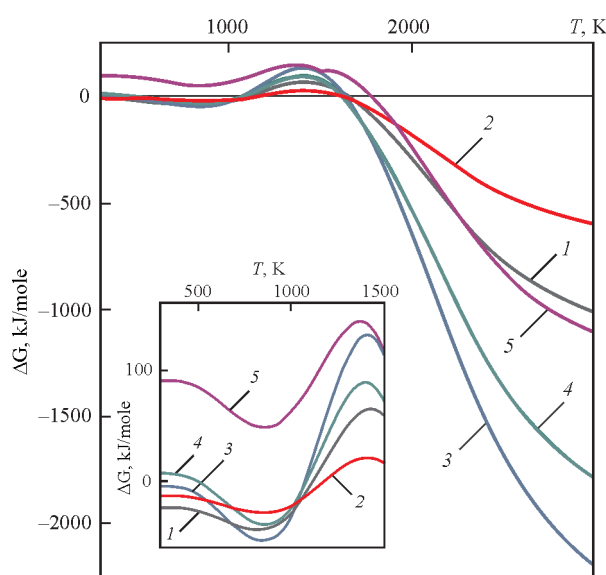


Figure 4. Temperature dependence of the change in the Gibbs energy of the reaction of silicon carbide with Fe: 1 — $\text{SiC} + 3\text{Fe} = \text{Fe}_3\text{Si} + \text{C}$; 2 — $\text{SiC} + 5/3\text{Fe} = 1/3\text{Fe}_5\text{Si}_3 + \text{C}$; 3 — $\text{SiC} + 6\text{Fe} = \text{Fe}_3\text{Si} + \text{Fe}_3\text{C}$; 4 — $\text{SiC} + 14/3\text{Fe} = 1/3\text{Fe}_5\text{Si}_3 + \text{Fe}_3\text{C}$; 5 — $\text{SiC} + 3\text{Fe} = \text{Fe}_3\text{C} + \text{Si}$

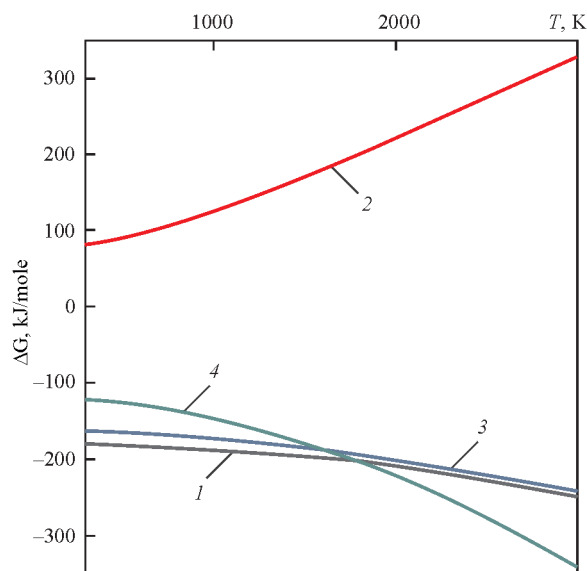


Figure 5. Temperature dependence of the change in the Gibbs energy in the reaction of ferrotitanium with silicon carbide (curve numbers correspond to the numbers of FeTi + SiC reactions)

the MChS and thermal spraying processes (high heating and cooling rates), which affects the completeness of the reactions of the initial components.

During the MChS of the powder mixture 79FeTi + 21SiC (wt.%), the initial components are grinded with their simultaneous mixing, introduction of silicon carbide particles into the volume of ferrotitanium with the further “cold” welding of particles and formation of agglomerates. As a result of MChS, after 5 h of treatment, a composite powder with a heterogeneous fine-dispersed structure with an average particle size of ~12 μm is formed (Figure 6).

The X-ray diffraction pattern of the produced CP (Figure 7) shows that during the MChS process, the X-ray lines broaden with the appearance of “halos” in the range of angles $2\theta = 34\text{--}52^\circ$, indicating a grinding of the crystallite size (up to 30 nm) and partial amorphization of the powder structure. Analysing the phase composition of CP, it should be noted that the X-ray diffraction lines corresponding to the $\text{Fe}_{0.2}\text{Ti}_{0.8}$ phase are absent in the X-ray diffraction pattern and the lines corresponding to the TiC and Ti_5Si_3 phases appear. The absence of diffraction lines of the Fe_3Si compound, the

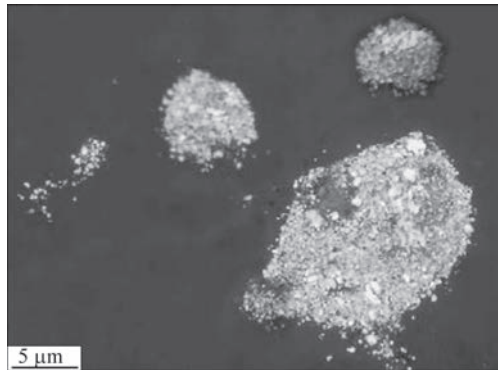


Figure 6. Microstructure of CP FeTi–SiC after 5 h of MChS

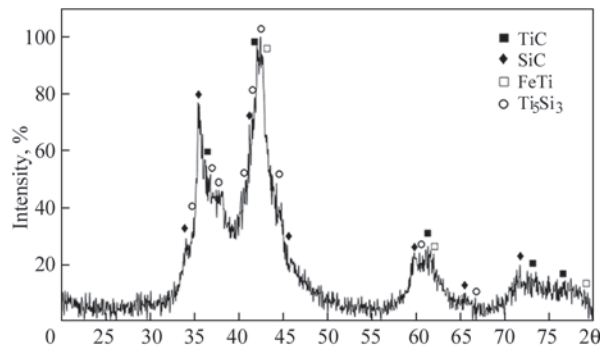


Figure 7. X-ray diffraction pattern of FeTi–SiC powder after 5 h of MChS

formation of which is possible according to equation 1, may be the result of the appearance of an amorphous halo, which complicates its identification. On the other hand, for the mechanically activated self-propagating synthesis in the MChS process, the value of the enthalpy-to-heat capacity ratio ($\Delta H/C_p$) should be greater than 2000 K [17]. Calculations have shown that for TiC, this ratio is 5400 K, for Ti_5Si_3 — 3100 K, and for Fe_3Si — 950 K. Therefore, the formation of iron silicide is thermodynamically less favourable, than the formation of TiC and Ti_5Si_3 compounds.

As a result of the formation of an amorphous nanocrystalline structure consisting of a FeTi matrix with dispersed inclusions of solid SiC, TiC, and Ti_5Si_3 phases, the microhardness of the particles of the produced CP is 8.2 ± 1.6 GPa.

One of the main requirements for the uniform supply of powder to a high-temperature jet during TS is its flowability. As a result of particle size grinding, in the MChS process, the specific surface area of the powder increases, which in turn reduces its flowability [18]. In order to provide flowability and optimize the particle size distribution of CP, before spraying, it was conglomerated with a 5 % aqueous solution of polyvinyl alcohol, followed by grinding and screening of particles, whose size falls in the range of 40–80 μm.

The X-ray diffraction phase analysis (Figure 8) revealed that the phase composition of the sprayed coatings is slightly different from that of CP FeTi–SiC, which indicates structural transformations in the powder particles that occur during the passage of particles through a high-temperature jet and during the formation of the coating layer. The degree of amorphousness of the coatings decreases relative to CP and the size of crystallites increases to 140 and 70 nm for plasma and detonation coatings, respectively. The absence of the SiC phase in the X-ray diffraction patterns also indicates the occurrence of phase transformation processes during spraying. In addition to the TiC and Ti_5Si_3 phases present in the phase composition of CP, phase transformations in the coatings result in the formation of the Fe_2Ti phase instead of FeTi, and in the case of plasma spraying, the Fe_2TiSi Heusler phase

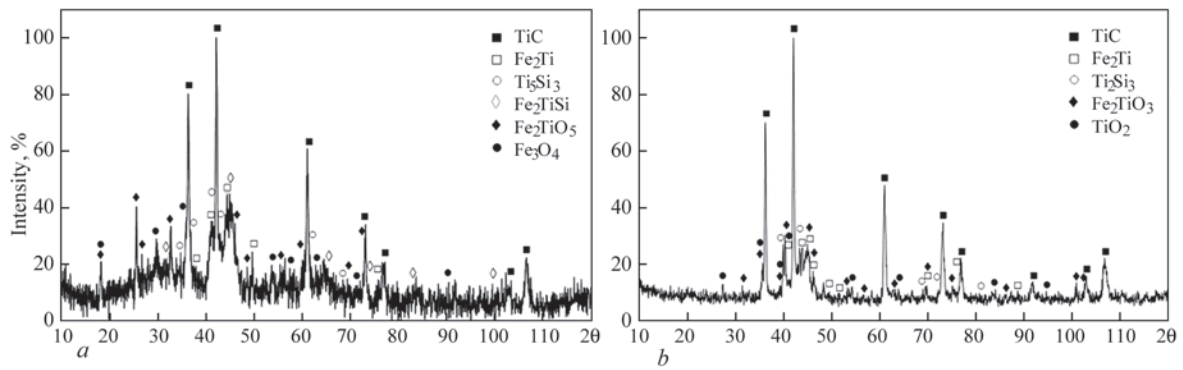


Figure 8. X-ray diffraction patterns of CP FeTi–SiC coatings produced by plasma (a) and detonation (b) spraying

is formed in the coating. During the presence of CP particles in a high-temperature jet, during spraying, they interact with air oxygen and oxidise the CP components, resulting in the formation of oxide phases in the coatings: pseudobrookite Fe_2TiO_5 and iron oxide Fe_3O_4 in the case of plasma spraying (Figure 8, a), ulvospinel Fe_2TiO_4 and titanium oxide TiO_2 in the case of detonation spraying (Figure 8, b).

As a result of plasma spraying, coatings with a heterogeneous structure and distinct structural components are formed (Figure 9, a). Defects in the structure of the plasma coating in the form of discontinuities and chipping of various shapes and sizes were found, the amount of which in the coating is ~ 13 vol. %. The size of defect ranges from 10 to 50 μm and their location across the coating cross-section is uneven. The presence of defects in the coating in the form of discontinuities is a consequence of insufficient thermal and kinetic energy of particles during spraying, which leads to a decrease in the impact consolidation and the degree of deformation of particles during the layer formation, on which the density of the coating depends. The size of defects of up to 50 μm indicates the presence of conglomerate-type particles in the powders after passing through the plasma jet, which are formed as a result of coagulation and fusion of particles of the conglomerated powder. Such particles do not undergo a melting stage and do not deform during the formation of the coating layer, and therefore the particles are not fixed in the coating due to the lack of a strong bond between the sprayed particles. As a

result, coatings with low cohesive strength are formed and defects in the form of chipping are formed in the coatings when producing microsections. It is possible to reduce the probability of such defects in the coating by optimising the process of plasma spraying of the FeTi–SiC composite powder by changing the technological parameters of plasma spraying.

The detonation spraying of CP FeTi–SiC results in the formation of a coating with a thin-lamellar heterogeneous structure. Small amounts of partially deformed particles are present in the coating. The oxides in the coating have the form of thin lamellae, located uniformly across the entire cross-section of the coating. The porosity of the coating is ~ 5 %. The absence of defects in the detonation coating, which are present in plasma coatings, is explained by the higher gas flow rate during the spraying process and, accordingly, the higher velocity of sprayed particles, which can reach ~ 800 m/s, while in plasma spraying, the maximum particle velocity can reach 200 m/s. Therefore, particles in detonation spraying acquire higher kinetic energy, which increases the degree of their deformation during the layer formation, resulting in the formation of dense coatings.

The microhardness of the coatings amounts to 8.5 ± 2.5 GPa in plasma spraying and 8 ± 2 GPa in detonation. The large variation in the measured microhardness values (6–11 GPa for plasma coating and 6–10 GPa for detonation coating) is explained by the heterogeneity of the structure of the coatings, composed of a metal component, carbide, silicide and

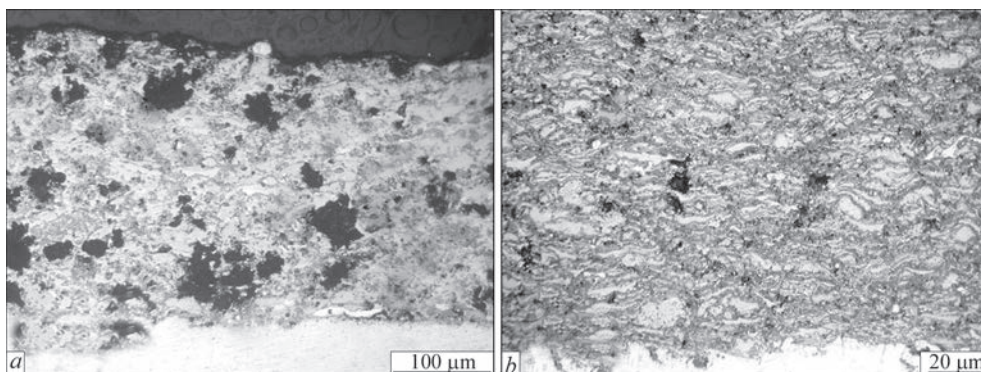


Figure 9. Microstructure of composite FeTi–SiC coatings produced by plasma (a) and detonation (b) spraying

Table 2. Mechanical properties of FeTi–SiC thermal coatings

Spraying method	Mechanical characteristics							
	H_{IT} , GPa	E , GPa	E^* , GPa	ε_{es} , %	σ_{es} , GPa	H_{IT}/E^*	H_{IT}^3/E^{*2}	H_{IT}^2/E^*
PS	6±02	102±2.3	98	1.87	1.84	0.061	0.022	0.37
DS	5.2±0.5	93±10	89.2	1.78	1.65	0.058	0.018	0.32

oxide phases. An increase in the microhardness of the plasma coating relative to CP is associated with the formation of the Fe₂TiSi phase in the coating, the hardness of which can reach from 19 to 30 GPa [20, 21]. A slight decrease in the microhardness of the detonation coating relative to CP is associated with the formation of a significant amount of oxide phases in the coating, which occurs due to the oxidation of powder components during the spraying process.

As a result of the studies carried out by the microindentation method, a number of characteristics of the mechanical properties of the outer layer of plasma and detonation FeTi–SiC coatings were obtained:

- H_{IT} — material hardness at indentation, GPa;
- E — modulus of elasticity, GPa;
- E^* — effective (contact) modulus of elasticity, GPa;
- ε_{es} — relative out-of-contact elastic strain, %;
- σ_{es} — stress of out-of-contact elastic deformation, GPa;
- H_{IT}/E^* — index of transition from elastic deformation to fracture or normalized hardness;
- H_{IT}^3/E^{*2} — index of resistance to plastic deformation;
- H_{IT}^2/E^* — parameter of elastic recovery, i.e. the ability of the material to absorb strain energy.

The results of microindentation of coatings are shown in Table 2.

The analysis of the obtained data shows that according to the main indices of mechanical characteristics, the coating produced by detonation spraying is somewhat inferior to the coating produced by plasma spraying, which is associated with a higher content of oxide components in detonation coatings. It should be noted that the difference in the values of microhardness and hardness obtained by microindentation (nanohardness) is explained by the difference in measurement procedures. The load during microindentation is much lower and therefore the imprints are limited to the area of a single deformed particle and reflect its properties. Whereas the results of microhardness measurement reflect the average value of the coating.

According to the method for evaluating the structural state of a material using the dependence of the hardness value (H_{IT}) on the value of the relative out-of-contact elastic strain (ε_{es}), proposed by the authors of [22], FeTi–SiC coatings produced by both plasma and detonation spraying, belong to the group of microcrystalline materials with a heterophase structure.

According to the indices of H_{IT}/E^* , H_{IT}^2/E^* , H_{IT}^3/E^{*2} , used as criteria for the wear resistance of strengthening coatings [23], the detonation coating is 1.1–1.2 times inferior to the plasma coating. Based on this, it should be expected that under sliding friction conditions, the FeTi–SiC coating produced by plasma spraying will have higher wear resistance than the coating of the same composition produced by detonation spraying.

CONCLUSIONS

On the basis of thermodynamic calculations of reactions between ferrotitanium and silicon carbide, the most favourable reaction in terms of interaction of components was established and the composition of the mixture of powders of the initial components was determined to produce a composite powder by the method of mechanochemical synthesis, at which the content of silicon carbide amounts to 21 wt.%. It was found that in the process of mechanochemical synthesis, a composite powder with an amorphous-nanocrystalline structure is formed, the phase composition of which, due to the non-equilibrium of the MChS process, differs slightly from the calculated one and consists of a FeTi metal matrix with dispersed inclusions of solid SiC, TiC and Ti₅Si₃ phases in it. The microhardness of particles is 8.2 ± 1.6 GPa.

As a result of thermal spraying, coatings with a heterogeneous structure were produced consisting of a Fe₂Ti metal matrix with ceramic inclusions of titanium carbide (TiC) and titanium silicide (Ti₅Si₃) and oxide phases: Fe₂TiO₅ and Fe₃O₄ in the case of plasma spraying, Fe₂TiO₄ and TiO₂ in the case of detonation spraying.

It was found that when using the detonation method of spraying FeTi–SiC powder, denser coatings with a porosity of ~5 % are formed, whereas during plasma spraying, the number of defects in the form of discontinuities and chipping is ~13 %, which is associated with low cohesive strength of the coating. In turn, detonation coatings have somewhat lower values of microhardness and mechanical characteristics (by 1.0–1.2 times).

Using the method of microindentation, it was found that, according to their structural state, the produced coatings of the FeTi–SiC system belong to the group of microcrystalline materials with a heterophase structure in terms of hardness and relative out-of-contact elastic strain, which are H_{IT} = 6 GPa, ε_{es} = 1.87 % for the coatings produced by plasma spraying, and H_{IT} = 5.2 GPa, ε_{es} = 1.78 % for the coatings produced by detonation spraying.

REFERENCES

- Wen, E., Song, R., Cai, C. (2019) Study of the three-body impact abrasive wear behaviour of a low alloy steel reinforced with niobium. *J. of Manufacturing Proc.*, **46**, 185–193. DOI: <https://doi.org/10.1016/j.jmapro.2019.08.026>
- Askari, M., Aliofkhaezai, M., Afrukhteh, S. (2019) A comprehensive review on internal corrosion and cracking of oil and gas pipelines. *J. of Natural Gas Sci. and Eng.*, **71**, 102971. DOI: <https://doi.org/10.1016/j.jngse.2019.102971>
- Dadbakhsh, S., Mertens, R., Hao, L. et al. (2019) Selective laser melting to manufacture “in situ” metal matrix composites: A review. *Adv. Eng. Mater.*, **21**, 1801244. DOI: <https://doi.org/10.1002/adem.201801244>
- Xiao, M., Zhang, Y., Wu, Y. et al. (2021) Preparation, mechanical properties and enhanced wear resistance of TiC–Fe composite cermet coating. *Inter. J. of Refractory Metals and Hard Materials*, **101**, 105672. DOI: <https://doi.org/10.1016/j.jrmhm.2021.105672>
- Wang, B.G., Wang, G.D., Misra, R.D.K. et al. (2021) Increased hot-formability and grain-refinement by dynamic recrystallization of ferrite in an in situ TiB₂ reinforced steel matrix composite. *Mater. Sci. and Eng.: A*, **812**, 141100. DOI: <https://doi.org/10.1016/j.msea.2021.141100>
- Tan, H., Luo, Z., Li, Y. et al. (2015) Effect of strengthening particles on the dry sliding wear behavior of Al₂O₃–M₂C₃/Fe metal matrix composite coatings produced by laser cladding. *Wear*, **324–325**, 36–44. DOI: <https://doi.org/10.1016/j.wear.2014.11.023>
- Chen, H., Lu, Y., Sun, Y. et al. (2020) Coarse TiC particles reinforced H13 steel matrix composites produced by laser cladding. *Surf. and Coat. Technol.*, **395**, 125867. DOI: <https://doi.org/10.1016/j.surfcoat.2020.125867>
- Jam, A., Nikzad, L., Razavi, M. (2017) TiC-based cermet prepared by high-energy ball-milling and reactive spark plasma sintering. *Ceramics Inter.*, **43**(2), 2448–2455. DOI: <https://doi.org/10.1016/j.ceramint.2016.11.039>
- Wang, Z., Lin, T., He, X. et al. (2015) Microstructure and properties of TiC-high manganese steel cermet prepared by different sintering processes. *J. Alloys Compd.*, **650**, 918–924. DOI: <https://doi.org/10.1016/j.jallcom.2015.08.047>
- Bansal, N.P. (2005) *Handbook of ceramic composites*. Springer. DOI: <https://doi.org/10.1007/b104068>
- Wang, S., Ma, C., Walsh, F.C. (2020) Alternative tribological coatings to electrodeposited hard chromium: A critical review. *Transact. of the Institute of Metal Finishing*, **98**(4), 173–185. DOI: <https://doi.org/10.1080/00202967.2020.1776962>
- Kübarsepp, J., Juhani, K. (2020) Cermets with Fe-alloy binder: A review. *Inter. J. of Refractory & Hard Metals*, **92**, 105290. DOI: <https://doi.org/10.1016/j.jrmhm.2020.105290>
- Burlachenko, O., Vihilianska, N., Senderowski, C. (2024) Cermet powders based on TiAl intermetallic for thermal spraying. *Mat. Sci. Forum*, **1113**, 77–85. DOI: <https://doi.org/10.4028/p-7ris3b>
- Samsonov, G.V., Vinitiskij, I.M. (1976) *Refractory joints: Refer. Book*. Moscow, Metallurgiya [in Russian].
- Barin, I. (1995) *Thermochemical data of pure substances*. DOI: <https://doi.org/10.1002/9783527619825>
- Itin, V.I., Najborodenko, Yu.S. (1989) *High-temperature synthesis of intermetallics*. Tomsk, Izd-vo Tomskogo Universiteta [in Russian].
- Solonin, Yu.M. et al. (2021) High-energy mechanical grinding to produce Cr₂AlC and Ti₂AlC max phases. *Powder Metallurgy and Metal Ceramics*, **60**(5–6), 259–267. DOI: <https://doi.org/10.1007/s11106-021-00236-y>
- Borysov Yu.S., Borysova A.L., Burlachenko O.M. et al. (2021) Composite powders based on FeMoNiCrB amorphizing alloy with additives of refractory compounds for thermal spraying of coatings. *The Paton Welding J.* **11**, 38–47. DOI: <https://doi.org/10.37434/tpwj2021.11.07>
- Firstov, S.O., Gorban, V.F., Pechkovsky, E.P. (2010) New methodological opportunities of modern materials mechanical properties definition by the automatic indentation method. *Nauka ta Innovacii*, **6**(5), 7–18. DOI: <https://doi.org/10.15407/scin.6.05.07>
- Mouchou, S. et al. (2023) Temperature dependence of the mechanical properties of Heusler Fe₂TiSi and Fe₂TiSn using the quasi-harmonic approximation. *Computational Condensed Matter*, **37**, e00852. DOI: <https://doi.org/10.1016/j.cocom.2023.e00852>
- Everhart, W., Newkirk, J.W. (2019) Mechanical properties of Heusler alloys. *Heliyon*, **5**, e01578. DOI: <https://doi.org/10.1016/j.heliyon.2019.e01578>
- Firstov, S.A., Gorban, V.F., Pechkovsky, E.P. (2009) New procedure of treatment and analysis of results of automatic indentation of materials. Kyiv, Logos [in Russian].
- Leyland, A., Matthews, A. (2000) On the significance of the H/E ratio in wear control: A nanocomposite coating approach to optimised tribological behaviour, *Wear*, **246**(1–2), 1–11. DOI: [https://doi.org/10.1016/S0043-1648\(00\)00488-9](https://doi.org/10.1016/S0043-1648(00)00488-9)

ORCID

N.V. Vihilianska: 0000-0001-8576-2095,
O.M. Burlachenko: 0000-0001-8576-295,
O.P. Gryshchenko: 0000-0003-2640-8656,
I.O. Koziakov: 0009-0004-1136-996X,
V.F. Gorban: 0000-0001-8887-0104

CONFLICT OF INTEREST

The Authors declare no conflict of interest

CORRESPONDING AUTHOR

N.V. Vihilianska
E.O. Paton Electric Welding Institute of the NASU
11 Kazymyr Malevych Str., 03150, Kyiv, Ukraine.
E-mail: pewinataliya@gmail.com

SUGGESTED CITATION

N.V. Vihilianska, O.M. Burlachenko, O.P. Gryshchenko, I.O. Koziakov, V.F. Gorban (2024) Formation of coatings of the FeTi–SiC system during thermal spraying of powder produced by the method of mechanochemical synthesis. *The Paton Welding J.*, **10**, 19–25. DOI: <https://doi.org/10.37434/tpwj2024.10.03>

JOURNAL HOME PAGE

<https://patonpublishinghouse.com/eng/journals/tpwj>

Received: 26.06.2024

Received in revised form: 01.08.2024

Accepted: 28.10.2024

OBTAINING WEAR-RESISTANT COATINGS BY SURFACING WITH POWDER CORE WELDING WIRE

Z. Mirijanashvili¹, G. Dadianidze¹, O. Tsagareishvili¹, B. Salaridze¹, L. Chkhartishvili^{1,2}

¹F. Tavadze Metallurgy and Materials Science Institute

8b Elizbar Mindeli Str., 0186, Tbilisi, Georgia

²Georgian Technical University

77 Merab Kostava Ave., 0160, Tbilisi, Georgia

ABSTRACT

A modification of hard and wear-resistant coatings fabricating technology by substrates surfacing with powder core welding wire is proposed. Nichrome or steel tapes are used as welding wire shells, while the specially produced $\text{CrB}_2\text{-Al}_2\text{O}_3$ and $(\text{TiCr})\text{B}_2\text{-Al}_2\text{O}_3$ composite powders, as well as commercially available Cr_3C_2 powder, serve for cores. The microstructure of one-, two- and three-layer surface welds reveals the presence of carbide–boride and aluminum oxide phases, which improve their tribological properties.

KEYWORDS: arc surfacing, hard powder, powder core wire, wear resistance

INTRODUCTION

Surfacing with powder core welding wire is known [1, 2] as one of the most effective technologies of coating various substrates. A special attention has been paid [3–6] to the production of powder core wires of new compositions intended for providing wear and corrosion-resistant coatings.

In the present work, for the first time nichrome tape (GOST 12766.2–90, 15×0.5 mm) is used as a powder welding wire shell instead of low-carbon steel-08KP (C 0.05–0.11, Mn 0.25–0.50, Si <0.03, and S and P together <0.04 %) one serving for shell material in standard welding wires with iron-based powder core (GOST 26101–84). Moreover, in order to increase the fabricated coatings hardness and wear resistance, for core there are utilized specially produced $\text{CrB}_2\text{-Al}_2\text{O}_3$ and $(\text{TiCr})\text{B}_2\text{-Al}_2\text{O}_3$ composite powders, in addition to commercial Cr_3C_2 powder.

OBTAINING COMPOSITE POWDERS FOR WELDING WIRE CORE

This technology, which is based on the aluminothermal reduction of a chloride–oxide charge, includes the following stages:

- Mixing the charge in a rotating mixer;
- Briquetting the charge;
- Reduction in argon atmosphere in a shaft-type furnace;
- Wet grinding the sinter in a ball mill; and
- Drying, sieving and packaging of powders.

During the full cycle, the loss of usable powder did not exceed 5 %. By comparing the main kinetic characteristics of the reduction process of metal chloride–oxide charge with aluminum and the results of thermographic and X-ray phase-analysis of the prod-

ucts obtained in this way, the optimal technological parameters for producing refractory compounds reinforced with aluminum oxide are developed and composite powders $\text{CrB}_2\text{-Al}_2\text{O}_3$ and $(\text{TiCr})\text{B}_2\text{-Al}_2\text{O}_3$ useful for welding wire powder core are obtained.

The size of the particles constituting the maximum fraction in these powders ranges from 125 to $100 \mu\text{m}$. And its share does not exceed 5 %. Other relatively important fraction contents are: 100–55, 50–20 and 20–5 μm — 15–20, 35–40 and 30–35 %, respectively. In addition, the particles of reinforcing oxide and carbide phases are practically evenly distributed in the powder sample volume.

By investigating some technological characteristics of powders, it is determined that their true, free bulk and rolling densities range within the intervals of 4.60–4.95, 1.05–1.20 and 1.50–1.65 g/cm^3 , respectively, while fluidity is of 39–42 s.

In order to prevent the cracks formation and improve the welding layer structure, the following powder mixture is added to the charge: rutile 30, calcium fluoride 20–21, ferrovanadium 0.35–0.50, ferrotitanium 0.8–1.0, boron carbide 1.0–1.5, sodium silicide–fluoride 1.5–2.0, marble 11–12, nitrided ferromanganese 0.3–0.5, copper 1.0–1.5, cobalt 1.0–1.5, graphite 1.0–1.5 and of Ce-group rare earth metals fluorides (CeF_3 , LaF_3 , NdF_3 , PrF_3 and YF_3) together 0.5–1.0 %.

The proportion of refractory compounds in the charge was constant, around 30–32 wt.%.

FABRICATING POWDER WELDING WIRES

Powder core wires are made from above listed powder materials. The scheme of this technology is presented in Figure 1. A general view of the laboratory equipment used for this purpose and coil of a powder welding wire made in this way is shown in Figure 2.

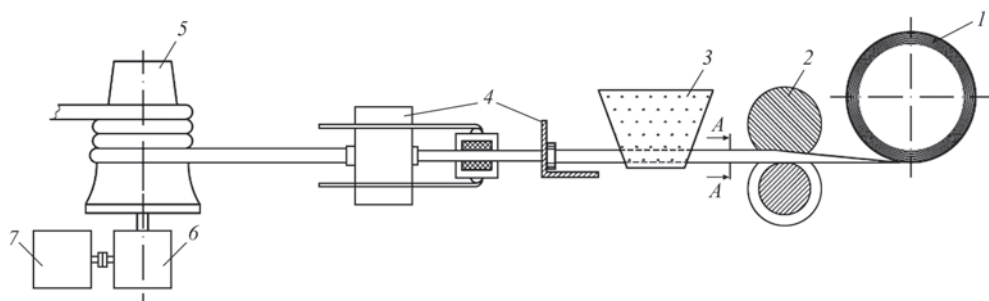


Figure 1. Schematic of powder core wire fabrication: 1 — tape coil; 2 — bending rollers; 3 — powder hopper; 4 — dies; 5 — coiler drum; 6 — reducer; 7 — electric motor

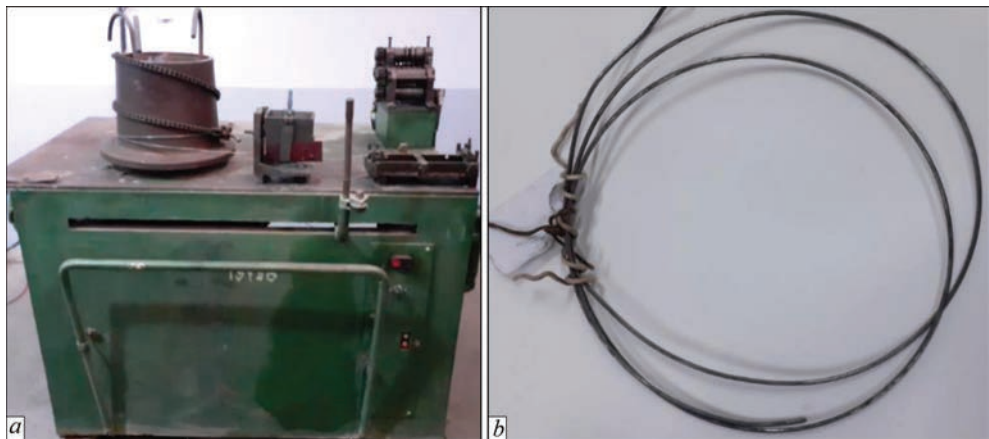


Figure 2. Powder core wire fabrication laboratory setup (a) and fabricated powder core wire (b)

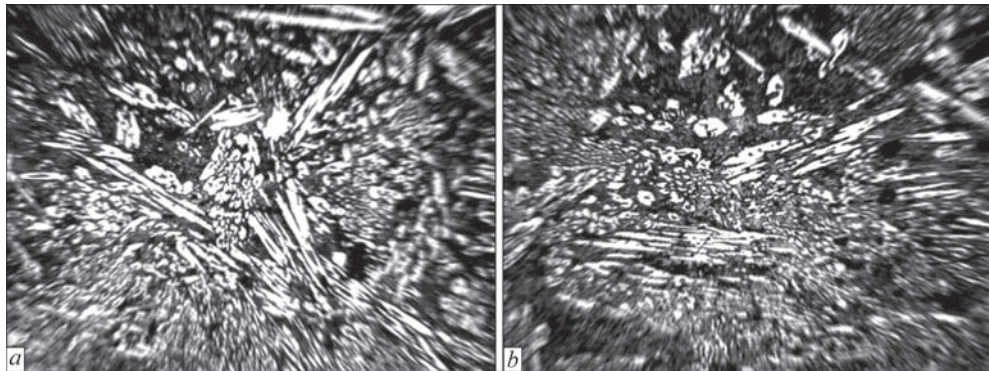


Figure 3. Microstructure of samples (a) and (b) with one-layer weld at ×100 magnification

Powder core wire welds are obtained in argon atmosphere on the steel-20 surface in one, two and three layers. The thickness of each layer is of 1.0–1.3 mm. By measuring the hardness and microhardness of the welding layer (Table 1), it was determined that the best result of the tested samples is given by the powder core wire with nichrome shell. When using steel-08KP as shell, formation of microcracks is noticed.

By metallographic study (Figures 3–5) it is determined that high hardness might be caused by carbide, boride and aluminum oxide inclusions, which has a positive effect on the coatings tribological properties. The hardness and microhardness values analyzes shows that the three-layer weld characteristics are higher than those of one- or two-layer welds.

Based on the microstructural analysis of one-layer weld, the different regions of the welded zone are

significantly different from each other. Carbide inclusions are fixed in all weld layers, however, in different shapes, sizes and relative positions. Carbide inclusions are large and elongated in shape and vary in size. Along with large carbide inclusions, relatively finer randomly oriented inclusions can be seen.

Hardness of one-, two- and three-layer welds are estimated as: 3.33, 5.64 and 6.38 GPa, respectively. In this way, the increase in the number of layers leads to a significant increase in microhardness, which in turn significantly changes tribological properties of the material.

Table 1. Typical values of hardness and microhardness measured at one-, two- and three-layer welds

Number of welded layers	1	2	3
Hardness, <i>HRC</i>	44.5	48.5	59.0
Microhardness, GPa	7.43	8.53	11.26

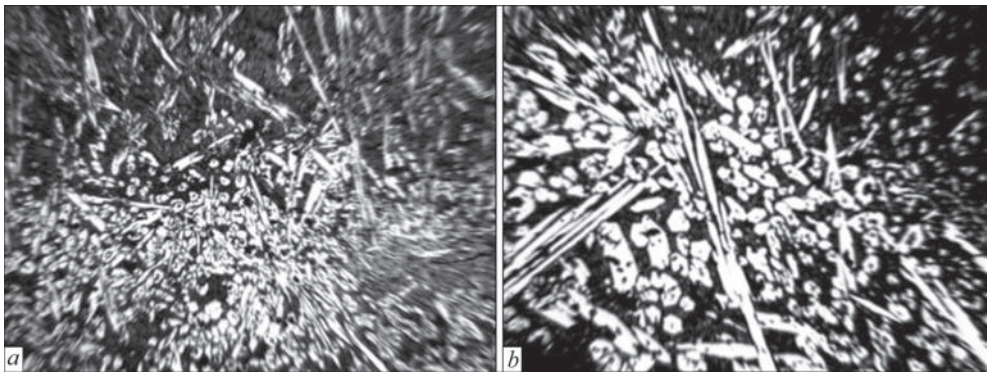


Figure 4. Microstructure of samples (a) and (b) with two-layer weld at $\times 100$ magnification

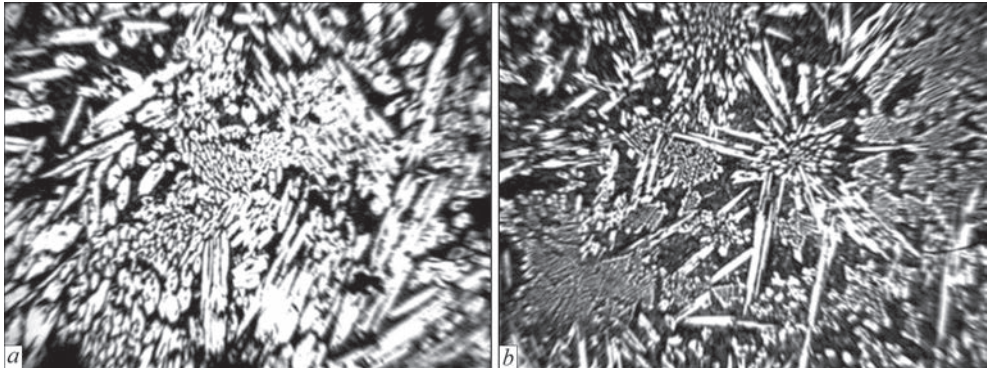


Figure 5. Microstructure of samples (a) and (b) with three-layer weld at $\times 100$ magnification



Figure 6. Inverter welding machine TIG/MMA-320 (a) and argon-arc welding process on universal welding rectifier VDU-506 (b)

The described structures were obtained by welding using powder core wires with shells made of nichrome.

TRIBOLOGICAL CHARACTERIZATION OF OBTAINED COATINGS

To evaluate the tribological properties of coatings fabricated by powder core wire welding, there are selected samples obtained with:

- Nichrome tape shell and Cr_3C_2 core;
- Steel-08KP tape and Cr_3C_2 core;
- Steel-08KP tape and CrB_2 core; and
- Steel-08KP tape and $(\text{TiCr})\text{B}_2$ core.

The surface of steel-20 samples were welded with powder core wires by argon-arc method (Figure 6) on the TIG/MMA-320 inventory welding machine (Georgian Technical University).

The powder core wires, shell of which is steel-08KP, and the powder core is made of $\text{CrB}_2\text{-Al}_2\text{O}_3$ or $(\text{TiCr})\text{B}_2\text{-Al}_2\text{O}_3$, practically do not differ from each other in the technological parameters of welding. At relatively low currents, up to 120 A, the quality of welding is poor, and above 140 A, the quality of welding is of average quality or sharply worsens, which is caused by overheating of the weld metal and an increase in the depth of welding.

The microstructure of the three-layer welded sample is characterized by carbide liquefaction zones. The white areas with microhardness of 7.28 GPa shown in Figure 5 belong to the carbide phase. The dark areas correspond to the structure of the base metal, which initially is in the ferritopearlite state, but in the welding zone it is not excluded that it is alloyed. Its micro-

hardness is of 5.12 GPa. One thing is worth noting: when approaching the border of the base metal from the center of the carbide inclusions, the value of microhardness decreases from 11.08 to 7.28 GPa.

The wear-resistant test of the steel-20 surface coated with powder core electrodes is conducted under dry friction conditions on the friction machine SMC-2 and at constant number of rotations: 1000 rpm. The loading force is of 25, 50 or 100 N. A roller made of tempered steel-U8 with diameter of 40 mm and hardness of 64 HRC is taken as a counterbody. The friction coefficient f and the wear mass loss of the samples are determined. During the tests to find the coefficient of friction, the values of loading force F acting on sample, moment of friction M and counterbody diameter d are recorded. The coefficient of friction is calculated by the formula: $f = 2M/Fd$. The wear resistance of the samples is assessed by the weight loss of the samples under dry friction conditions.

The wear resistance of welds made with powder core wires is studied on samples with one-, two- and three-layer coatings, when the used powder core wire is made of steel-08KP tape and powders $\text{CrB}_2\text{-Al}_2\text{O}_3$ or $(\text{TiCr})\text{B}_2\text{-Al}_2\text{O}_3$. For these coatings, there are studied the relationship between the sliding distance and the friction coefficient. For layers welded with powder core wires (steel-08KP shell and Cr_3C_2 or $\text{CrB}_2\text{-Al}_2\text{O}_3$ and $(\text{TiCr})\text{B}_2\text{-Al}_2\text{O}_3$ core) on steel-20 under Ar pressure, it is determined that the friction coefficient is almost equal after passing different distance of 1200 to 1400 m. The surface of the welded sample is stable and therefore does not significantly affect the wear resistance. However, after passing a distance from 1200 to 1350 m, it experiences a slight fall in a certain section, which affects the mass weight loss, however does not significantly affect the wear resistance.

As mentioned above, metallographic studies and hardness measurements revealed that high hardness is caused by inclusions of carbide, boride and aluminum oxides, which positively affects the tribological properties of coatings obtained in this way.

Compared with samples welded with nichrome tape wires, in structures obtained using powder core wires with 08KP steel shells, the corrosion resistance of the coating decreases, but its wear resistance increases by 20 %.

CONCLUSIONS

In the present work, nichrome tape was used for the first time as a shell of powder core wire. In order to increase

the formed coatings hardness and wear resistance, specially produced $\text{CrB}_2\text{-Al}_2\text{O}_3$ or $(\text{TiCr})\text{B}_2\text{-Al}_2\text{O}_3$ or commercial Cr_3C_2 powders, whose mass fraction was about 30 %, were used as cores of powder welding wire. In these powders, particles of reinforcing and strengthening oxide (aluminum oxide) and boride (chromium and titanium-chromium diborides) phases are evenly distributed in the volume. The microstructure of one-, two- and three-layer welds indicates the presence of inclusions of carbide-boride and aluminum oxide phases, which positively affects their tribological properties.

REFERENCES

1. Sheinman, E.L. (2005) Abrasive wear. Review. *Friction & Wear*, 26(1), 100–111.
2. Gordeziani, A. (2013) *Electrophysical technologies for metal processing and strengthening*. Tbilisi, Tech. Univ. Press.
3. Gusev, A.I., Usol'tsev, A.A., Kozyrev, N.A. et al. (2018) Flux-cored wire for the surfacing of parts subject to wear. *Steel Transl.*, 48(11), 724–731.
4. Mirijanashvili, Z., Khutsishvili, M., Dadianidze, G., Saralidze, B. (2020) Development of new wear-resistant welding material. In: *Proc. of Inter. Sci. Tech. Conf. on Environ. Protec. Sustain. Develop.*, Tbilisi, Tech. Univ. Press, 31–36.
5. Junsheng, M., Xiaoping, Sh., Shaojun, Zh. et al. (2021) *Powder-cored welding wire, preparation method and application thereof, porous coating and preparation method thereof*. Pat. CN 110819931 B, October 12.
6. Hanguang, F., Xianwu, L., Haiyun, N. et al. (2023) *High-boron iron-based alloy wear-resistant welding wire and using method thereof*. Pat. CN 113878262 B, March 21.

ORCID

L. Chkhartishvili: 0000-0003-3926-4524

CONFLICT OF INTEREST

The Authors declare no conflict of interest

CORRESPONDING AUTHOR

L. Chkhartishvili

Georgian Technical University

77 Merab Kostava Ave., 0160, Tbilisi, Georgia

E-mail: levanchkhartishvili@gtu.ge

SUGGESTED CITATION

Z. Mirijanashvili, G. Dadianidze, O. Tsagareishvili, B. Salaridze, L. Chkhartishvili (2024) Obtaining wear-resistant coatings by surfacing with powder core welding wires. *The Paton Welding J.*, 10, 26–29.

DOI: <https://doi.org/10.37434/tpwj2024.10.04>

JOURNAL HOME PAGE

<https://patonpublishinghouse.com/eng/journals/tpwj>

Received: 12.08.2024

Received in revised form: 12.09.2024

Accepted: 21.10.2024

USING THE HEREDITY EFFECT FOR CONTROL OF THE STRUCTURE OF THE DEPOSITED METAL DURING ELECTRIC ARC SURFACING WITH FLUX-CORED WIRES (Review)

A.A. Babinets

E.O. Paton Electric Welding Institute of the NASU
11 Kazymyr Malevych Str., 03150, Kyiv, Ukraine

ABSTRACT

Modern views on the relationship between structure and properties in steels and alloys are considered. It is shown that a promising method of influencing the structure and properties of the deposited metal is the use of the heredity effect — the transfer of properties from the initial charge materials to the finished products. A detailed classification of the types of heredity is given according to its manifestations in steels and alloys, which can be divided into three main interrelated groups — metallurgical, structural and technological. It is shown that from the point of view of the influence of initial materials on the structure and properties of finished parts, heredity can be considered both positive and negative. The main factors affecting the degree of manifestation of the effect of structural heredity in steels and alloys are defined and described. Such factors include: chemical composition and degree of doping with chemical elements; degree of defectiveness of the initial structure; size, shape and structure of the initial charge materials; use of modifying additives or external physical influences. The main problems and prospects of using the heredity effect in electric arc surfacing are described. The main directions that will allow controlling the structure and properties of the deposited metal by influencing the degree of manifestation of the heredity effect in it have been determined. The most promising are methods of control by changing the initial parameters of surfacing materials, as well as by means of regulation of heat input due to technological or physical influences. The use of the heredity effect in various surfacing methods can provide a significant impact due to producing the optimal structure of the deposited metal and the absence of harmful impurities in it.

KEYWORDS: electric arc surfacing, deposited metal, flux-cored wire, heredity, structure, operational properties

INTRODUCTION

The main task to be solved at wear-resistant electric arc surfacing is development of such materials and technologies, which will provide the specified chemical composition, structure, high quality and other necessary properties of the deposited metal. Taking into account the operating conditions of specific parts, this is most often achieved through complex alloying of the deposited metal by such elements as Cr, Mo, W, V, Ti, which are added in the form of ferroalloys or other components to the composition of the charge of electrode or filler surfacing materials [1, 2]. Today, however, the technical and economic possibilities for improvement of the deposited metal properties due to such an approach have been practically exhausted.

The structure and properties of the deposited metal can be also controlled by different physical, chemical and technological actions, for instance by its modification and alloying [3]. However, the influence of modifying and microalloying elements is rather complicated, particularly at application of complex additives. They can simultaneously promote improvement of certain properties of the deposited metal, and form undesirable inclusions, which can become the nuclei of cracks or other defects.

It is known that the metal structure and properties can be controlled due to the effect of structural heredity, i.e. the transfer and preservation of the structure (for instance, fine-grained) from the initial charge materials to the finished part structure, leading to an increase of their operational properties [4].

Such an approach is used, for instance, in metallurgical production. On the other hand, the effect of structural heredity is almost not used in surfacing (welding) production. When studying the regularities of formation and change of the deposited metal structure, the attention is usually focused on the influence of alloying element content and surfacing thermal cycle on them. The influence of the initial structure of electrode or filler materials on the deposited metal structure is almost unstudied. At the same time, such a connection certainly exists in the “initial surfacing material – weld pool – deposited metal” system [4, 5].

The main problems of application of structural heredity effect at different surfacing methods, first of all the arc, are apparently associated with the special features of these methods and distinguish them from metallurgical processes [4]:

- deposited metal crystallization occurs on a solid substrate, which is partially remelted, and, hence, its

initial chemical composition and structure influence the deposited metal structure and properties;

- unlike a metallurgical furnace the temperature-time parameters of the weld pool are not stationary; they may also differ at application of different surfacing methods, and are rather difficult to control.

At the same time, application of some technological measures to control the structural heredity effect at arc and plasma surfacing methods are known [4–6], which resulted in improvement of the deposited metal structure and properties.

THE OBJECTIVE OF THE WORK

is analysis of the features of the heredity effect (i.e. preservation of primary object features in the secondary objects) in steels and alloys; factors, influencing it, as well as determination of the prospects for and ways of using this effect at arc surfacing of parts to optimize their structure and operational properties.

BASIC CONCEPTS ABOUT THE CONNECTION BETWEEN THE STRUCTURE AND PROPERTIES AND HEREDITY EFFECT IN STEELS AND ALLOYS

It is widely known that the properties of steels and alloys are determined by their structure and features of structure change under the impact of external physical, chemical or technological factors, to which also such high-temperature processing methods as surfacing (welding) certainly belong [1–6]. In the general case it is assumed that a finer structure of steel or alloy ensures better properties (physical, mechanical, technological, service, etc.) of the finished parts.

The “heredity” term for metals and alloys is usually used to describe the phenomenon at which the shape of any elements of the metal structure is preserved after direct (at cooling) and reverse (at heating) polymorphous transformation. The heredity of the crystallographic orientation is ensured by ordering of rearrangement of one lattice into another one, and restoration of the grain shape is provided by preservation of chemical heterogeneity (segregation of impurities and inclusions along the old grain boundaries) [7].

In metallurgy the positive or negative influence of the initial charge materials on the melt structure, and through it also on the structure and physico-mechanical properties of solid metal, was called “metallurgical heredity”. Its manifestations are associated with preservation in the melt of nonmetallic phases, gases, impurities and elements of the crystalline structure of initial metal, due to technological background of production, preparation, melting, deoxidation and crystallization of the charge metal [7–13].

Proceeding from different views on the processes associated with the heredity phenomenon, it can be classified in different ways. In keeping with [13], heredity is the totality of many processes, among which the following physical phenomena can be singled out in particular:

- deformational heredity, which is characterized by incomplete recovery of the properties of deformed and recrystallized metal. Deformational heredity depends on the nature of the metal and is manifested irrespective of the presence of polymorphous transformation;

- phase heredity, which is determined by crystallographic correspondence of the dislocation structures of the phases at polymorphous transformation and is the base for thermomechanical treatment of the alloys from metals, which undergo a polymorphous transformation (for instance, iron). This phenomenon is also responsible for defect accumulation at thermal cycling;

- boundary heredity, which is associated with incomplete healing of defects in regions, corresponding to old grain boundaries after migration of the latter. This kind of heredity is very resistant (sometimes it is not relieved at heating to premelting temperatures), and it strongly depends on the influence of impurities, included into the solid solution and precipitating in the form of phases.

In [14–17] the authors give another classification of heredity, based on manifestations of the characteristic features at manufacture of parts from steels and alloys. In keeping with this classification, heredity can be divided into three main interrelated groups: metallurgical, structural and technological:

1. Metallurgical heredity is the ability of the cast metal to preserve the structural features and properties of the initial charge materials and liquid metal. It is due primarily to the chemical composition, charge quality, state of the melt and its treatment conditions (temperature, mixing, flux treatment, deoxidation, modification, etc.). At each production stage, certain structural elements appear in the melt, which have hereditary characteristics of cast metal properties at this stage.

2. Structural heredity is observed in those cases, when at close chemical composition, content of impurities and nonmetallic inclusions of initial materials and approximately the same conditions of melt cooling the solidified metal has different micro- and macrostructure. This is attributable to preservation in the metal after the phase or structural transformation, of certain features of its initial structure at different levels (macroscopic, micro- and submicroscopic). One of the kinds of structural heredity after the phase or

structural transformation is presence of chemical heterogeneity in the steel, which is manifested in preservation of segregation areas, forming at melt crystallization.

At first, the structural heredity was understood only as regeneration of coarse grains in the preheated steel. Modern concepts about structural heredity are not limited by pure restoration of the grain size at heat treatment. Structural heredity is manifested both in the form of restoration of grain dimensions and in the form of preservation of their orientation, or modification of the grain boundary, according to the initial structure [15, 16]. It may be accompanied by decomposition of the characteristic structural elements and preservation of the initial coarse-grained structure that is particularly important for the processes of high-temperature treatment, as it may lead to lowering of the mechanical properties of the deposited metal.

3. Technological heredity associated with preservation of special features of the structure of the initial components during the next operations of part manufacture. It is due to the influence of diverse technological factors. Forming of certain characteristics of technological heredity occurs at all the stages of melting, crystallization, deformation, deformation-heat, heat treatment, etc. In the opinion of the author of [17], in the majority of the cases these are exactly the technological factors which are responsible for forming of the structural features and manifestations of the metallurgical and structural heredity in steels and alloys.

The influence of material preparation and technological parameters of surfacing on the quality of the manufactured parts apparently can be an example of technological heredity at surfacing: monitoring the content of gases, nonmetallic inclusions, impurities in the deposited materials; controlling the heat input and crystallization conditions; use of additional external treatment of the molten metal pool, etc. [4].

In view of the influence of initial materials on the structure and properties of finished products, heredity can be regarded both as positive and negative. Transfer of the initial material fine-grained structure to the deposited metal structure or its certain modification that leads to an improvement of the part operational properties can be as example of the positive influence. For instance, in [18] an example of positive heredity is formation in the overheated coarse-grained steel of primary boundaries of austenite grains of a complex (serrated) shape, which were inherited from the initial fine-grained metal structure. Producing such a complex grain shape due to the structural heredity effect, increases the steel crack resistance, as well as its strength characteristics. Another example of positive

heredity is improvement of the degree of steel sheet protection from local impact loads of a considerable intensity as a result of hereditary thermomechanical strengthening which consists in inheriting the dislocation substructure, formed during previous high-temperature deformation, by austenite newly formed in case of heating, and also by martensite at further quenching [19].

Negative heredity can be manifested, contrarily, in preservation or restoration of the coarse-grained initial structure of source materials, preservation of the content of impurities, etc., that may impair the properties of the produced deposited metal and requires taking of additional technological measures [9]. Conditionally the simplest method to remove the negative structural heredity which is manifested as preservation of the coarse-grained structure, is conducting heat treatment [20]. For instance, in [21, 22] it is shown that in medium manganese steels, the heredity effect can be manifested, depending on heat treatment mode, resulting in formation of coarse ferrite grains in metal layers with a low manganese content, leading to lowering of steel ductility, because of crack propagation along the interface of the coarse- and fine-grained regions. After heat treatment of such steel at a sufficiently high temperature cementite can dissolve, forming ultra-fine uniformly distributed austenite grains, thus increasing the steel ductility.

However, in some cases the manifestations of negative heredity cannot be completely removed by heat treatment. In [23] the case of structural heredity in cast steel of 30Kh2N4MF type was studied. It was determined that after preliminary high-temperature tempering fine grains form in steel at heating, which at reheating to 1050–1150 °C is replaced by coarse grains, coinciding by their size, shape and crystallographic orientation with the initial cast austenite grains. This restoration is attributable to nucleating orienting impact of residual austenite, which did not decompose at high-temperature tempering and was preserved at reheating to critical range temperatures.

In metallurgy the negative heredity is most often eliminated due to application of different methods, such as preparation and selection of the charge component ratio; optimal selection of melting and pouring technologies; metal refining due to melt vacuumizing; electroslog remelting, electromagnetic stirring, treatment by ultrasound or electric current, electrohydropulse treatment, alloying, modification, etc. [7, 14, 24].

Application of the majority of the abovementioned methods involves certain difficulties, primarily, economic. Expensive equipment, high energy costs, problems of fitting into the available technological processes complicate application of these methods

of melt treatment in metallurgical production. Application of the majority of the above-listed methods of removing the negative heredity in arc surfacing methods is significantly complicated.

Thus, heredity is not just a peculiarity of transformation in real crystalline alloys, which is manifested in the form of inheriting of the initial structure shape and dimensions by the final structure, which can be revealed by metallographic methods [13]. Heredity in steels and alloys is a totality of many phenomena, leading to preservation in them of the special features of the structure, phase-structural state and properties of the initial material after various technological impacts, which result in the respective structural and phase transformations [14–17]. Such a definition is based on the concept of realization of the possibilities of forming certain hereditary characteristics (structural features) in steels and alloys at all the stages of the technological process of part manufacturing, also by the methods of arc surfacing.

MAIN FACTORS INFLUENCING THE EFFECT OF STRUCTURAL HEREDITY IN STEELS AND ALLOYS

Chemical composition and degree of alloying by chemical elements are the important factors, determining the degree of manifestation of structural heredity, depending on which the steels can be divided into several groups (see Table 1), where “+” symbol denotes the manifestation of structural heredity, and “–” mean its absence [9].

For manifestation of structural heredity, carbon content in the steel should not be lower than 0.2 %. Here, the higher is the steel alloyed by such carbide-forming elements as Cr, Mo, W, V, Ti, the wider the temperature range, in which the structural heredity forms. Alloying influences the critical heating rate, at which grain size restoration can take place. For instance, structural heredity is readily manifested in structural alloyed and high-alloyed steels (high-speed, maraging, corrosion-resistant, etc.) and here it little depends on the heating rate. For low-carbon low-alloyed steels with regular ferrite-pearlite structure the possibility of formation of structural heredity is practically excluded [9]. Lowering of carbon content from 0.08 to 0.008 % prevents restoration of the initial austenite grains even at very rapid heating [16].

Influence of the heating rate on the process of grain formation at heating and cooling of steel with the ordered structure is given in Figure 1 [9]. At rapid heating (100–200 °C/min) of the quenched and untempered steel a special crystallographically ordered mechanism of austenite formation is realized, resulting in restoration of the initial structure grains. As the

Table 1. Influence of steel type and heating rate on structural heredity [9]

Steel type	Heating rate		
	High	Moderate	Slow
Low-carbon low-alloyed	–	–	–
Alloyed	+	–	+
High-alloyed	+	+	+

heating rate is reduced, the processes of tempering and normal diffusion-controlled mechanism of austenite formation, accompanied by grain refinement, develop. At intermediate heating rates (100–150 °C/min), when complete martensite decomposition has enough time to take place before the start of $\alpha \rightarrow \gamma$ -transition, the structural heredity of steel is not manifested. Here $\alpha \rightarrow \gamma$ -transition coincides with recrystallization, and fine grains form at once, i.e. the normal unordered recrystallization mechanism is implemented. At rather slow heating (1–2 °C/min) of many steel austenite also forms by the crystallographically ordered mechanism, resulting in restoration of the initial structure grains at such heating, i.e. the structural heredity is strongly expressed.

Initial structure defects and other structural features of steels and alloys certainly influence the occurrence of the heredity effect, but these dependencies are insufficiently studied. It is known that relative to initial structure defects heredity depends on the nature of initial defectiveness, particularly, of dislocation structure, as well as on the composition and conditions of steel or alloy heat treatment [13, 16]. The heredity effect grows and is preserved to higher temperature values at heating, if the grain boundaries

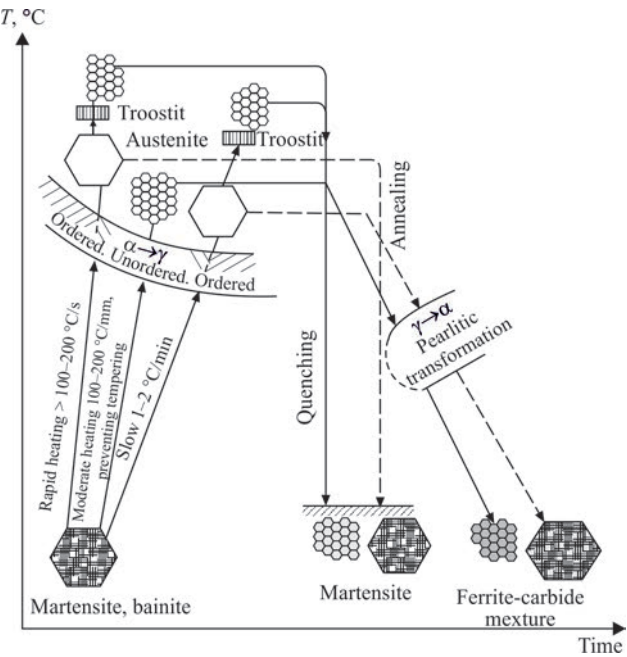


Figure 1. Scheme of recrystallization of steel with initial ordered structure at heating and cooling [9]

are preliminarily enriched in additives. This effect is greater, the more the additives differs from the matrix by its properties and the stronger is their interaction. This is confirmed by the data of [25], where the influence of charge material structure on the properties of cast iron melts was studied, and where it was determined that microadditives not only enhance the energy inequality of different interatomic interactions, but also lead to appearance of noticeable structural features in the solid state.

In metallurgical production the considerable influence of admixtures in the charge on the structure and properties of the finished products is the subject of many papers. Application of a low-grade charge leads to melt contamination by impurities, usually uncontrolled, which noticeably influence the nature of metal solidification. Some of these impurities are resistant and influence structure formation not only during blast furnace smelting, but also during subsequent remelting operations, with manifestation of the heredity effect [9]. By the data of [26] the peculiarities of intercrystalline boundary structure in steels and alloys also are very important for manifestation of the heredity effect.

Application of modifiers can also influence the degree of manifestation of structural heredity in steels and alloys, for instance, enhancing the grain refinement effect. As was noted above, one of the methods of manufacturing products from steels and alloys with a more homogeneous fine-grained structure is application of their modification technologies. The essence of the process consists in introducing special additives (modifiers) into the liquid metal, which initiate the process of heterogeneous formation of a large number of crystallization nuclei (modifiers of the 1st kind), or surface-active additives, which slow down the increase of solid-phase grain size during melt crystallization (modifiers of the 2nd kind).

In keeping with the data of technical literature, not only chemical elements or compounds, but also materials, which were prepared accordingly, i.e. their initial properties were modified, can be such modifiers. For instance, it is possible to use as modifying additives the materials of the same chemical composition, but with a highly-dispersed structure and improved mechanical properties, which were produced due to high-rate crystallization [14, 27, 28]. So, investigations of the influence of such modifiers revealed an essential increase of the dispersity and homogeneity of the cast structure, mechanical properties and brittle fracture resistance of carbon steels with different carbon content as a result of hereditary modification [27].

Similar results were obtained in [28], where the possibility of purposeful increase of the dispersity of

the cast structure of steel at introducing additives of analogous composition dispersion-structured by rapid crystallization into the melt was demonstrated in the case of 45L and R6M5L steels. Such additives preserve in the melt the incorporated in them hereditary features (short-range order), lead to formation of a significant number of crystallization nuclei and ensure formation of a homogeneous fine-grained structure over the entire cross-section of the castings (Figure 2). For R6M5L steel the grain size is decreased by 4–5 numbers, compared to initial values. Hereditary modification performed in such a way, is sufficiently controllable and versatile with rather long-term technological viability.

Thus, incorporating the necessary hereditary elements in the initial charge components and specially structured modifiers opens up the possibility of actively influencing the structure and properties of steels and alloys.

The size (granulometric composition) and shape of the initial surfacing materials also influence the metal final structure. In terms of refinement of its microstructure, a promising approach seems to be introducing into the liquid metal the additives of fine-, micro- or nanosized charge materials, which obviously, can enhance the effect of heredity, similar to the effect of chemical elements-modifiers [29]. For instance, in keeping with the data of [11], one of the most probable factors influencing the manifestation of structural heredity, is the initial size of graphite inclusions, on which the degree of their dissolution in the melt depends.

At present, only some publications are available, which are devoted to the problem of heredity in surfacing production. The majority of the works, where attention is paid to the processes at the stage of formation of the initial powder materials and influence of their particle shape and size on the final mechanical properties of the produced steels and alloys, pertain to metallurgical production. Somewhat generally it can be considered that the smaller are the charge initial dimensions, the finer will be the metal structure and the higher its operational properties [30].

For the surfacing (welding) production valid is the statement that the size of charge material powder particles in electrode or filler wires should meet certain requirements as to granulation. It affects such characteristics as friability, flowability, etc. of the charge, which determine the dozing quality and homogeneity at wire filling and, hence, influence the surfacing process stability and deposited metal quality. From practical experience it is known that in terms of improvement of the homogeneity of flux-cored wire charge, presence of a dust-like fraction with <50 μm particle

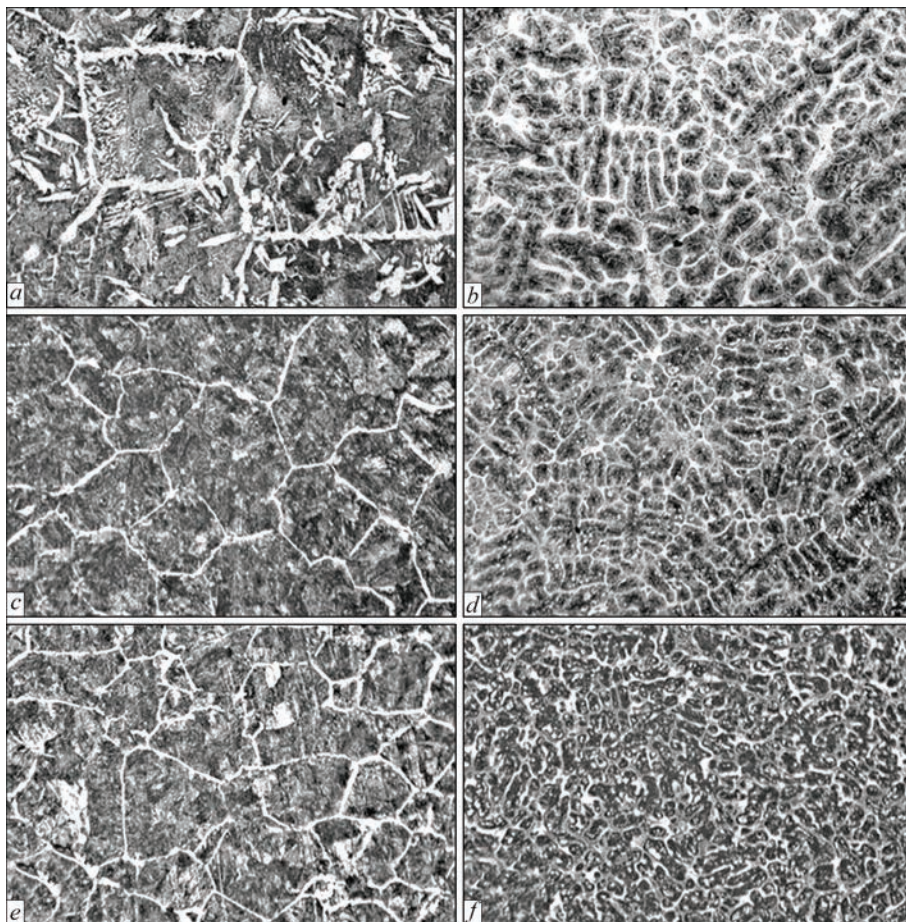


Figure 2. Transformation of the structure of 45L (*a, c, e*) and R6M5L steels (*b, d, f*), depending on dispersity of the modifying additive structure in the quantity of 20 % [28]: *a, b* — without additives; *c, d* — $V_{\text{cool}} = 350 \text{ }^{\circ}\text{C/s}$; *e* — $V_{\text{cool}} = 650 \text{ }^{\circ}\text{C/s}$ ($\times 100$)

size and of coarse particles of more than $300 \text{ }\mu\text{m}$ size is undesirable in powder materials used for flux-cored wire manufacture.

At the same time, there are practically no data on the influence of the size of initial charge material particles on the size of the produced final structure of the deposited metal. It may be related, primarily, to the high temperature in the melting zone. It is common knowledge that for arc surfacing methods the temperature in the arc column, through which the molten metal drop passes, can reach $6000\text{--}8000 \text{ }^{\circ}\text{C}$. Here, the temperature of the drop proper reaches $2150\text{--}2350 \text{ }^{\circ}\text{C}$ [1, 2]. It is obvious that under such conditions the majority of hereditary characteristics inherent to the initial charge materials, is lost and it is difficult to establish a connection between the properties of primary and secondary objects.

Proceeding from that, the influence of structural heredity can be manifested to the greatest degree in such surfacing technologies, where the surfacing materials are fed into the melting zone, bypassing the highest temperature zone, and where there is no rigid connection between arc current and surfacing material melting rate. So, in [5] the influence of the powder initial structure and granulometric composition on

the structure of the deposited metal of 10R6M5 type produced by plasma surfacing, was studied. The filler powder consisted of a mixture of fine ($40\text{--}125 \text{ }\mu\text{m}$) and coarse ($200\text{--}400 \text{ }\mu\text{m}$) fractions, taken in different proportions. It is found that addition of 15 % of coarse fraction powder to fine-grained powder does not lead to any particular changes in the deposited metal structure (Figure 3, *a*). Increase of the content of powders of coarse fractions ($200\text{--}250$ or $315\text{--}400 \text{ }\mu\text{m}$) up to 30 % led to refinement of the deposited metal structure (Figure 3, *b*).

At further increase of the abovementioned fraction content to 45 %, the deposited metal preserves a mostly disoriented structural pattern, but coarser dendrites appear, which grow to the crystallization centers, which are the coarse powder particles (Figure 3, *c*). If such particles do not have enough time to melt completely, then they also act as crystallization centers (Figure 3, *d*) [5].

The given results show that when feeding the surfacing material in the form of a filler (at plasma-powder surfacing) the coarse powder particles ($\geq 200 \text{ }\mu\text{m}$) can become additional crystallization centers. In this case, their influence is similar to the action of granulated powders, which are added to the flux-cored wire

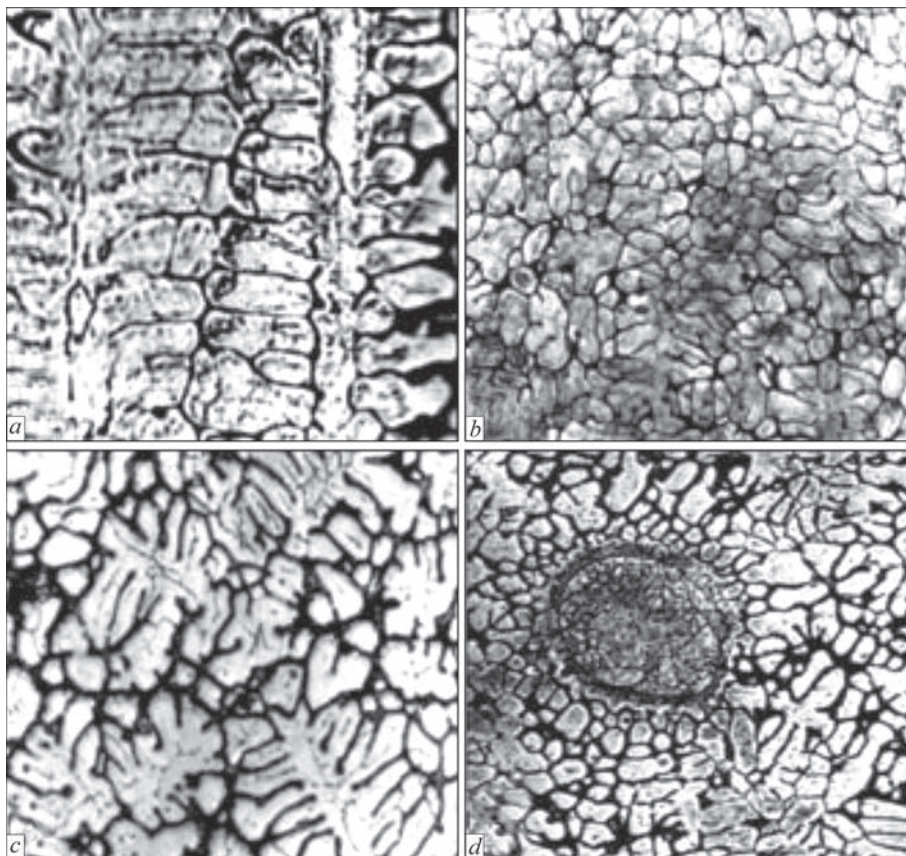


Figure 3. Microstructure of 10R6M5 deposited metal, produced at addition of coarse powder fractions into fine filler powder [5]: *a* — coarse fraction content 15 %; *b* — 30 %; *c* — 45 %; *d* — unmolten inclusion ($\times 400$)

core and are used in the form of electrode or filler materials in arc surfacing.

In [31] it is shown that application of granulated powder allows achieving more uniform filling of the flux-cored powder in arc surfacing, compared to standard wire with a charge from ferroalloys. Both the wires ensured production of deposited metal of the class of wear-resistant tool steel 35V9Kh3GSF. It was noted that the process of surfacing with flux-cored wire with granulated powder is stable, deposited metal formation is good, pores or other defects are absent. The resistance of rolling rolls surfaced by experimental wire with granulated powder was equal to the resistance of rolls surfaced by standard flux-cored wire based on ferroalloys. Here, the smaller the size of granulated powder grains, the higher is the wire fill factor that, obviously, should have influenced the welding-technological properties of the flux-cored wire and the deposited metal quality.

Another example of application of the abovementioned approaches and certain leveling of the influence of the welding arc high-temperature region at surfacing can be use of ultra-dispersed compositions of refractory metals in the flux-cored wire charge [6, 29, 30]. Application of such particles can have a positive influence on the deposited metal quality and can improve its operational properties.

So, in [6] the influence of ultra-dispersed carbide compositions added to the charge of flux-cored electrode wires on the properties of the deposited metal of the type of tool steels 35V9Kh3GSF and 30Kh4V2M2FS used at surfacing tools for hot pressure treatment of metals, was studied. The structure of metal deposited with standard flux-cored wires, consist of lath martensite (laths are elongated in one direction) and a small amount of residual austenite (Figure 4, *b*, *e*).

The structure of the metal deposited with experimental flux-cored wires with additives of ultra-dispersed carbide compositions, is more dispersed, and it has a somewhat different composition: alongside the laths it includes lamellar martensite (Figure 4, *d*, *g*). Residual austenite content is somewhat higher than in the metal deposited with standard wire. Alloying element distribution in the metal deposited with flux-cored wires using ultra-dispersed carbide compositions is more uniform, than at application of flux-cored wires with standard charge [6]. The mentioned features of application of ultra-dispersed carbide compositions in the flux-cored wire charge had a positive influence on the service properties of the deposited metal, improving its wear- and heat resistance.

It is obvious that by changing the technological parameters of the surfacing process it is possible to

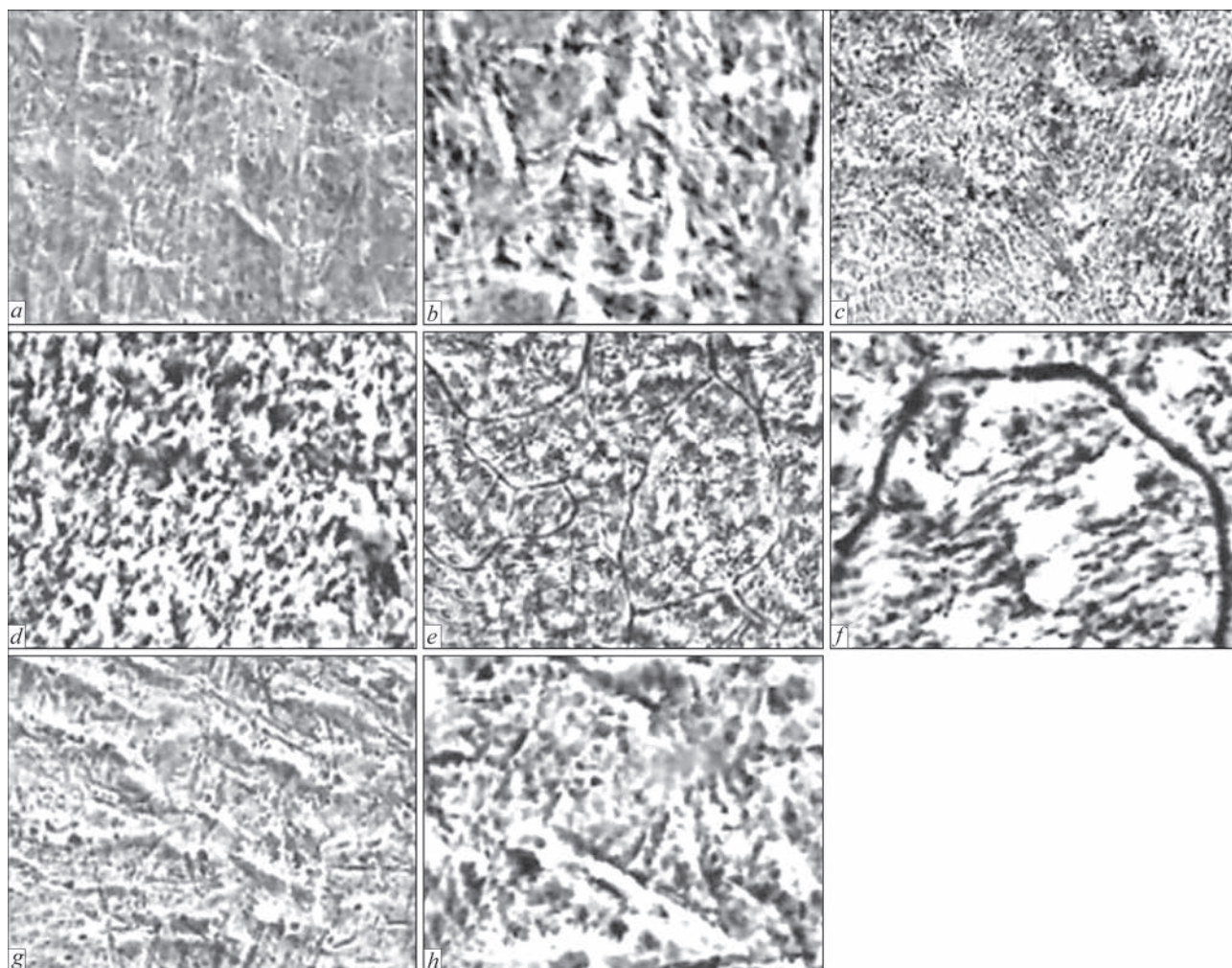


Figure 4. Microstructure of metal surfaced by flux-cored wires [6]: *a, b* and *e, f* — PP-Np-35V9Kh3GSF and PP-Np-30Kh4V2M2FS standard wires, respectively; *c, d* and *g, h* — experimental wires of similar type with additives of ultra-dispersed carbide compositions; *a, c, e, g* — $\times 900$; *b, d, f, h* — $\times 2000$

influence in a certain way the degree of manifestation of the structural heredity effect, as it is known that the solidification morphology, and, hence, the deposited metal microstructure, depend on the deposition rate, current and arc voltage, i.e. on the surfacing energy input. Moreover, by adjusting the amount of heat supplied to and removed from the part, it is possible to control the shape of the fusion line, penetration depth, and, therefore, the composition, structure and properties of the deposited metal to a certain extent [1, 2]. Thus, within certain limits, the degree of structural heredity can be controlled using methods, aimed at changing the metal melt crystallization conditions by varying the surfacing modes.

It is necessary to control the heating and cooling temperature and rate [32] and, depending on metal type, to avoid cyclic heating to high temperatures. For instance for high-speed steels heating up to 1260–1280 °C and subsequent quenching provides a rather fine-grained structure, but after reheating to the same temperature the steel structure is characterized

by very large grain size, leading to brittle naphthalene-like fracture of the tool in service [10].

For instance, for high-speed steel of R6M5 grade the critical melt temperature is 1500 °C (Figure 5). Crystallite grain size under the conditions of melt overheating in the temperature range of 1460–1500 °C changes after remelting, i.e. the dispersity and homogeneity of the initial structure are inherited at remelting in the subcritical temperature range. Now increase melt temperature above the specified temperature range leads to the process of radical restructuring of steel melts, transition to a more equilibrium state and loosing to a certain extent the characteristics of the initial charge billet [10].

Negative example of the heredity effect can result from repeated cyclic heating in multipass welding (surfacing) of heat-resistant [33, 34], high-strength [35] and stainless steels [36]. Structural heredity is manifested in the austenite memory effect, arising under the influence of high heating rates and peak welding or surfacing temperatures. As a result the initial coarse-grained structure is restored, because austenite cannot recrystallize.

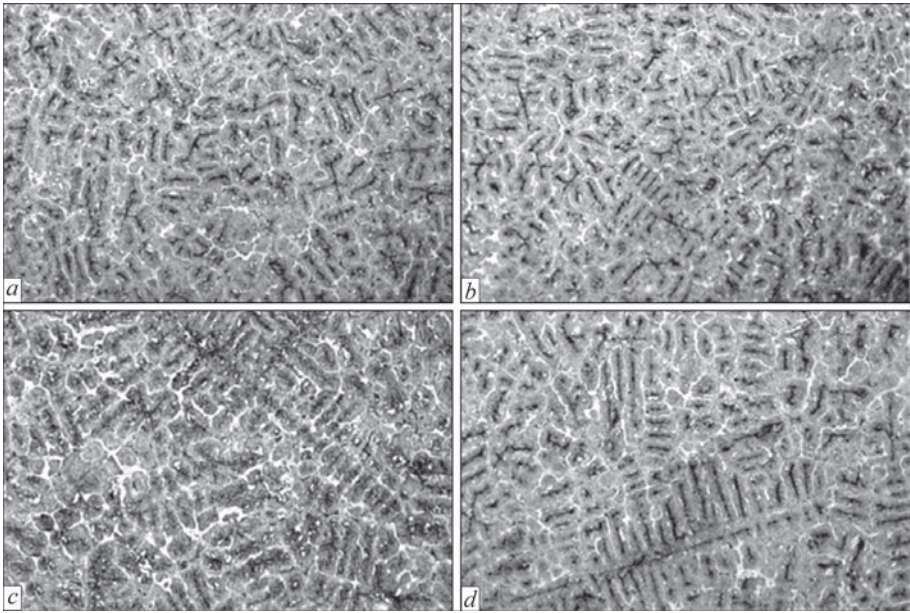


Figure 5. Structure of R6M5 steel, depending on remelting temperature [10]: *a* — 1460; *b* — 1500; *c* — 1540; *d* — 1620 °C (×100)

tallize, leading to higher brittleness and lower toughness in the zone of reheated metal regions. To avoid this effect, it is recommended to control the welding (surfacing) energy input at the level of 8 kJ/cm [35].

The influence of one-, two- and three-time remelting on transformation of the cast structure of the initial charge metal was studied in the case of R6M5L

steel [10, 12]. It was found that at subsequent remelting the grain size of the steel cast structure increases naturally with each remelting, the most significantly after three remelting operations. The size of R6M5L steel increases by 4–5 numbers on average after three-time remelting, compared to the grain of initial structural states of the billets (Figure 6). On the other hand,

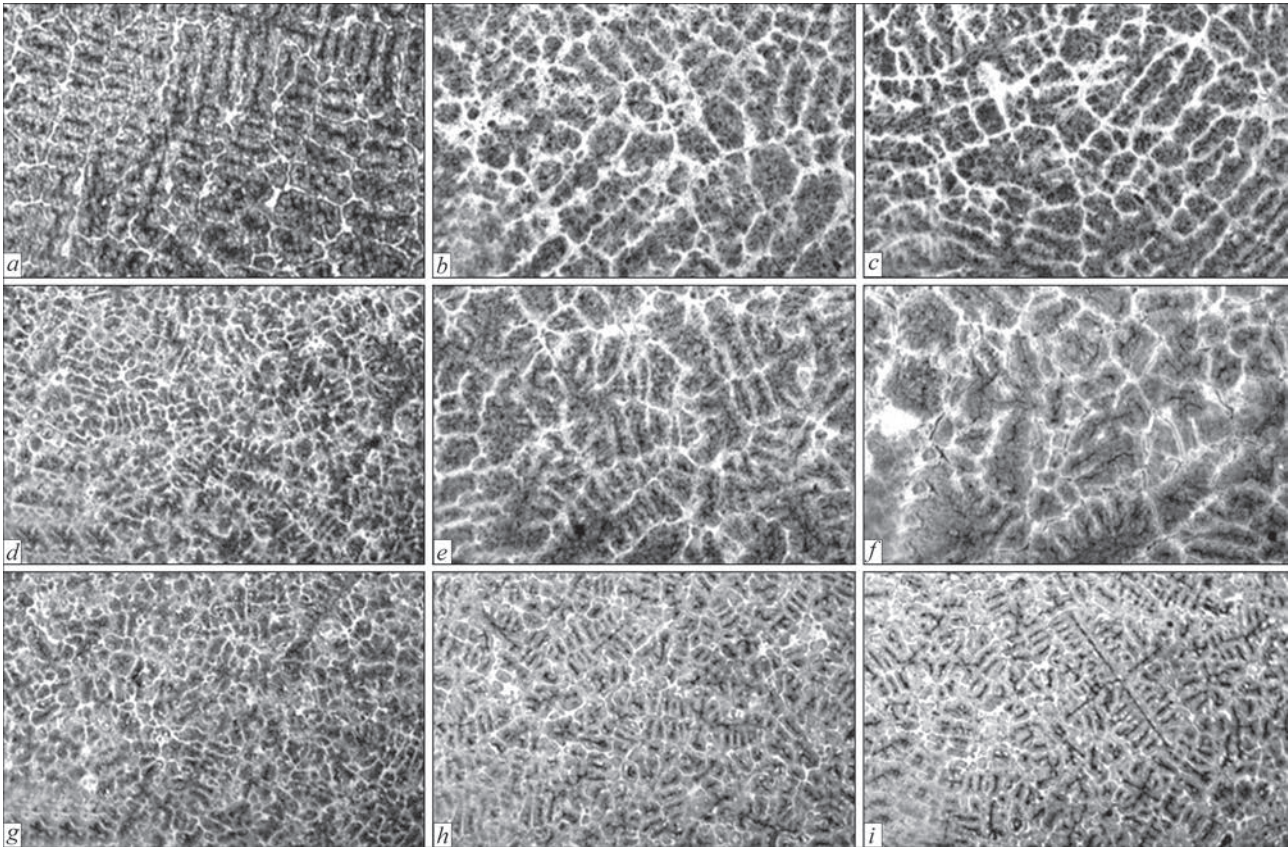


Figure 6. Transformation of R6M5L steel structure, depending on the number of remelting operations and crystallization conditions of the initial billet [12]: *a, d, g* — single remelting; *b, e, h* — double remelting; *c, f, i* — triple remelting; *a-c* — $V=2$; *d-f* — 350; *g-i* — 700 °C/s (×100)

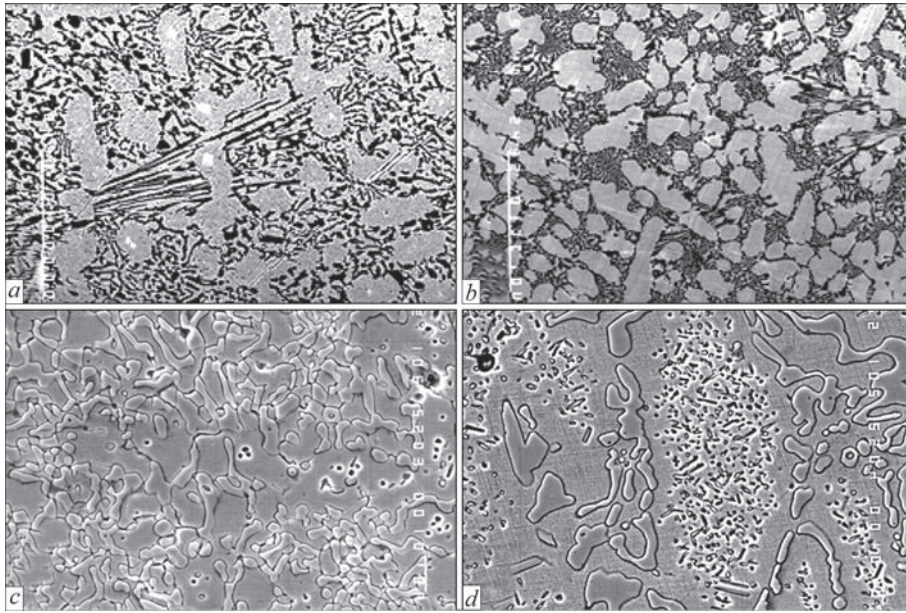


Figure 7. Microstructure of 250Kh25NT alloy [24]: *a, b* — cast state; *c, d* — after heat treatment; *a, c* — control metal; *d* — experimental metal; *a, b* — $\times 400$; *c, d* — $\times 1000$

at an essential increase of cooling rate ($700\text{ }^{\circ}\text{C}/\text{min}$) the incorporated level of non-equilibrium of the steel initial structures increases in proportion at crystallization of charge billets, and at subsequent remelting the high degree of non-equilibrium of rapidly cooled initial steels is preserved, compared to normal cooling steels that is indicative of the high stability of hereditary characteristics of initial billet structures formed at primary crystallization [12].

Application of different methods of external physical impact is another factor, which can influence the structural heredity effect. So, when studying the influence of electrohydropulse treatment (EHPT) of the metal melt on structural heredity of high-chromium wear-resistant cast irons it was determined that EHPT of the melt changes the structure formation conditions due to preservation of the hereditary structural characteristics at the change of aggregate state. Charge remelting by the traditional technology and with EHPT application showed that refinement of the structural components (eutectic carbides and matrix grains) occurred in the studied metal in the cast state. Further heat treatment revealed the presence of the characteristic structural features of the charge material (Figure 7) [24].

Such structural changes are attributable to EHPT influence on finer structural levels [24] that was confirmed by the results of X-ray phase analysis. Thus, the features of the melt structure formed by EHPT in it are fixed by structural elements and are preserved up to phase transition temperatures in the liquid and solid state, and are inherited at subsequent technological impacts (heat treatment).

The methods of weld pool treatment by high-frequency sound or mechanical vibrations will probably have certain potential as to enhancement of the heredity effect manifestation [37, 38]. For instance, in [37] it is shown that part treatment by ultrasonic vibrations during its arc welding results in formation of a more fine-grained structure, both in the weld and in the HAZ. Application of high-frequency (100 Hz) mechanical vibrations also leads to refinement of the deposited metal structural components and improvement of its structural homogeneity that has a positive effect on its service properties [38].

WAYS TO USE THE STRUCTURAL HEREDITY EFFECT IN ARC SURFACING

At present only separate publications are known in scientific-technical literature, which are devoted to the problem of the connection between the crystal-line structure of the initial solid materials with similar structures of the deposited metal, and the “heredity” term is practically not used in surfacing [4–6].

It follows from the conducted analysis, however, that investigation and development of the methods to control the structural heredity effect in arc surfacing can be a reserve for improvement of the operating properties of the surfaced parts. The main directions of investigations to improve the deposited metal structure and properties can be the ways to influence the following:

1. Initial parameters of surfacing materials: their chemical composition, impurity content, granulometric composition, structure and/or shape. In this case, using specially prepared electrode and/or filler materials for surfacing, it is possible to transfer the positive

properties from them to the deposited metal through the weld pool melt: fine-grained structure, uniform distribution of the strengthening phases (carbides, carbonitrides, carboborides), certain dendrite orientation, etc.

2. Weld pool crystallization rate by changing the value of heat input (energy input) through regulation of the electric and technological surfacing modes (current, voltage, surfacing material feed rate, use of pulsed, hybrid technologies, etc.).

As shown by previous studies, these methods of influence are rather promising. So far, however, only the influence of several individual factors has been studied, and the impact of other factors, also at their complex application, remains almost unstudied, for instance, influence of the granulometric composition and type of the surfacing metal materials at their application in the charge of flux-cored electrode and/or filler wires.

Based on this, it is necessary to take a balanced approach to selection of the base alloying system of experimental materials, considering the above determined features of manifestation of the heredity effect in steels and alloys. Carbon content in the deposited metal should be not lower than 0.2 %. Here, with increase of the degree of alloying with such elements as Cr, Mo, W, V, Ti, the structural heredity effect should be manifested under regular temperature conditions of metal crystallization during arc surfacing. Thus, promising materials in terms of effectiveness of manifestation of the structural heredity phenomenon in them, are alloyed and high-alloyed steels: tool, high-speed, maraging, corrosion-resistant, etc.

CONCLUSIONS

1. One of the promising, but practically unstudied methods to control the structure, and, therefore, also the properties of the deposited metal, is using the structural heredity effect, which is applied in metallurgy and foundry with the purpose of transfer and preservation of the fine-grained structure of the initial materials in the finished part structure, leading to an improvement of its operational properties.

2. Unlike metallurgy, application of structural heredity effect in surfacing production is complicated by the features inherent to all the fusion processes of surfacing (welding), namely influence of the initial chemical content and structure of the base metal, which is remelted and penetrates into the weld pool and deposited metal; as well as complex and fast-flowing temperature-time parameters of weld pool existence.

3. It has been preliminarily established that in arc surfacing methods the deposited metal structure and

properties can be controlled, using the heredity effect, in several ways, which can be applied separately or in a combination: by varying the initial parameters of surfacing materials (chemical and granulometric composition, structure, shape, etc.) and influencing metal pool solidification through regulation of the electric and technological surfacing modes and/or application of physical methods of its external treatment.

REFERENCES

1. Ryabtsev, I., Fomichov, S., Kuznetsov, V. et al. (2023) *Surfacing and additive technologies in welded fabrication*. Springer Nature Switzerland AG. DOI: <https://doi.org/10.1007/978-3-031-34390-2>
2. Ryabtsev, I.A., Kuskov, Yu.M., Pereplyotchkov, E.F., Babinets, A.A. (2021) *Surfacing. Control of base metal penetration and formation of deposited layers*. Kyiv, Interservice [in Russian].
3. Babinets, A.A., Ryabtsev, I.O. (2021) Influence of modification and microalloying on deposited metal structure and properties (Review). *The Paton Welding J.*, **10**, 3–10. DOI: <https://doi.org/10.37434/tpwj2021.10.01>
4. Ryabtsev, I.A. (2006) Structural heredity in the initial materials – metal melt – solid metal system (Review). *The Paton Welding J.*, **11**, 8–12.
5. Ryabtsev, I.A., Pereplyotchkov, E.F., Mits, I.V., Bartenev, I.A. (2007) Effect of initial structure and particle size composition of powder on structure of metal 10R6M5 deposited by the plasma-powder cladding method. *The Paton Welding J.*, **10**, 18–22.
6. Ryabtsev, I.A., Kondratiev, I.A., Gadzyra, N.F. et al. (2009) Effect of ultra-dispersed carbides contained in flux-cored wires on properties of heat-resistant deposited metal. *The Paton Welding J.*, **6**, 10–13.
7. Luchkyn, V.S., Tuboltsev, L.H., Padun, N.Y. et al. (2008) Structural characteristics of heredity of liquid cast irons and steels. *Fundamentalni ta Prykladni Problemy Chornoy Metalurgii*, **18**, 122–137 [in Russian].
8. Janerka, K., Jezierski, J., Bartocha, D., Szajnár, J. (2012) Heredity of the structure and properties of grey cast iron melted on a basis of steel scrap. *Advanced Materials Research*, **622–623**, 685–689. DOI: <https://doi.org/10.4028/www.scientific.net/amr.622-623.685>
9. Kutsova, V.Z., Kovzel, M.A., Nosko, O.A. (2007) *Phase transformations in special alloyed steels*. Dnipro, NMetAU [in Ukrainian].
10. Kondratyuk, S.Ie., Prymak, I.N., Shcheglov, V.M., Pliakhtur, O.O. (2009) Inheritance of the structure and manifestations of liquation during remelting of R6M5 steel. *Metaloznavstvo ta Obrobka Metaliv*, **3**, 3–10 [in Ukrainian].
11. Gubenko, A.Ja. (1991) Influence of the initial structural state of the melt on the properties of alloys. *Litejnoe Proizvodstvo*, **4**, 19–20 [in Russian].
12. Kondratyuk, S.Ie., Stoianova, O.M., Pliakhtur, O.O. (2012) The structural heredity of steels is related to the disbalance and and structural heredity of the charge materials. *Metaloznavstvo ta Obrobka Metaliv*, **1**, 3–9 [in Ukrainian].
13. Bokshetjn, S.Z., Bernshtejn, M.L. (1971) *Structure and properties of metal alloys*. Moscow, Metallurgiya [in Russian].
14. Kondratyuk, S., Veis, V., Parkhomchuk, Z. (2019) Structure formation and properties of overheated steel depending on thermokinetic parameters of crystallization. *J. of Achievements in Materials and Manufacturing Eng.*, **97(2)**, 49–56. DOI: <https://doi.org/10.5604/01.3001.0013.8537>

15. D'yachenko, S.S. (2000) Heredity in phase transformations: Mechanism of the phenomenon and effect on the properties. *Metal Sci. and Heat Treatment*, 42(4), 122–127. DOI: <https://doi.org/10.1007/BF02471324>
16. Meshkov, Yu.Ya., Pereloma, E.V. (2012) The effect of heating rate on reverse transformations in steels and Fe–Ni-based alloys. *Phase Transformations in Steels*, 1, 581–618. DOI: <https://doi.org/10.1533/9780857096104.4.581>
17. Timofeev, G.V. (2012) Structural heredity in rolled large sections from continuously cast billets. *Fundamentalni ta Prykladni Problemy Chornoy Metalurgii*, 25, 192–198 [in Russian].
18. Romaniv, O.N., Tkach, A.N., Vol'demarov, A.V. (1980) Method of complex improvement of the mechanical properties of low-tempered structural steels. *Materials Sci.*, 15, 373–378. DOI: <https://doi.org/10.1007/BF00720461>
19. Garasym, J. A., Bondarevskaya, N. A., Teliovich, R. V. et al. (2021) Influence of high-speed heat-setting on armor resistance of high-strength sheet metal of protective purpose. *Metallofiz. Noveishie Tekhnol.*, 43(9), 1235–1246. DOI: <https://doi.org/10.15407/mfint.43.09.1235> [in Ukrainian]
20. Delin, H., Zhang, F., Dingqiang, L., Yan, C. (1994) Re-investigation of austenite grain boundary inheritance in alloy steel. *Heat Treatment of Metals*, 1, 27–32, 50.
21. Ding, F., Guo, Q., Hu, B., Luo, H. (2022) Influence of softening annealing on microstructural heredity and mechanical properties of medium-Mn steel. *Microstructures*, 2, 2022009. DOI: <https://doi.org/10.20517/microstructures.2022.01>
22. Yang, D.P., Du, P.J., Wu, D., Yi, H.L. (2021) The microstructure evolution and tensile properties of medium-Mn steel heat-treated by a two-step annealing process. *J. Mater. Sci. and Technol.*, 75, 205–215. DOI: <https://doi.org/10.1016/j.jmst.2020.10.032>
23. Dang, S.-E., He, Y., Liu, Y., Su, Z.-N. (2014) Structural heredity of 30Cr2Ni4MoV steel. *Transact. of Materials and Heat Treatment*, S2, 61–65.
24. Volkov, G.V. (2011) Structural heredity in alloys after electrohydropulse treatment in the liquid state. *Naukovi Notatky*, 31, 56–62 [in Russian].
25. Tret'yakova, E.E., Rovbo, M.V., Hakimov, O.P., Churkin, V.S. (1991) Influence of the initial structure of cast irons on the surface tension of their melts. *Litejnoe Proizvodstvo*, 4, 11–12 [in Russian].
26. Movchan, B.A. (1970) *Crystallite boundaries in cast metals and alloys*. Kyiv, Tekhnika [in Russian].
27. Kondratyuk, S., Veis, V., Parkhomchuk, Z. (2020) The effect of thermal treatment of the melt before crystallization on the structure and properties of castings. *Archives of Materials Sci. and Eng.*, 104(1), 23–29. DOI: <https://doi.org/10.5604/01.3001.0014.3866>
28. Kondratyuk, S.E., Stojanova, E.N., Shcheglov, V.M. et al. (2013) Hereditary modification of steels with dispersed structured charge components. *Procesy Lytlya*, 2, 19–23 [in Russian].
29. Heath, G. (2006) Nanotechnology and Welding – Actual and possible future applications. In: *Proc. of the Castolin-Eutectic Seminar, 25 Oct 2006. Brussels, Belgium*, 25–35.
30. Klimpel, A., Kik, T. (2008) Erosion and abrasion wear resistance of GMA wire surfaced nanostructural deposits. *Archives of Mater. Sci. and Eng.*, 2, 121–124.
31. Kondratiev, I.A. (2015) Flux cored wire filled with granular alloy. In: *Surfacing. Technologies, Materials, Equipment*. Kyiv, PWI, 53–54 [in Russian].
32. Hu, Y., Chen, W., Han, H., Bai, R. (2016) Effect of cooling rate after finish rolling on heredity in microstructure and mechanical properties of 60Si2MnA spring steel. *Metallurgical Research & Technology*, 113(5), 508. DOI: <https://doi.org/10.1051/metall/2016024>
33. Peng, K., Yang, C., Lin, S., Fan, C. (2017) Effect of arc distance on HAZ thermal cycles and microstructural evolution 10CrNi3MoV steel. *Int. J. Adv. Manuf. Technol.*, 90, 3387–3395. DOI: <https://doi.org/10.1007/s00170-016-9639-4>
34. Arora, K.S., Pandu, S.R., Shajan, N. et al. (2018) Microstructure and impact toughness of reheated coarse grain heat affected zones of API X65 and API X80 linepipe steels. *Int. J. of Pressure Vessels and Piping*, 163, 36–44. DOI: <https://doi.org/10.1016/j.ijpvp.2018.04.004>
35. Lu, H., Xing, S., Chen, Z. et al. (2014) Microstructure and properties of GMAW multipass welding of Q-T high strength steel Q690D. *Heat Treatment of Metals*, 39(10), 120–124. DOI: <https://doi.org/10.13251/j.issn.0254-6051.2014.10.031>
36. Lu, X., Cen, Y., Wang, H., Wu, M. (2013) Structure and mechanical properties on DH40 ship building steel joints by multi-layer and multi-pass welding technology. *Transact. China Weld. Inst.*, 34(2), 79–83.
37. Kirian, V.I., Kajdalov, A.A., Novikova, D.P. et al. (2007) Improvement of welded joint structure under the impact of wide-band ultrasonic vibrations during welding. *The Paton Welding J.*, 2, 38–40.
38. Pokhmurskaya, G.V., Student, M.M., Vojtovich, A.A. et al. (2016) Influence of high-frequency mechanical vibrations of the item on structure and wear resistance of Kh10R4G2S deposited metal. *The Paton Welding J.*, 10, 20–25. DOI: <https://doi.org/10.15407/tpwj2016.10.04>

ORCID

A.A. Babinets: 0000-0003-4432-8879

CORRESPONDING AUTHOR

A.A. Babinets

E.O. Paton Electric Welding Institute of the NASU

11 Kazymyr Malevych Str., 03150, Kyiv, Ukraine.

E-mail: a_babinets@ukr.net

SUGGESTED CITATION

A.A. Babinets (2024) Using the heredity effect for control of the structure of the deposited metal during electric arc surfacing with flux-cored wires (Review). *The Paton Welding J.*, 10, 30–41.

DOI: <https://doi.org/10.37434/tpwj2024.10.05>

JOURNAL HOME PAGE

<https://patonpublishinghouse.com/eng/journals/tpwj>

Received: 27.05.2024

Received in revised form: 30.07.2024

Accepted: 28.10.2024

CONTINUOUS PRODUCTION OF LARGE VOLUMES OF PLASMA ACTIVATED WATER FOR AGRICULTURE

S.V. Petrov¹, S.G. Bondarenko², Sh. Roshanpour³, A.M. Shakhnovsky²

¹The Gas Institute of the NASU

39 Degtyarivska Str., 03113, Kyiv, Ukraine

²National Technical University of Ukraine “Igor Sikorsky Kyiv Polytechnic Institute”

37 Prosp. Beresteiskyi, 03056, Kyiv, Ukraine

³Plasma Dynamics SRL

11/13, Via del Progresso, Vicenza, Italy, 36100

ABSTRACT

This article is devoted to the issues of using plasma technology to produce plasma-activated water, which serves as liquid nitrogen fertilizers. The use of plasma-activated water in crop production is associated with seed treatment, subsequent stimulation of seed germination, and the stimulation of agricultural crop growth. The study proposes a new plasma system for the direct production of activated water based on a hybrid electric discharge, which combines equilibrium and non-equilibrium plasma. This system operates in a mixture of air and water. The process of plasma-chemical treatment is implemented in a plasma module with a pulsation mode of electric discharge combustion in an aqueous solution. This system is environmentally friendly, as it does not use additional chemicals (since air and water plus electricity are used as raw materials) and does not produce waste. Using the developed plasma system, plasma-activated water with a high content of stable active forms of oxygen and nitrogen (NO_3^- , NO_2^- , H_2O_2 , O_3 , etc) was obtained. Such plasma-activated water has high potential for effective use, as the long-lived active compounds contained in the activated water can participate in plant metabolism and serve as nutrients for them. The small size and weight of the plasma unit, along with its sufficiently high productivity, allow its use in small and medium-sized farms. This ensures environmentally friendly fertilizer production on-site, provides flexibility to meet changing demand, significantly reduces transportation costs, and minimizes losses. The substantial energy consumption required for the production of plasma-activated water can be offset by integration with renewable energy sources.

KEYWORDS: plasma agriculture, hybrid plasma, nitrogen fixation, plasma/liquid interfacial, plasma chemical reactor, plasma fertilizer production, plant growth

INTRODUCTION

Nitrogen fertilizers are essential for the growth of agricultural crops and, consequently, for feeding the growing population. Modern fertilizer production has supported the growth of industrial societies for more than a century. Approximately 40–60 % of global food production is related to the use of commercial fertilizers. According to statistical data, the global production volume of ammonia (NH_3) in 2019 was 235 mln t, making it the second most produced chemical commodity after sulfuric acid (H_2SO_4) [1]. Ammonia plays an important role in the agricultural industry for the production of fertilizers. The primary raw material for the production of nitrogen fertilizers is fossil fuel, and their production is significantly dependent on the extraction of coal and natural gas. The most commonly used method for ammonia production is the Haber-Bosch process. The drawbacks of this technology include high levels of greenhouse gas emissions, exceeding 2.16 kg CO_2 -equivalent per kg of NH_3 , as well as a large amount of energy consumption — more than 30 GJ per ton of NH_3 [2].

As a result, the cost of produced fertilizers depends on market conditions and tends to be high, while greenhouse gas emissions during their production are very significant. In this context, farmers often find themselves making decisions based on prices rather than plant needs, leading to inefficient nitrogen use and low application efficiency. Moreover, entrenched supply chains often overlook the nuances of developing economies, making nitrogen unavailable where it is most needed. Over the past few decades, the world has dramatically changed due to a sharp increase in population. The consequence of this population growth is high demand for food, water, and energy resources. The application of nitrogen fertilizers is one solution to the food security issue that has arisen globally. However, it should be noted that environmental sustainability is at risk due to excessive use of chemical nitrogen fertilizers, which negatively impact all segments of the environment, namely soil, water, and air, and also affects the health of humans and animals. Several strategies are employed to cushion the harmful impact of nitrogen fertilizers. In particular, the use of compost and organic manure, slow-release and controlled-release fertilizers, as well as nano-fertilizers is encouraged. Another widely accepted solution for reducing the excessive use of chemical fertilizers is

to improve the nitrogen uptake efficiency of agricultural crops. Thus, the issue of the form and role of nitrogen fertilizers requires rethinking [3]. The current challenge is to shift the paradigm in the field of nitrogen fertilizers in agriculture towards environmentally friendly production, borrowed from nature, obtaining them solely from nitrogen and oxygen in the air with minimal energy consumption at the point of application. The specific rate of fixed nitrogen should be close to 200 grams per 1 kWh of consumed electricity.

It is expected that new plasma technologies, which provide maximum efficiency with minimal costs, will contribute to the sustainable development of various sectors of the economy. In this regard, a unique method of transferring chemical reactivity and energy from plasma to water without the presence of any chemical substances is currently being actively researched. The interaction of plasma with water results in the creation of a new product with noticeable and diverse activity, referred to as plasma-activated water (PAW) [4]. PAW is environmentally friendly and promising solution for a wide range of applications: from water treatment and biomedicine to agriculture. The application of PAW minimizes the stages of the production process and either eliminates or significantly reduces the use of expensive and/or hazardous reagents. PAW is also used for the inactivation of microorganisms (bacteria, fungi, viruses, algae, pests, etc.), preservation of food products (fruits, vegetables, dairy and meat products, including seafood, etc.), disinfection of dental and medical equipment surfaces, removal of pesticides, selective destruction of cancer cells, preparation of viral vaccines, seed germination, plant growth, as a source of nitrogen fertilizers, and more. It follows that the application of PAW allows for the avoidance of disinfectants (chemicals), preservatives, fertilizers,

pharmaceutical ingredients, and other substances that cause various environmental and health issues. Despite the promising developments in this field, there are currently only a few examples of the practical application of plasma water activation [5–7]. The presented study focuses on the production of PAW. It analyzes issues related to the plasma-chemical synthesis of reactive particles present in the water, as well as various mechanisms that regulate the activity of PAW in agricultural applications, the problems of PAW efficiency and selectivity, and the possibilities for scaling the process. The aim is to advance the understanding of the fundamental aspects of PAW chemistry necessary for optimizing biochemical activity and transitioning this environmentally and human health-safe technology into an energy-efficient strategy for practical application.

The interaction of plasma with water alters its physicochemical properties, which is associated with the formation of reactive oxygen-nitrogen species (RONS). Figure 1 shows the formation of RONS [8, 9].

In the initial stage, dissociation of oxygen, nitrogen, water molecules, and others occurs in the presence of high-energy electrons. These dissociated particles combine to form various compounds, such as NO_x , O_3 and H_2O_2 . Due to the airflow, these particles (via diffusion or convection) enter the liquid-gas interphase boundary, where all short-lived particles disappear, while long-lived ones survive. Subsequently, these “surviving” particles, upon dissolving in water, react with each other and with water molecules, leading to the formation of stable RONS (NO_3^- , NO_2^- , H_2O_2 , O_3 , etc.).

Furthermore, if certain readily accessible metals such as Mg, Al, Zn, and Cu are separately immersed in water activated by plasma, they undergo oxidation

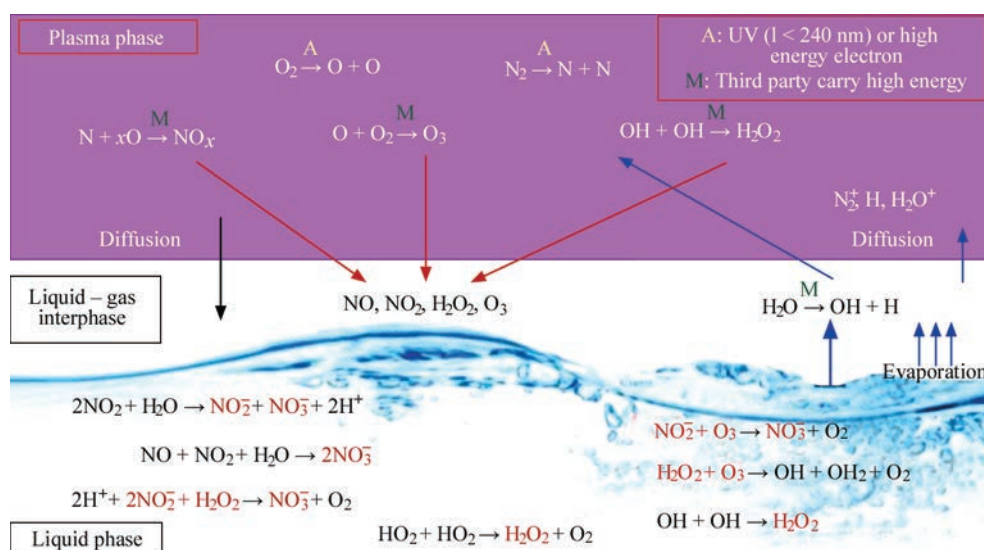


Figure 1. Scheme explaining the physicochemical changes occurring in water (the formation of RONS) as a result of the interaction of plasma with water [8]

in the water, releasing electrons that reduce hydrogen ions to hydrogen atoms. The liberated hydrogen atoms then reduce plasma-excited nitrogen back to ammonia. The reduction of hydrogen ions by metals not only regulates pH but also enhances the rate of ammonia synthesis by providing additional hydrogen donors. This process opens up new avenues for further research in sustainable nitrogen fixation [10].

In the study [11], hydroxyl radicals were apparently introduced for the first time into the electrocatalytic nitrogen oxidation reaction (NOR) to produce nitrates. Here, cobalt tetraoxide (Co_3O_4 , Figure 2, *a*) serves not only as an electrocatalyst but also as a nanozyme (in conjunction with hydrogen peroxide, producing OH), thereby making this compound suitable as a highly efficient electrocatalyst for NOR to synthesize nitrates. $\text{Co}_3\text{O}_4 + \text{OH}$ demonstrates excellent performance in NOR, employing an environmentally friendly approach. This compound is the most active catalyst among non-precious metals reported for the NOR process to date. Additionally, this catalyst exhibits long-term electrochemical and structural stability. Energy barriers for the conversion of N_2 to N_2OH^* (the rate-determining step) were determined from Figure 2, *b*. It was found that the introduction of the hydroxyl radical OH ($\text{Co}_3\text{O}_4/\text{H}_2\text{O}_2$ system) significantly reduces the energy barrier and accelerates the reaction. Figure 2, *c* illustrates the entire scheme of the electrocatalytic NOR process.

Below, we will discuss the application of PAW for seed germination, plant growth, as well as its use as a nitrogen source for various agricultural and aquaculture purposes. PAW can be utilized to enhance seed germination rates. Setting aside the methods of producing PAW, we will focus on the influence of

concentrations of major components NO_3^- , NO_2^- can also be oxidized to NO_3^- or it can interact with H_2O_2 , resulting in the formation of peroxynitrous acid (ON-OOH). The presence of nitrogen in the soil is a primary factor influencing plant growth and determining crop yield. From this perspective, increasing nitrate concentrations through plasma processing potentially serves as a crucial nitrogen source for plant growth and development.

In study [12], PAW was obtained by surface treatment of water using gliding arc discharge with a power of 4.96 W for up to 20 min, resulting in an average nitrate and nitrite concentration of 6 mg/L. Water absorption capacity is crucial for seed germination as it induces swelling and softening of seed coats. PAW significantly improves the water uptake rate by radish, alfalfa, and pea seeds [12]. The water uptake rates for PAW-irrigated seeds (radish, alfalfa, and pea) were $59.94 \pm 0.2\%$, $147 \pm 1.0\%$, and $147.70 \pm 1.3\%$ after 10 hours of irrigation, respectively, which was higher compared to seeds treated with non-ionized water (58.49 ± 0.3 , $120 \pm 0.9\%$, $120.59 \pm 1.2\%$, respectively). Overall, using PAW for seedling irrigation led to favorable physical and chemical changes in them, resulting in significantly higher yields over a shorter period.

PAW can serve as an alternative to chemical fertilizers in agriculture. The effect of PAW treatment at two concentrations (1.5 or 3.0 mg/L NO_3^-) on various morphological, physiological, biochemical parameters, and yield of *Lactuca Sativa* L., cultivated in pots of two different volumes (400 or 3200 cm³), was studied in research [13]. The study results indicated that both PAW concentrations did not affect germination at the beginning of the process. A positive effect of treat-

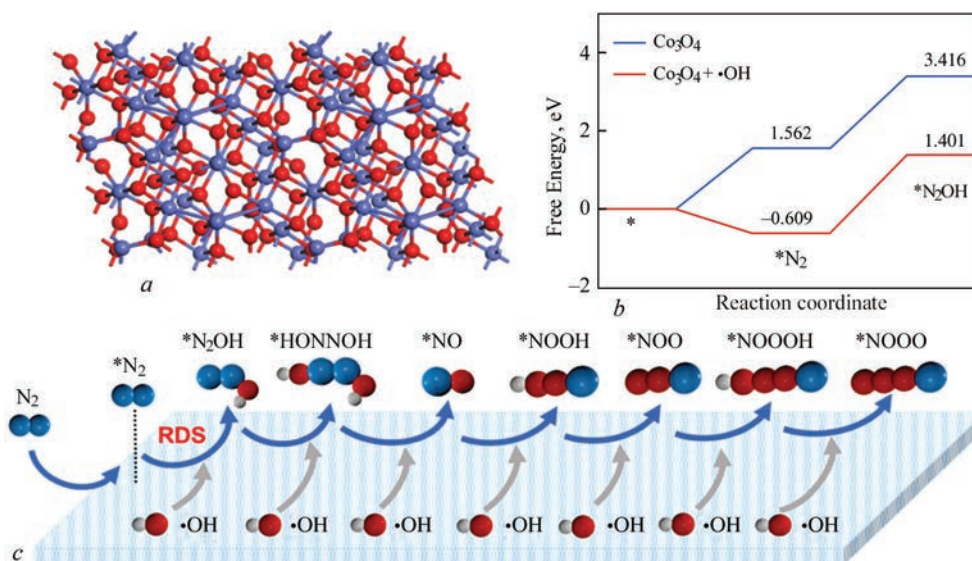


Figure 2. To the use of a Co_3O_4 catalyst: *a* — crystal structure of Co_3O_4 ; *b* — free energy diagram of the electrooxidation reaction N_2 on Co_3O_4 and $\text{Co}_3\text{O}_4 + \text{OH}^-$; *c* — simplified mechanism of NO_3^- production on the surface of catalysts [11]

Table 1. Physicochemical properties of the PAW

Water samples	pH	Nitrite NO ₂ ⁻ , mg/L	H ₂ O ₂ , mg/L	Nitrate NO ₃ ⁻ , mg/L	Conductivity, us/cm
Deionized water (DW)	5.74±0.06	0.00	0.00	0.00	1.53±0.13
PAW5 min (PAW5)	3.62±0.02	1.09±0.11	0.09±0.01	25.29±2.88	118.10±2.26
PAW7 min (PAW7)	3.34±0.03	1.24±0.12	0.14±0.01	49.05±2.61	218.50±9.64
PAW12 min (PAW12)	2.94±0.08	1.85±0.07	0.27±0.02	102.67±6.30	460.33±15.25
PAW19 min (PAW19)	2.62±0.07	3.68±0.12	0.88±0.04	202.87±8.74	972.93±32.41
PAW40 min (PAW40)	2.37±0.04	5.17±0.16	1.31±0.04	389.08±12.24	1847.00±79.19

ment was observed in the increase of lettuce length at the 1.5 mg/L NO₃⁻ concentration, while chlorophyll content significantly increased at the 3.0 mg/L NO₃⁻ concentration. Dry weight was notably higher in lettuce treated with PAW grown in larger pots after 57 days. Nitrite content in lettuce grown in larger pots was lower compared to lettuce grown in smaller pots, regardless of PAW concentration.

PAW samples in [14] were obtained using five different treatment durations and utilized in the experiment. The samples are denoted as PAWi (i — plasma treatment time in minutes): PAW5, PAW7, PAW12, PAW19 и PAW40 (see Table 1).

The use of PAW increases the total root length and the number of root hairs in *Arabidopsis* roots, which serves as a typical model for studying plant genetics and developmental biology (Figure 3).

In [15], the foliar application of PAW was evaluated on plant growth during the vegetative period. Periodic application of PAW positively influenced the chlorophyll content in maize leaves. Chlorophyll content decreased over time with maximum application of distilled water by 34.6 and by 24.7 % with PAW at the same doses. Foliar application of PAW significantly increased the electrical capacity of roots, aboveground biomass, and nutrient content in dry matter, except for nitrogen. Periodic application of PAW increased nitrogen content in aboveground dry matter by 13.3 %. The chemical activity of PAW was assessed based on hydrogen peroxide, nitrite, and nitrate formation. The

average concentration of hydrogen peroxide in PAW was (0.7±0.2) mg/L (0.022±0.004 mmol/L), nitrite concentration was (1.071±0.005) mg/L, and nitrate concentration was (24.7±2.3) mg/L.

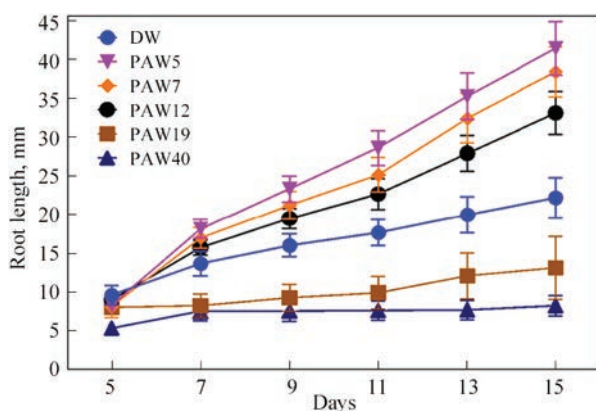
The results obtained by the authors [16] indicate that PAW can effectively stimulate the growth of wheat seedlings and positively influence their metabolism, particularly in nutrient-deficient soil.

The enhanced response to the use of PAW is likely associated with increased water absorption, which leads to accelerated utilization of seed nutrient reserves and nitrogen metabolism during the vegetative growth of wheat. Seeds grown in PAW interact with H₂O₂ primarily in the early stages of growth during imbibition and germination, while NO₂⁻ and NO₃⁻ are metabolized after the seeds begin to grow.

At Kwangwoon University, Seoul, South Korea, physiological, biochemical, and molecular changes were observed in tomato seedlings treated with PAW compared to the control seedlings [17]. The altered chemical properties of water under the influence of cold plasma are shown in Figure 4, *a–c*.

The effects of PAW treatment at different time intervals are presented in Figure 5, *a–c*. Pre-germinated lettuce plants were grown in pots with soil and irrigated with PAW or solutions of H₂O₂ and/or NO₃⁻. After 5 weeks, growth parameters, leaf quantity and quality, fresh and dry plant mass, chlorophyll content of photosynthetic pigments, photosynthesis rate, and the activity of antioxidants and superoxide dismutase (SOD) enzymes were determined. Lettuce plants irrigated with PAW, compared to the chemically equivalent solution of H₂O₂ and NO₃⁻, had the same dry mass, but PAW induced higher content of photosynthetic pigments, higher photosynthesis rate, and lower SOD activity. NO₃⁻ primarily contributed to an increase in dry weight, content of photosynthetic pigments, photosynthesis rate, and better plant appearance. H₂O₂ contributed to an increase in dry weight and induced SOD activity. Overall, H₂O₂ and NO₃⁻ at appropriate concentrations can stimulate plant growth and influence their physiological properties.

In the study [18], the role of PAW was evaluated by examining its effects on lettuce plants and compar-

**Figure 3.** Effect of PAW on root length at the developmental stage of *Arabidopsis* [14]

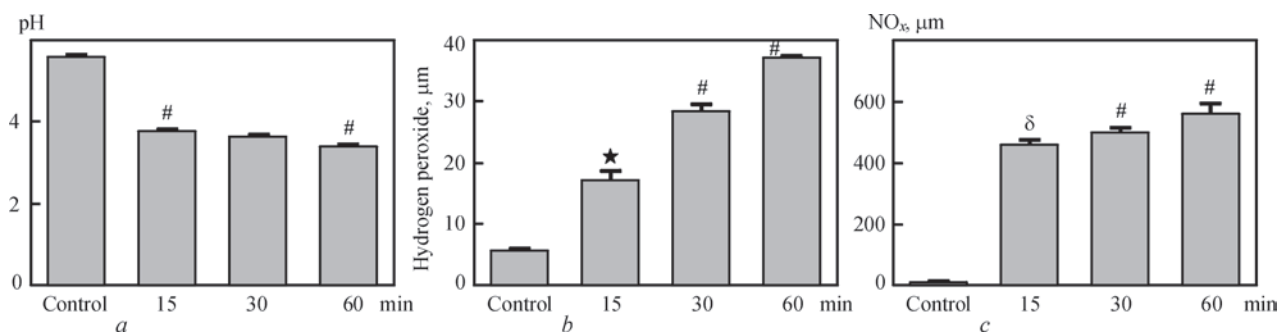


Figure 4. Biochemical properties of PAW: *a* — pH; *b* — H_2O_2 ; *c* — NO_x before and after different times of water exposure to plasma. Mean \pm SE ($n=3$) of each experiment represented in terms of error bars. The SE between the mean of the control and the treatment group was analyzed by student t-test. p-value denoted by * ($p < 0.05$), δ ($p < 0.01$), # ($p < 0.001$) [17]

ing the influence of PAW with the effects of H_2O_2 and/or NO_3^- (considering solutions of various concentrations). chemical composition and pH of plasma activated water (PAW) and various $\text{H}_2\text{O}_2/\text{NO}_3^-$ solutions are shown in Table 2.

The Company VitalFluid B.V. from Eindhoven University positions itself as global leader in PAW application [19]. The synthesized in plasma liquid nitrogen fertilizer is referred to as “Organic nitrogen VitalFluid”. In organic plant cultivation, the USDA (U.S. Department of Agriculture) does not permit the use of nitrogen fertilizers in a form directly available

for crop uptake. Typically, nitrogen is applied in an organic form, which must be processed by microorganisms before becoming available to the crop. Nitrogen fertilizers in the form of PAW are readily accessible for assimilation, providing a clear advantage over organic fertilizers.

The VitalFluid B.V. company developed an organic nutrient solution in accordance with USDA standards using PAW and tested it in a pilot production system. A greenhouse experiment (crop cultivation area of 120 m^2) was conducted with tomato crops grown in a hydroponic system on a peat substrate, fol-

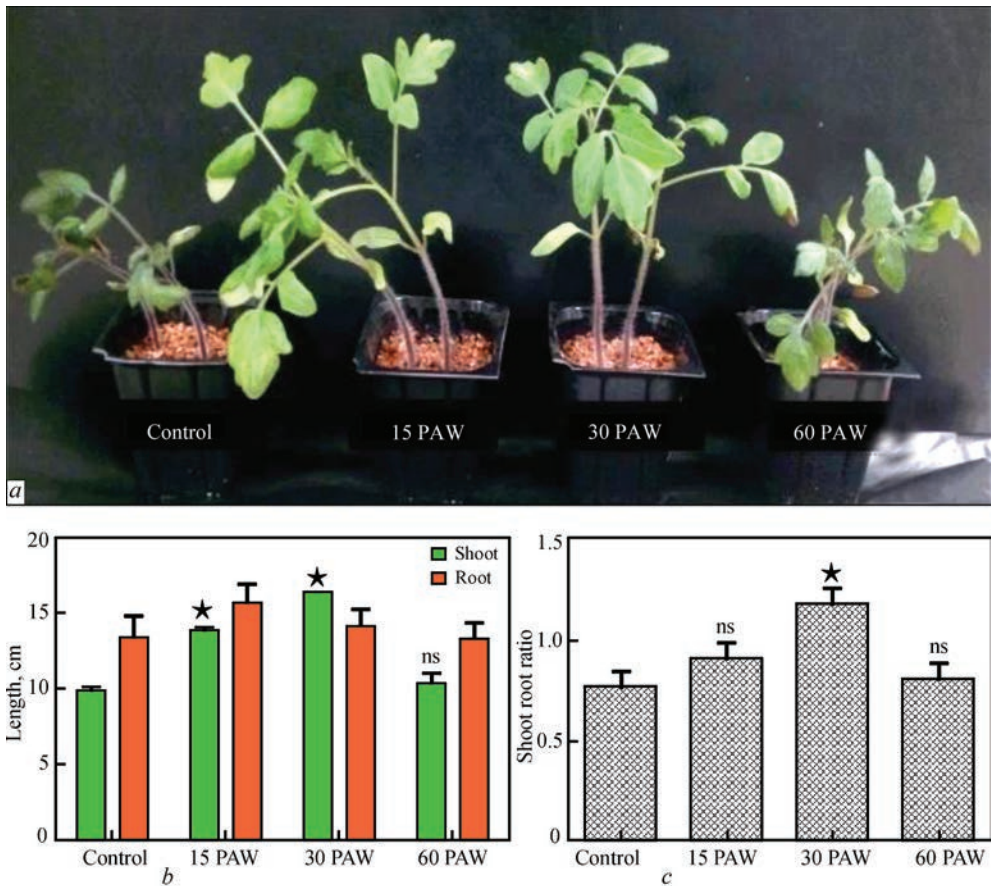


Figure 5. Effect of PAW treatment at different time intervals: *a* — on the physiological state of tomato seedlings (28 days) grown in vermiculite; *b* — shoot and root length (cm); *c* — shoot and root length ratio; \pm SE of mean ($n = 3$) of each experiment represented in terms of error bar. Significant difference between the mean of control and treatment group was analyzed by student t-test. p-value denoted by * ($p < 0.05$), δ ($p < 0.01$), and # ($p < 0.001$) [17]

Table 2. Chemical composition and pH of PAW and various H₂O₂/NO₃⁻ solutions

Solution/variant (abbrev.)	H ₂ O ₂ , mM	NO ₃ ⁻ , mM	pH
Control (tap water)	—	~0.02	~7.5
PAW	~0.42	~0.85	~7.5
H ₂ O ₂ (4)	0.4	—	~7.6
H ₂ O ₂ (1)	1.0	—	~7.7
H ₂ O ₂ (10)	10.0	—	~7.8
NO ₃ ⁻ (85)	—	0.85	~7.9
NO ₃ ⁻ (2)	—	2.0	~7.9
NO ₃ ⁻ (20)	—	20.0	~7.9
H ₂ O ₂ (4) + NO ₃ ⁻ (85)	0.4	0.85	~7.9
H ₂ O ₂ (10) + NO ₃ ⁻ (20)	10.0	20.0	~7.4

lowing USDA organic cultivation principles. Half of the greenhouse section served as the control (following USDA principles). In the other half of the greenhouse, nitrogen fertilizers in the form of PAW were provided by VitalFluid. On average, 10 mmol/L of NO₃⁻ of natural (plasma) nitrogen was applied. At the beginning of the experiment, the yield was the same for both treatments, but crop development was entirely different. The crop grown with VitalFluid clearly had sufficient nitrates for growth, while the reference crop suffered from nitrogen deficiency, leading to reduced productivity (Figure 6) [20].

Using natural PAW nitrogen as the primary nitrogen source in USDA organic tomato production has been shown to provide opportunities for water and nutrient savings through drainage water reuse. This can improve resource efficiency in USDA organic tomato production.

The literature on plasma agriculture has described in detail the effectiveness of various approaches to using PAW, from seed to field. It can be concluded that, in general, plasma-treated water has a significant effect on seed germination and seedling growth. Plants irrigated with plasma-treated water have increased yields. The studies conducted show that PAW can act as both a plant growth stimulator and an immune inducer. Thus, special attention should be paid to better

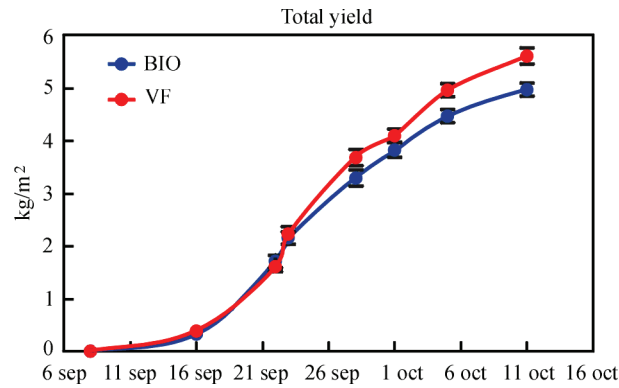


Figure 6. Cumulative yield of tomatoes (kg/m²) for VitalFluid (VF) and for reference sample (BIO) [20]

understanding the potential of cold plasma in plant growth, development and protection. Numerous laboratory tests have been performed that demonstrate clear benefits of using PAW and the feasibility of moving to large-scale field practice. The solution to this problem is related to the development of affordable and reliable high-performance plasma equipment.

AIMS OF RESEARCH

The aim of the study is to investigate the potential for high-performance activation of water or aqueous solutions using a hybrid electrical discharge in bubble water for the efficient production of PAW — liquid nitrogen fertilizers.

To achieve this goal, the following objectives must be accomplished:

- develop and implement a plasma system operating with a hybrid electrical discharge (with both equilibrium and non-equilibrium zones) in a water-bubble medium.
- determine the operating parameters of the system that ensure direct fixation of NO_x in the plasma flow reactor with a hybrid mode of electrical discharge operation.

MATERIALS AND METHODS

To accomplish the objectives, a plasma system utilizing a flow-type plasma-jet plasma-chemical reactor has been developed.

The developed reactor system for NO_x synthesis includes a plasma-jet reactor equipped with a recuperative cooling-heating system, a power supply, water

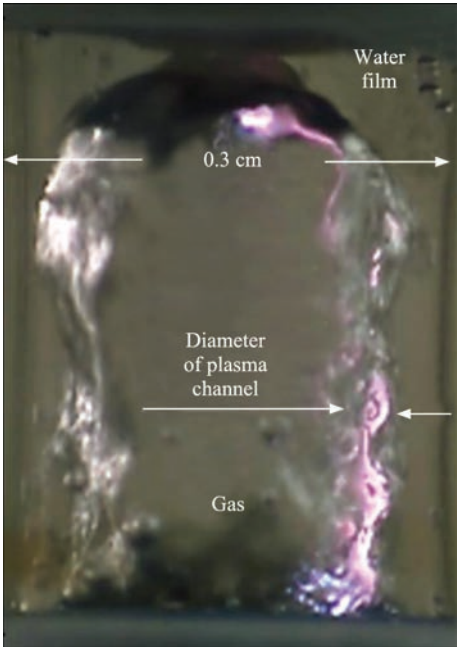


Figure 7. Zoomed in photo of the discharge region and filamentary plasma channel formed along the surface of the water film for the argon carrier gas [21]

and air supply systems, and monitoring and measurement equipment.

The electrical discharge in the plasma-chemical reactor occurs on the surface of air bubbles in water (Figure 7) [21]. This phenomenon underpins the technology for direct nitrogen fixation in water.

The power supply system for the electrical discharge is built using resonant inverters with a capacity of up to 20 kW. Experiments were conducted by varying the frequency of the applied voltage from 5 to 100 kHz. Bipolar pulses with a voltage amplitude of 4000 V are applied to the reactor electrodes. Air flow rates during the experiments did not exceed 2 m³/hour. Tap water was used in the experimental studies, with a maximum flow rate of 2 tons per hour.

A critical aspect in developing the technological equipment is determining the energy consumption during the discharge process. This determination was carried out by analyzing current and voltage oscillograms during discharge (Figure 8).

To obtain oscillograms, a dual-channel DSO3202A Digital Storage Oscilloscope with a bandwidth of 200 MHz and high sampling rate was used. Digitalization of the oscillograms was performed using the OriginPro 2017 software. Following digitalization, the acquired data facilitated the necessary calculations in the Mathcad mathematical software. Specifically, power calculations were conducted for all phases of discharge combustion.

The parameters of PAW were monitored using ion chromatography on a compact IC-flexometer 930 (manufactured by Thermo Scientific) with a Dionex

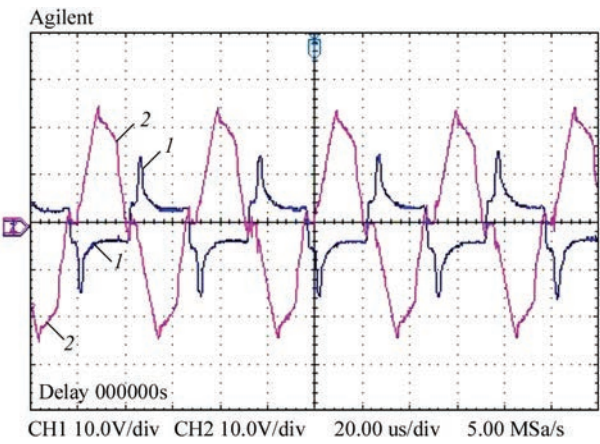


Figure 8. Typical oscillogram of voltage (1) and current (2) for an optimal discharge shape (breakdown voltage 3000 V and current amplitude 14 A)

IonPac AG9-HC guard column and an analytical column Dionex IonPac AS9-HC. The Horiba NO₃ analyzer was used as the measuring instrument. For rapid analyses, QUANTOFIX® indicator test strips were employed. pH values of the solution were measured using a D-51 HORIBA pH meter, and conductivity was assessed with a COND5021ST device from Sato Shouji Inc. The analysis of NO and NO₂ content in exhaust gases was performed using a Testo 340 gas analyzer. Conductivity of both tap water and PAW was monitored using a COND5021ST device from Sato Shouji Inc.

RESULTS

In order to address the research objectives, ERA LLC, in collaboration with GEFEST PE, has developed a new plasma system for direct high-throughput pro-

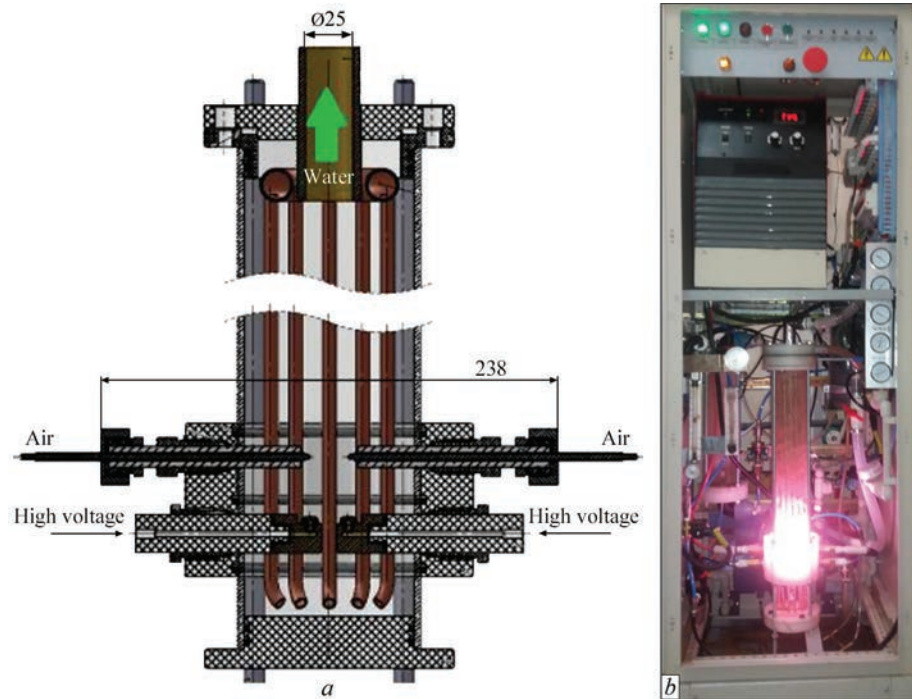


Figure 9. Plasma system for high-performance production of PAW: *a* — plasma module; *b* — system in operation

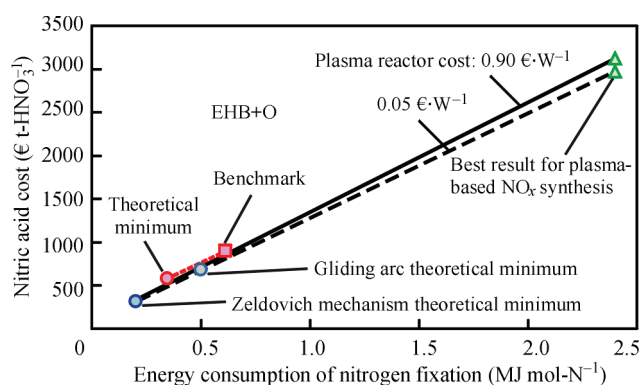


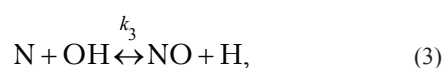
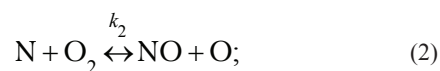
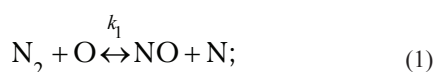
Figure 10. Impact of energy consumption of the plasma NO_x synthesis process on the total cost of nitric acid production [22]

duction of PAW. This system integrates both equilibrium and non-equilibrium plasma states and operates in an air-water mixture. The process is implemented within a plasma module utilizing a pulsating mode of electrical discharge combustion in a flowing bubble stream of water (Figure 9, *a*, *b*).

When conducting the research, it was taken into account that a very important indicator characterizing operating costs is energy consumption. It is obvious that energy consumption has a great impact on the overall cost of RONS production (NO_3^- , NO_2^- , H_2O_2 , O_3 , etc.), while increasing capital costs has little impact on the overall economics of the process. The assessment of energy consumption's impact on the cost of nitric acid in the plasma synthesis of NO_x is depicted by solid and dashed lines in Figure 10 [22]. Analysis of Figure 10 demonstrates that the plasma NO_x synthesis process becomes competitive compared to the Haber–Bosch process based on electrolysis combined with the Ostwald process at an energy consumption of $0.7 \text{ MJ mole-N}^{-1}$.

Among the various nitrogen fixation processes, one of the most promising methods is low-temperature non-equilibrium plasma [23–25]. Compared to the Haber–Bosch process and the early Birkeland–Eyde process, non-equilibrium plasma allows for a larger portion of the supplied energy to activate N_2 at room temperature and atmospheric pressure. The energy consumption for nitrogen fixation with non-equilibrium plasma can be lower than in standard ammonia synthesis, determined by thermodynamics.

The development by the authors is based on two principles. Firstly, extended Zeldovich mechanism was taken as a basis. The extended Zeldovich mechanism [26] is a chemical mechanism describing the oxidation of nitrogen and the formation of NO_x , according to reactions:



where: k_1 and k_2 are reaction rate constants according to Arrhenius law.

Secondly, non-equilibrium plasma affects electrochemical processes influencing chemical bonding of molecules within the plasma and/or on the surfaces of processed materials. Conversely, equilibrium plasma, characterized by high energy density, ensures efficient performance. However, achieving non-equilibrium states with high energy densities is challenging. Therefore, the authors have developed a hybrid plasma processing method that combines both equilibrium and non-equilibrium plasma, leveraging the advantages of each. The electrical discharge in the reactor (Figure 9, *a*) ignites around air bubbles in water (Figure 7). The power supply system for the electrical discharge is based on a resonant inverter with a capacity of up to 20 kW at a frequency of 20 kHz. Bipolar pulses with a voltage amplitude of 4000 V are applied to the electrodes. The formed sheath around the discharge occupies a volume hundreds of times larger than the discharge channel itself, creating a non-equilibrium plasma environment where all plasma-chemical reactions occur.

The radical termolecular reaction (3) between OH and N is still poorly understood, but under conditions of a water plasma discharge, it has a significant influence on the formation of NO in the presence of nitrogen. cobalt tetraoxide (Co_3O_4) can act as an electrocatalyst (in combination with hydrogen peroxide, producing OH), and can be used as a highly efficient electrocatalyst for nitrate synthesis.

In the exhaust gases at the outlet of the plasma module (Figure 9, *a*), NO remains which is not soluble in water. The final stage of the process involves the absorption of NO_2 by water. During the oxidation of NO to NO_2 , several side reactions occur, resulting in the formation of a mixture of nitrogen oxides: NO, N_2O_3 , NO_2 , N_2O_4 , N_2O . The composition of the mixture can vary significantly, but NO_2 is always the predominant component. To enhance the absorption of NO_2 by water, it is necessary to increase pressure and decrease temperature, while maintaining elevated water temperature in the discharge zone. To meet these conflicting conditions, the plasma module design includes an internal heat exchanger, and a separator with gas-water separation is installed in the pneumatic line. Subsequently, this gas containing NO is mixed with ozone for complete oxidation to NO_2 , followed by dissolution in water in a bubbling reactor (Figure 11).

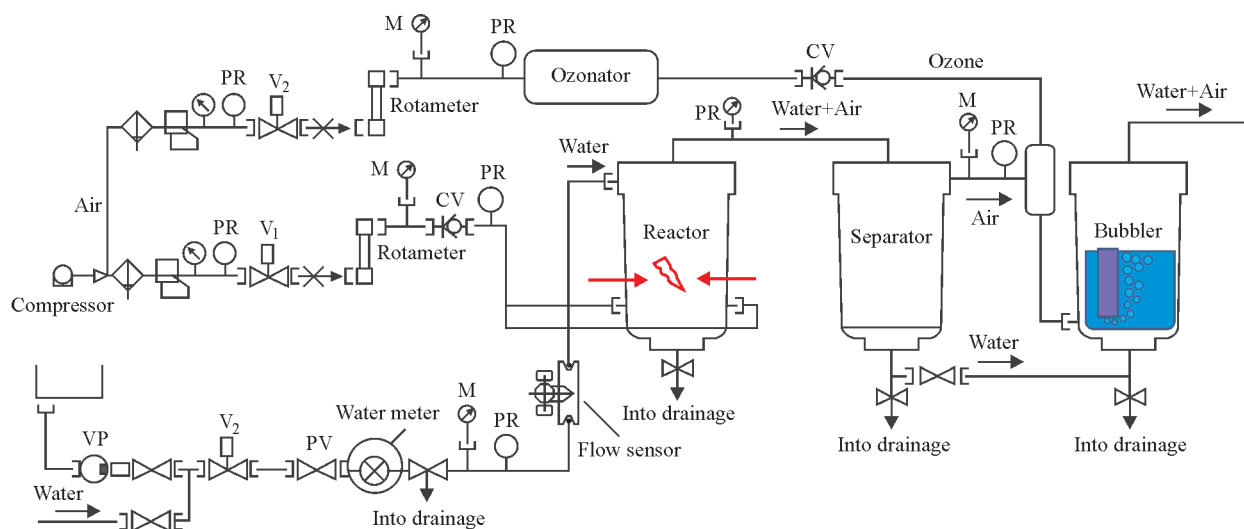


Figure11. Pneumatic hydraulic diagram of the plasma system

Table 3. Parameters of the plasma system for the production of PAW and liquid nitrogen fertilizers

Parameter	Magnitude
Power	10 kW
Water consumption	up to 2 t/h
Air consumption	up to 5 m³/h
NO ₃	up to 6 mol NO ₃ ⁻ per hour (0.4 kg)
Concentration NO ₃ ⁻	up to 500 mg NO ₃ ⁻ per liter
Installation dimensions	0.7×0.7×1.5 m
Installation weight	150 kg

The parameters of the plasma system for the production of PAW and liquid nitrogen fertilizers are presented in Table 3.

The system is scalable up to 100 kW with a capacity of up to 20 t/h. Typical research results are presented in Table 4.

In this series of experiments, air was introduced into the system.

DISCUSSION

The authors, along with several other researchers, are developing a process that simulates lightning flashes in nature. Understanding the chemical processes occurring during induced plasma discharge in water will lead to an understanding of the impact of PAW on seed germination and plant growth.

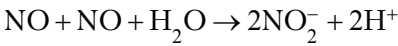
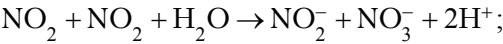
Table 4. Research results

Power, kW	Gas	Gas consumption, m³/hour	Water consumption, L/hour	Ozone, g/hour	Water conductivity, µS/cm	NO, ppm	NO ₃ ⁻ , mg/L	NO ₂ ⁻ , mg/L	O ₂ , mg/L
4.3	Air	0.8	240	–	240/500	2200	150	30	7
4.3	Air	0.8	240	10	240/530	330	180	40	7
–	Air	0.8	240	–	240	–	–	–	0

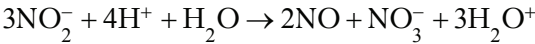
The electric discharge in the surrounding air primarily produces NO and NO₂. During lightning flashes, the air transitions from the gaseous phase to the plasma phase, splitting N₂ and O₂ molecules into active radicals. As demonstrated in [16], upon contact with water, hydroxyl radicals (OH*) are formed, which quickly recombine into hydrogen peroxide (H₂O₂):



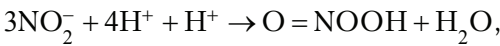
gaseous NO₂ dissolves in water, forming nitrites NO₂⁻ and nitrates NO₃⁻:



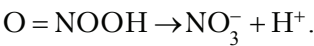
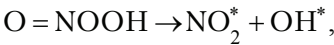
in an acidic environment NO₂⁻ can be oxidized to NO₃⁻



or NO₂⁻ reacts with H₂O₂ to form an intermediate compound, peroxynitrous acid:



which is an unstable product and over time decomposes either into NO₃⁻ or into the radicals NO₂* and OH*:



Thus, the resulting reactive particles dissolve in water and produce PAW. In this form, a mixture of long-lived active oxygen and nitrogen species (H_2O_2 , NO_2^- , NO_3^- , and others) is considered a clean and stable alternative to chemical fertilizers. Such PAW can be effectively utilized for various agricultural purposes [27–29].

The new plasma process, based on phenomena borrowed from nature, is currently in the developmental and testing stage. Plasma sources used in plasma agriculture may vary in design and operating principle. However, their primary goal is to generate plasma and deliver RONS to seeds, plants, soil, or water. Plasma generation devices can range from portable units to larger systems, depending on the scale of agricultural operations and their requirements. The choice of device for plasma generation in water plasma treatment plays a crucial role in obtaining a variety of RONS. In several studies [30–33], a comprehensive analysis was conducted on the efficiency of RONS generation from different types of plasma sources. Various plasma reactors were investigated, including spark discharges, glow discharges, corona discharges, laser discharges, radiofrequency cross discharges, dielectric barrier discharges, arc discharges, microwave discharges, and plasma jets in contact with water.

In the plasma system developed by the authors, a hybrid plasma is utilized, combining equilibrium and non-equilibrium plasmas. The plasma module operates in a pulsating mode of electric discharge combustion (transitioning from arc to diffuse discharge, accompanied by a significant increase in plasma volume by orders of magnitude) within a flowing bubble stream of water. The conductivity of the liquid plays a crucial role in plasma formation and electrical breakdown. Electrical breakdown is a pivotal phase for generating plasma discharge. Analysis of oscillograms (Figure 8) revealed that a system with rapid voltage rise time exhibits much higher tolerance to liquid conductivity and can sustain a stable discharge. Highly reactive particles are produced specifically in the electric discharge in the presence of water and air, dissolving into water to form PAW. Some authors also note that using air as the feed gas in the plasma setup leads to a greater variety of RONS compared to using other gases such as argon, N_2 , and O_2 . The plasma system (Figure 11) includes ozone injection for oxidizing residual NO.

As indicated by the research results presented in Table 4, the system with a hybrid plasma discharge ensures sufficiently high levels of RONS concentration in PAW. The results obtained during the study suggest that the developed plasma system can be used for the direct high-yield production of PAW.

The increase in the amount of air passed through the discharge zone enhances the content of RONS in PAW. Similar results have been obtained in studies [14, 17].

It should be noted, however, that as demonstrated by a series of practical studies, different concentrations of RONS in PAW have varying effects on the development of different agricultural crops and seed germination. For instance, in study [30], correlations between the characteristics of PAW and their impact on various crops were analyzed. Such data allow for the adjustment of RONS content in activated water to target specific agricultural crops. High-concentration solutions can be diluted with water if necessary. Plasma-treated solutions remain stable for several days of storage [13], allowing for the transportation of PAW and its prolonged use over time. PAW has significant potential for effective use in various agricultural applications, as long-lived liquid RONS (H_2O_2 , NO_2^- , NO_3^-) can participate in plant metabolism or serve as nutrients [16].

Nitrites and nitrates in PAW act as nitrogen fertilizers and contribute to enhanced seedling growth. As noted in [16], NO_3^- primarily enhances dry biomass, photosynthetic pigment content, photosynthesis rate, and overall plant appearance; and H_2O_2 contributes to increased dry biomass. Additionally, PAW improves seed germination and early seedling development [16].

It should also be noted that agricultural plants are highly susceptible to pathogen attacks. However, PAW contains various RONS in concentrations that can help activate plant defense systems [17].

The small size of the developed plasma system for PAW and liquid nitrogen fertilizer production, and also its lightweight and sufficiently high productivity in generating RONS (Table 3) enable developed plasma system's use in small and medium-sized farms, as well as its shared use among multiple farms.

CONCLUSION

The analysis of the current state of PAW application in agriculture has shown its potential to enhance many key crop production indicators. A primary challenge lies in transitioning from laboratory conditions to industrial-scale applications. High-throughput production of PAW holds promise through the use of hybrid plasma discharge, combining non-equilibrium and equilibrium (arc) discharges with water plasma. Experimental research results on PAW production have demonstrated the effectiveness of hybrid plasma generation technologies in producing water enriched with active substances. Such PAW can be effectively used for seed germination, plant growth, and development. PAW presents an alternative to chemical nitrogen fer-

tilizers in agriculture. Plasma technology for atmospheric nitrogen fixation enables the production of liquid nitrogen fertilizers directly at agricultural sites, eliminating issues related to transportation, product loss, and environmental protection. The advancement of plasma agricultural technologies can be further facilitated by integrating plasma systems with inexpensive renewable electricity sources. The potential of PAW lies in its relative simplicity and convenience of production, although standards development is needed for widespread adoption in crop cultivation.

REFERENCES

1. Soloveichik, G. (2017) NH_3 Energy future of ammonia production: Improvement of Haber–Bosch process or electrochemical synthesis? In: *Topical Conf.: AIChE Annual Meeting, October 29–November 3, 2017, Minneapolis*. <https://nh3fuelassociation.org/wp-content/uploads/2017/11/NH3-Energy-2017-Grigorii-Soloveichik.pdf>
2. Ghavam, S., Vahdati, M., Wilson, I.A.G., Styring, P. (2021) Sustainable ammonia production processes. *Frontiers in Energy Research*, **9**, 580808. DOI: <https://doi.org/10.3389/fenrg.2021.580808>
3. Tyagi, J., Ahmad, S., Malik, M. (2022) Nitrogenous fertilizers: impact on environment sustainability, mitigation strategies, and challenges. *Inter. J. of Environmental Sci. and Technology*, **19**, 11649–11672. DOI: <https://doi.org/10.1007/s13762-022-04027-9>
4. Zhou, R., Zhou, R., Wang, P. et al. (2020) Plasma-activated water: Generation, origin of reactive species and biological applications. *J. of Physics D: Applied Physics*, **53**, 30. DOI: <https://doi.org/10.1088/1361-6463/ab81cf>
5. Petrov, S.V. (2021) *Innovatsionnye plazmenno-struinye tekhnologii*. LAMBERT Academic Publ. [in Russian].
6. Bogaerts, A., Neyts, E.C. (2018) Plasma technology: An emerging technology for energy storage. *ACS Energy Letters*, **3**(4), 1013–1027. DOI: <https://doi.org/10.1021/acsenrgylett.8b00184>
7. Anastasopoulou, A. (2018) *Conceptual process design of plasma-assisted nitrogen fixation through energy, environmental and economic assessment*. Technische Universiteit Eindhoven. https://pure.tue.nl/ws/portalfiles/portal/105883898/20180919_CO_Anastasopoulou.pdf
8. Rathore, V., Nema, S.K. (2021) Optimization of process parameters to generate plasma activated water and study of physicochemical properties of plasma activated solutions at optimum condition. *J. of Applied Physics*, **129**(8). DOI: <https://doi.org/10.1063/5.0033848>
9. Kaushik, N.K., Ghimire, B., Li, Y. et al. (2018). Biological and medical applications of plasmaactivated media, water and solutions. *Biological Chemistry*. **400**(1), 39–62. DOI: <https://doi.org/10.1515/hsz-2018-0226>
10. Lamichhane, P., Paneru, R., Nguyen, L.N. et al. (2020) Plasma-assisted nitrogen fixation in water with various metals. *Reaction Chemistry & Eng.*, **5**, 2053–2057. DOI: <https://doi.org/10.1039/d0re00248h>
11. Wang, Z., Liu, J., Zhao, H. et al. (2023) Free radicals promote electrocatalytic nitrogen oxidation. *Chemical Sci.*, **14**, 1878–1884. DOI: <https://doi.org/10.1039/D2SC06599A>
12. Guragain, R.P., Baniya, H.B., Pradhan, S.P. et al. (2021). Influence of plasma-activated water (PAW) on the germination of radish, fenugreek, and pea seeds. *AIP Advances*, **11**, 125304. DOI: <https://doi.org/10.1063/5.0070800>
13. Stoleru, V., Burlica, R., Mihalache, G. et al. (2020) Plant growth promotion effect of plasma activated water on *Lactuca sativa* L. cultivated in two different volumes of substrate. *Scientific Reports*. **10**, 20920. DOI: <https://doi.org/10.1038/s41598-020-77355-w>
14. Ka, D.H., Priatama, R.A., Park, J.Y. et al. (2021) Plasma-activated water modulates root hair cell density via root developmental genes in *Arabidopsis thaliana* L. *Applied Sci.*, **11**(5), 2240. DOI: <https://doi.org/10.3390/app11052240>
15. Škarpa, P., Klofáč, D., Krěma, F. et al. (2020) Effect of plasma activated water foliar application on selected growth parameters of maize. *Water*, **12**(12), 3545. DOI: <https://doi.org/10.3390/w12123545>
16. Kučerová, K., Henselová, M., Slováková, L., Hensel, K. (2019) Effects of plasma activated water on wheat: Germination, growth parameters, photosynthetic pigments, soluble protein content, and antioxidant enzymes activity. *Plasma Process and Polymers*, **16**(3), 1800131. DOI: <https://doi.org/10.1002/ppap.201800131>
17. Adhikari, B., Adhikari, M., Ghimire, B. et al. (2019) Cold atmospheric plasmaactivated water irrigation induces defense hormone and gene expression in tomato seedlings. *Scientific Reports*, **9**, 16080, 1–15. DOI: <https://doi.org/10.1038/s41598-019-52646-z>
18. Kučerová, K., Henselová, M., Slováková, L. et al. (2021) Effect of plasma activated water, hydrogen peroxide, and nitrates on lettuce growth and its physiological parameters. *Applied Sci.*, **11**(5), 1985. DOI: <https://doi.org/10.3390/app11051985>
19. VitalFluid (2024) *Plasma activated water*. <https://vitalfluid.com/plasma-activated-water/>
20. (2021) *Plasma activated water in USDA-organic fertilization*. <https://vitalfluid.com/wp-content/uploads/2022/03/Newsletter-2-VitalFluid-in-USDA-organic-tomato-cultivation.pdf>
21. Wang, H., Wandel, R.J., Tachibana, K. et al. (2018) The influence of liquid conductivity on electrical breakdown and hydrogen peroxide production in a nanosecond pulsed plasma discharge generated in a water-film plasma reactor. *J. of Physics D: Applied Physics*, **52**(7). DOI: <https://doi.org/10.1088/1361-6463/aaf132>
22. Rouwenhorst, K.H.R., Jardali, F., Bogaerts, A., Lefferts, L. (2021) From the Birkeland–Eyde process towards energy-efficient plasma-based NO_x synthesis: A techno-economic analysis. *Energy & Environmental Sci.*, **14**, 2520–2534. DOI: <https://doi.org/10.1039/d0ee03763j>
23. Muzammil, I., Lee, D.H., Dinh, D.K. et al. (2021) A novel energy efficient path for nitrogen fixation using a non-thermal arc. *RSC Advances*, **11**(21), 12729–12738. DOI: <https://doi.org/10.1039/d1ra01357b>
24. Winter, L.R., Chen, J.G. (2020) N_2 fixation by plasma-activated processes. *Joule*, **5**(2), 300–315. DOI: <https://doi.org/10.1016/j.joule.2020.11.009>
25. Vervloessem, E., Gorbanev, Y., Nikiforov, A. et al. (2022) Sustainable NO_x production from air in pulsed plasma: Elucidating the chemistry behind the low energy consumption. *Green Chemistry*, **24**, 916–929. DOI: <https://doi.org/10.1039/D1GC02762J>
26. Ganz, S.N., Parkhomenko, V.D. (1976). *Obtaining fixed nitrogen in plasma*. Kyiv, Vishcha Shkola [in Russian].
27. Judée, F., Simon, S., Baillyb, C., Dufour, T. (2018) Plasma-activation of tap water using DBD for agronomy applications: Identification and quantification of long lifetime chemical species and production/consumption mechanisms. *Water Research*, **133**, 47–59. DOI: <https://doi.org/10.1016/j.watres.2017.12.035>
28. Sharma, H.P., Patel, A.H., Pal, M. (2021) Effect of plasma activated water (PAW) on fruits and vegetables. *Ameri-*

- can *J. of Food and Nutrition*, 9(2), 60–68. DOI: <https://doi.org/10.12691/ajfn-9-2-1>
29. Rahman, M., Hasan, M.S., Islam, R. et al. (2022) Plasma-activated water for food safety and quality: A review of recent developments. *Inter. J. of Environmental Research and Public Health*, 19(11), 6630. DOI: <https://doi.org/10.3390/ijerph19116630>
30. Konchekov, E.M., Gusein-zade, N., Burmistrov, D.E. et al. (2023) Advancements in plasma agriculture: A review of recent studies. *Inter. J. of Molecular Sci.*, 24(20), 15093. DOI: <https://doi.org/10.3390/ijms242015093>
31. Gao, Y., Francis, K., Zhang, X. (2022) Review on formation of cold plasma activated water (PAW) and the applications in food and agriculture. *Food Research Inter.*, 157, 111246. DOI: <https://doi.org/10.1016/j.foodres.2022.111246>
32. Bruggeman, P.J., Kushner, M.J., Locke, B.R. et al. (2016) Plasma-liquid interactions: a review and roadmap. *Plasma Sources Sci. and Technology*, 25, 053002. DOI: <https://doi.org/10.1088/0963-0252/25/5/053002>
33. Zjup, W., Chen, H., Yuan, D. et al. (2021) Review of low-temperature plasma nitrogen fixation technology. *Waste Disposal & Sustainable Energy*, 3, 201–217. DOI: <https://doi.org/10.1007/s42768-021-00074-z>

ORCID

S.V. Petrov: 0000-0003-0373-8003

S.G. Bondarenko: 0000-0001-9590-4747
 Sh. Roshanpour: 0000-0002-4272-9217
 A.M. Shakhnovsky: 0000-0003-2963-4026

CONFLICT OF INTEREST

The Authors declare no conflict of interest

CORRESPONDING AUTHOR

S.V. Petrov

The Gas Institute of the NASU

39 Degtyarivska Str., 03113, Kyiv, Ukraine

E-mail: vizana.sp@gmail.com

SUGGESTED CITATION

S.V. Petrov, S.G. Bondarenko, Sh. Roshanpour, A.M. Shakhnovsky (2024) Continuous production of large volumes of plasma activated water for agriculture. *The Paton Welding J.*, 10, 42–53. DOI: <https://doi.org/10.37434/tpwj2024.10.06>

JOURNAL HOME PAGE<https://patonpublishinghouse.com/eng/journals/tpwj>

Received: 10.07.2024

Received in revised form: 16.09.2024

Accepted: 21.10.2024

OKOSCAN 73HS

HIGH SPEED
RAIL TESTING
SYSTEM
OKOSCAN 73HS








METRO (SUBWAY, MRT) OKOSCAN 73MS



UDS2-77

SINGLE RAIL
TESTING
SYSTEM



UDS2-73 RAILWAY





OKOndt GROUP

ProNDTSolution
sales@ndt.com.ua
 (38044) 531 37 26 (27)
www.ndt.com.ua

77th ANNUAL ASSEMBLY OF THE INTERNATIONAL INSTITUTE OF WELDING AND INTERNATIONAL WELDING AND JOINING CONFERENCE



This year the 77th Annual Assembly of the International Institute of Welding and the International Conference on Welding and Joining took place from July 7 to 12 on the island of Rhodes in Greece at the Rhodes Palace Hotel and Convention Center. This prestigious international event brought together experts from around the world to discuss the latest developments and innovations in welding technologies. Prominent industry representatives and researchers shared their findings and discussed future trends in the field. Almost 1000 participants from 51 countries also had the opportunity to attend seminars and networking events to deepen their knowledge and make new contacts.

Such events are extremely important for Ukrainian scientists, especially under the conditions of modern challenges that the scientific community of Ukraine is facing. Participation in international conferences, such as the Annual Assembly of the International Institute of Welding, provides an opportunity to exchange experience with colleagues from around the world, and to become familiar with the latest scientific achievements and technologies. For Ukrainian researchers, this is also an important step towards integration into the world scientific community, establishment of new international contacts and involvement in the joint projects. Years of pandemic and military aggression in the territory of Ukraine significantly limited the opportunities for direct communication with colleagues from other countries. Therefore, the chance to participate in the 77th IIW Annual Assembly and the International Conference was used to the maximum.

Thanks to the support of the Ministry of Education and Science of Ukraine, CRDF Global, the team of the In-



ternational Institute of Welding and the Greek Institute of Welding, the Ukrainian delegation, led by Illia Klochkov, Academic Secretary of the E.O. Paton Electric Welding Institute of the National Academy of Sciences of Ukraine, representative of Ukraine in IIW, Cand. of Sci. (Eng.) went to Greece. The delegation also included Maksym Iurzhenko, the Corresponding Member of the National Academy of Sciences of Ukraine, Dr. of Sci. (Eng.), Head of the Plastics Welding Department and Sviatoslav Motrunich, Cand. of Sci. (Eng.), Senior Staff Scientist of the Department of Welded Structure Strength.



The heat that prevailed this July in Kyiv is difficult to compare with that on the island of Rhodes. However, in the halls where this scientific event was held, the atmosphere was even hotter: reports, speeches, presentations, discussions on the sidelines, meetings with old colleagues and new acquaintances — all this created a unique atmosphere of the event. Here are the official statistics of registered participants:

- full members — 466;
- full participants (young specialists) — 147;
- full participants (students) — 205;
- participants of the International Conference — 25;
- participants of the International Conference (students and young specialists) — 17;
- accompanying persons — 68;
- participants of the Symposium on “Intelligent Manufacturing” — 11.

Germany was the most represented this year with 155 participants. It is followed by China — 132, Greece — 128, Japan — 86, USA — 81, South Korea — 68.

The Ukrainian delegation, together with representatives of the Institute, who presented their reports online, consisted of ten scientists. They were Maksym Khokhlov, who presented the report on “Thermomechanical

processes in zones of FSW butt joints of sheet magnesium alloy”, Svitlana Maksymova — “Influence of Ge and In on the structure and thermodynamic characteristics of high-entropy MnCoNiCu alloys”, Oleksandr Yarovytsyn — “On the issue of probability assessment and prevention of the occurrence of the “immersion plasticity cracking” mechanism in the conditions of the process of 3D multilayer deposition with a welding arc on nickel and cobalt alloys”, Serhiy Maksymov — “Effectiveness of application of the pulsed nature of arc burning in wet underwater welding”, Serhiy Schwab — “Production and application of powder of a biomedical titanium alloy of Ti–Zr–Nb system in metal flux-cored wire for WAAM technology”, Roman Selin — “Narrow-gap welding of titanium alloy samples with a width of 45–60 mm by a controlled magnetic field”, Yevgenia Chvertko — “Welding of rod artistic constructions”.

One of the main areas of PWI activity is to attract young scientists to the technology sector, to promote their professional development and integration into the international scientific and technical community. The Institute recognizes the importance of training a new generation of researchers and welding engineers capable of not only supporting but also promoting advanced technologies in the field of welding and materials science. For this purpose, PWI supported the participation of its young talents in the online format in the meetings of IIW Working Commissions. Thanks to such support, young Ukrainian scientists had the opportunity to participate in the discussion of the latest scientific and technical achievements.

Members of the Ukrainian delegation, who had the opportunity to attend the event on the Greek island, presented the following reports: Maksym Iurzhenko — “High-speed welding of polymer materials”, Sviatoslav Motrunich — “High-cycle fatigue of 3D-printed titanium alloy TA15 produced by electron beam additive manufacturing”, “Manufacture of a high-hardness, high-entropy, tantalum-doped eutectic alloy using arc additive manufacturing” and “Structural integrity of 3D-printed Ti–6.5Al–1Mo–1V titanium alloy billets”. It should be noted that Sviatoslav Motrunich presented reports both at the meeting of the relevant Working Commission and at the International Conference on Welding and Joining.

As part of IIW activities, a tradition has been established long ago of honoring those who have achieved significant results in welding and related areas. These awards received their names in honor of outstanding personalities who were the founders of IIW or made a significant contribution to the development and implementation of scientific and technical achievements in the field of welding, joining and related processes. Usually, the award ceremony takes place during the official opening ceremony of the event. In 2024, the award winners were:

- Fellow of the IIW, awarded to Károly Jármai, Patrio Mendez, Gerhard Posch, Volker Schöppner, Chuan-song Wu and Yixiong Wu;
- Evgeny Paton Award — Suck-Joo Na;

- Arthur Smith Award — David Fink;
- Yoshiaki Arata Award, — Boian Alexandrov;
- Thomas Medal — Teresa Melfi;
- Chris Smallbone Award — Emmanuel Afrane Gyasi;
- Walter Edström Medal — John C. Lippold;
- Henry Granjon Category A Award — Rui Yu;
- Henry Granjon Category B Award — Derek Shaffer;
- Henry Granjon Category C Award — Aravindh Nammalvar Raja;
- Halil Kaya Gedik Award — Sergio Amancio
- Welding in the World Best Paper Award, Category A: Welding Processes and Additive Manufacturing awarded to Florian Muller;
- Welding in the World Best Paper award, Category B: Materials and Metallurgy awarded to Nellikode Savyasachi;
- Welding in the World Best Paper Award, Category C: Structural Integrity, Design and Fitness for Service awarded to Kalle Lipiäinen;
- André Leroy Prize — Guy Brooks & Michael Pitt.

Almost 30 years ago, our Institute established one of IIW most prestigious awards — the Evgeny Paton Prize. According to the results of a secret vote, which was held among the representatives of member countries of the International Institute of Welding, this year’s winner among many applicants was Suck-Joo Na, Professor of the Korea Advanced Institute of Science and Technology. The award was presented to the laureate by Illia Klochkov, Academic Secretary of the E.O. Paton Electric Welding Institute of the National Academy of Sciences of Ukraine.

For its part, the International Institute of Welding recognized a Ukrainian representative for her significant contribution to the activities of the governing bodies of this international organization during 2021–2024. The award was given to Yevgenia Chvertko, former IIW Vice-President, who, with her tireless work, contributed to the strengthening of Ukraine’s position in this organization.

Representatives of the Ukrainian delegation held a series of meetings in Rhodes — from short greetings to long, substantive negotiations. Each of these meetings had its own importance, as they created the basis for establishing new professional contacts and strengthening the already existing partnerships. We sincerely hope that these negotiations will bring mutually beneficial results for both parties.

I would especially like to note the meeting with David Lake, President of Weld Australia organization, the head of the organization, which at a very difficult time for Ukraine initiated support for us within the international welding community, thereby helping and continuing to help the promotion of the Institute, and Ukraine as a whole, in the international arena. We are grateful to Weld Australia for both significant financial support and willingness to cooperate within bilateral and multilateral agreements.

In Rhodes, the Ukrainian delegation actively promoted the activities of the Institute. Particular attention was paid to the presentation of the International Conference “Welding and Related Technologies 2024”, which will

be held from October 7 to 10, 2024 in the picturesque city of Yaremche (Ukraine). This event should become a unique platform for the exchange of experience between scientists, engineers and industry specialists, promote the development of international cooperation, as well as popularization of the latest achievements in the field of welding and related technologies. The Conference has already aroused considerable interest among potential participants from different countries of the world, which makes it one of the key events of the year in the field of welding in Ukraine.

This year's meeting in Rhodes became an ideal place for a substantiative exchange and professional communication around the topic of welding and related fields. If we summarize the work of the 77th Annual Assembly of the International Institute of Welding and the International Conference on Welding and Joining, then, according to official information:

- in the period from July 7 to July 12, 2024, 18 meetings of IIW Commissions and Working Groups were held;
- at the International Conference “Energy Infrastructures and Transportations across the seas”, held on July 11 and 12, 2024, 87 presentations were made and 17 posters were presented;
- social events included an opening ceremony and awards ceremony, an Ice Breaking event for young professionals, a welcome reception, a Greek night and a closing ceremony at the gala banquet;
- presentation of sponsors' products took place;
- a photo exhibition of a collection of works of art made using the welding methods was held.

And what next... Next we will look forward to 2025, when the 78th IIW Annual Assembly and International Conference on Welding and Joining is scheduled to take place in Magazzina del Cotone in Genoa, Italy, from June 22 to 27.

Editorial Office of the Journal

VII INTERNATIONAL CONFERENCE “WRT-2024”

On October 7–10, 2024, the VII International Conference “Welding and Related Technologies WRT-2024” was held in Yaremche, Ukraine, bringing together scientists from Australia, Canada, China, Czech Republic, France, Germany, Israel, Italy, Japan, Mexico, Poland, Ukraine, USA, and representatives from more than 30 research organisations, private companies and industrial enterprises. The event was held in a mixed format. The working language of the Conference was English.

The VII International Conference “Welding and Related Technologies WRT-2024” was held as an associated event of the International Institute of Welding (IIW) and with the financial support of the US Civilian Research and Development Foundation (CRDF Global). The Conference was organized by the E.O. Paton Electric Welding Institute of the NAS of Ukraine. The International Association “Welding” and the NGO “Virtus” were co-organizers of the Conference.

A total of 159 participants from 13 countries of the world took part in the event. Interesting presentations from 5 invited speakers were heard. 18 specialists in the field of welding and related technologies presented the results of their research and development works in person, 20 scientists spoke online, and 19 participants made poster presentations. An online section was also held in parallel at the E.O. Paton Electric Welding Institute of the NAS of Ukraine in Kyiv.

The most popular topic area of the Conference in terms of the number of presented papers was “Innovative technologies, materials and equipment for welding and related processes” — 19 papers, 10 papers were presented in the topic “New structural and functional materials, nanomaterials, composites”, the topic areas “Mathematical modelling of welding and related processes”, “Non-destructive testing and technical diagnostics” and “Modern technologies of special electrometallurgy” were presented in 7 papers each, and 6 papers were presented in the topic area “Additive technologies”.

It is worth noting the extremely positive atmosphere of the event, the high level of speakers, fruitful exchange of opinions and interesting communications. All the presentations aroused great interest, which was reflected in the inspired, lively discussions among the participants and the audience. Thus, all participants had a great opportunity to enrich their knowledge and exchange experiences. Welding science and technologies are alive in Ukraine and around the world and have significant development prospects.

We invite everybody to participate in the VIII International Conference “Welding and Related Technologies WRT-2026” in 2026!

Editorial Office of the Journal